PALEOGEOGRAPHIC AND PALEOCLIMATIC RECONSTRUCTION ALONG THE MAHANADI DELTA

Ph.D. THESIS

by

CHINMAY DASH

DEPARTMENT OF EARTH SCIENCES
INDIAN INSTITUTE OF TECHNOLOGY ROORKEE
ROORKEE – 247 667 (INDIA)
JULY, 2019

PALEOGEOGRAPHIC AND PALEOCLIMATIC RECONSTRUCTION ALONG THE MAHANADI DELTA

A THESIS

Submitted in partial fulfilment of the requirements for the award of the degree

of

DOCTOR OF PHILOSOPHY

in

EARTH SCIENCES

by

CHINMAY DASH

DEPARTMENT OF EARTH SCIENCES
INDIAN INSTITUTE OF TECHNOLOGY ROORKEE
ROORKEE – 247 667 (INDIA)
JULY, 2019

INDIAN INSTITUTE OF TECHNOLOGY ROORKEE
ROORKEE

CANDIDATE'S DECLARATION

I hereby certify that the work which is being presented in the thesis entitled **"PALEOGEOGRAPHIC AND PALEOCLIMATIC RECONSTRUCTION ALONG THE MAHANADI DELTA"** in partial fulfilment of the requirements for the award of the Degree of Doctor of Philosophy and submitted in the Department of Earth Sciences of the Indian Institute of Technology Roorkee, Roorkee is an authentic record of my own work carried out during a period from July, 2013 to July, 2019 under the supervision of Dr. Pitambar Pati, Associate Professor, Department of Earth Sciences, Indian Institute of Technology Roorkee, Roorkee.

The matter presented in this thesis has not been submitted by me for the award of any other degree of this or any other institution.

Chinmay Dash

(CHINMAY DASH)

This is to certify that the above statement made by the candidate is correct to the best of my knowledge.

27/12/19

Signature of Supervisor

The Ph.D. Viva-Voce Examination Mr. Chinmay Dash, Research Scholar, has been held on 27.12.2019.

27/12/2019

Chairperson, SRC

External Examiner

This is to certify that the student has made all the corrections in this thesis.

27/12/19

Signature of Supervisor

Head of the Department

Date: 27.12.2019

Abstract

The present study on Mahanadi delta has two broad objectives: (i) to define implications of sea-level fluctuations on channel morphologic changes in deltaic environment and, (ii) to reconstruct Indian Summer Monsoon variability from lake sediment records.

Contrary to previous laboratory-based investigations lacking empirical evidence on fluvial response to base-level changes, the present work is focused on correlating concepts of base-level controlled channel morphologic changes with field-based observations. Various paleo-fluviogeomorphic features such as anastomosing-meandering transition, paleo-dendritic channels, and lateral shift of river mouths, which are indicative of base-level change have been studied and correlated with past marine transgression and regression events. Past studies on borehole cuttings indicate that the Mahanadi delta has experienced several episodes of marine transgression and regression events. Paleo-barrier spits, relict ridges, and paleo-marine terraces in the inner Mahanadi deltaic region are evidence of past coastline positions. Ground Penetrating Radar study along paleo-strandlines of the Mahanadi delta reveals several stratal termination units in the sub-surface sediment layers. These subsurface depositional units may have developed due to repeated marine transgression/regression and sequential deposition of sediments. Major rivers in the Mahanadi delta e.g. Mahanadi, Devi, Brahmani, and Baitarani, show episodic anastomosing and meandering characteristics corresponding to transgressive and regressive events, respectively. The paleo-anastomosing branches along the paleo-strandline positions can be observed in satellite imagery. Dendritic drainage patterns formed due to flow accumulation along the coast have been observed along the paleo-strandlines. Based on OSL ages and affinity to strandline positions, two generations of Holocene dendritic channels can be distinguished in the Mahanadi deltaic region. Paleo-dendritic channels with age > 5 ka BP correspond to Early-Mid Holocene strandline position and, with age group < 5 ka BP correspond to the Late Holocene strandline position. The Early to Mid and Mid to Late Holocene paleo-dendritic channels developed along the transgressive coasts and later were abandoned when the coastline regressed. Lateral shifting of river mouths in response to sea-level changes have been observed in the lower deltaic plain. The delta distributaries such as Bhargavi, Kushavadra, Brahmani and Baitarani rivers

show lateral shift of river mouth before meeting the Bay of Bengal. Age of Kushabhadra River paleochannel indicating paleo-flow direction dates back to ~ 7 ka BP. Similarly, the paleo-flow paths of the Brahmani River date back to ~ 6 ka BP. The river mouth shift directions of both the rivers are parallel to the Early Holocene strandline. Major rivers in the delta have migrated up to the present coastline with base-level adjustments to changing coastline, while the small channels ended abruptly with a retreat in sea level. Paleochannels along the paleo-strandlines indicate last fluvial activity along the paleo-coastlines. When compared to fluvial morphological patterns along paleo-strandlines of major deltas around the world, the Mahanadi delta shows similar paleo-fluvial morphology with changing coastline.

Two sediment cores from Anshupa Lake and Chilka Lake were analyzed to study paleoclimatic changes and their effect on sedimentation in the Mahanadi delta region. Sediment core from Anshupa Lake dates back (^{14}C) to 1400 AD, provides evidence of the Little Ice Age (LIA). The average sedimentation rate during LIA was 0.12 cm/yr and it drastically changed to 0.45 cm/yr in the post LIA period. During the LIA period, the sedimentation rate was highest in the 16th century (0.35 cm/yr) and lowest in the 18th century (0.09 cm/yr). Down core variation of mineral magnetic, organic carbon and stable isotope record suggest that LIA extended from 1450 AD to 1850 AD. The χlf values vary from ~ 5× 10^{-8} m^3 kg^{-1} to ~ 60× 10^{-8} m^3 kg^{-1}. The χlf values are lower at the Dalton (~ 5× 10^{-8} m^3 kg^{-1}) and Munder Minimums (~ 9× 10^{-8} m^3 kg^{-1}), while the 16th century showed an increasing trend. The χfd % value varies from ~0 to ~13%. The χARM value varies from 0.785 × 10^{-5} m^3 kg^{-1} to 0.021 × 10^{-5} m^3 kg^{-1}. The saturation isothermal remnant magnetization value varies from 627.0126× 10^{-5} Am^2 kg^{-1} to 33.094× 10^{-5} Am^2 kg^{-1}. χfd %, χARM and SIRM show similar trend as shown by χlf values. The χlf shows a positive correlation with reconstructed sunspot numbers. Spectral analysis of χlf values shows significant periodicity of 74, 64, 44 and 11 years. These periodicities suggest a solar influence on Indian Summer Monsoon. Organic carbon and nitrogen percentage vary from 1.5 to 6 % and 0.07 to 0.7 %, respectively. The δ^{13}C value of organic carbon fluctuates from – 21.028 to − 26.528 ‰. The downcore variation of δ^{13}C and TOC reflects two phases of climate during LIA. Phase-I (1450 to 1700 AD) reflects relatively high content of TOC and more negative values δ^{13}C indicating relatively warmer climatic condition. During Phase-II (1700-1850 AD), TOC deposition relatively decreased and δ^{13}C

became comparatively positive reflecting relatively cold climate. The inter-parametric ratio χARM/SIRM is > 200 around 1600 AD, suggesting the presence of bacterial magnetism. Bacterial magnetite develops due to a high influx of nutrients into the lake. The bacterial magnetism correlates with high nutrient supply to the lake ecosystem due to a relatively warm period during the 16th century, as suggested by an increasing trend in χlf values. The organic carbon percentage, C/N ratio and stable isotope record indicate comparatively increased rainfall during the 16th century than the 17th and 18th centuries. From these geochemical parameters, it is inferred that the 17-18th century corresponding to Dalton Minimum was the coldest period with reduced precipitation and the 16th century was a relatively warmer period during LIA. Several events of drought, high rainfall, and the onset of aridity can be correlated with similar events documented in speleothems from different parts of India. The sediment core from Chilka Lake dates back to 9039 cal yr. BP. Sedimentation rate fluctuates from ~ 0.2 cm/year to ~ 0.007 cm/year, with maximum sedimentation from 8,000 cal yr BP to 6,000 cal yr BP and minimum sedimentation from 6,000 cal yr BP to 2,000 cal yr BP. Down core variation of mineral magnetic parameters reveals wide fluctuation in χlf values. The χlf values range from 6.4× 10^{-8} m^3 kg^{-1} to 43× 10^{-8} m^3 kg^{-1}. The χlf values are minimum from 6,000 cal yr BP to 2,000 cal yr BP, suggesting mid-Holocene weakening of Indian Summer Monsoon. χARM varies from 0.71 × 10^{-5} $m^3 kg^{-1}$ to 0.021 × 10^{-5} m^3 kg^{-1}. The saturation isothermal remnant magnetization values vary from 636.33× 10^{-5} $Am^2 kg^{-1}$ to 44.905× 10^{-5} $Am^2 kg^{-1}$. The downcore variation of χlf, χARM, and SIRM show a similar trend. An increasing trend in these mineral magnetic parameters are observed during early to mid (8,000 cal yr BP to 6,000 cal yr BP) and late Holocene period (>2,000 cal yr BP). The study of Chilka Lake core suggests Holocene warm period extended from 9,000 cal yr BP to 6,000 cal yr BP, and the mid-Holocene period was relatively cold. Regional records on flourishing and extinction of river valley civilizations are found to be correlated with climatic records obtained from Chilka Lake core. Spectral analysis of χlf values shows significant periodicities of 1058, 690, 484, 396, 288, 212, 207, 183 and 158 years, suggesting a possible solar influence on Holocene variation of Indian Summer Monsoon. Paleoclimatic study from two sediment cores suggests that magnetic susceptibility (χlf) data is highly correlating with regional climatic records. Spectral analysis of χlf in both the cores indicates that periodicities in ISM can be obtained from high-resolution

magnetic susceptibility data. We have thus explored the potential of using magnetic susceptibility (χlf) as a proxy for paleorainfall variations in a tropical region.

Acknowledgment

It would be an immense pleasure to acknowledge all individuals I came across during these six years of Ph.D. research work for their contributions towards the completion of my Ph.D. thesis and making it successful.

At the outset, I would love to acknowledge my research guide **Prof. Pitambar Pati** for his incomparable lead throughout the project from scratch. His peerless research discussion, time-to-time, and bit-by-bit research work monitoring and guidance, fieldwork inspection, motivation, and for a concerted attempt to read, re-read, editing and inputs in all chapters of my thesis.

The major work of this thesis was carried out with the help of **Prof. Shankar** (Mangalore University). Every aspect of paleoclimatic data interpretation was carried out with his guidance. His continuous support and discussion with my research work helped in gaining in-depth knowledge about paleoclimatic studies.

All my heartfelt gratitude for **Prof. Manoj Kumar Jaiswal** (Assistant Professor, IISER Kolkata) for his time, help and patience for OSL dating and fruitful discussion about geomorphological studies in my research work.

I want to express my thanks to **Dr. Pankaj Kumar** (IUAC) for his help in geochronological studies. His continuous guidance helped me in chronological data interpretation. I want to express my thanks to **Mr. Rajveer Sharma** (IUAC) for his help during laboratory analysis.

Secondly, I would take this opportunity to express my sense of obligation to my research committee members **Prof. Amit Kumar Sen** and **Dr. Debi Prasad Kanungo** who have coordinated timely progress of my Ph.D. research, constructive suggestions for the improvement of scientific communications, insightful comments and scientific inputs in the research from the beginning of this project. My sincere thanks for **Prof. Sunil Bajpai** (Head of Department) and other former HODs for all their support in official documentation and approvals.

Furthermore, I also thank all my research mates and colleagues who have been all-time associated with me in my six years stint in IIT Roorkee. I am indebted to **Kamlesh, Dr. Aditya Verma, Dr. Vijay Sharma, Ankit Gupta,** and **Narendra Patel** for helping me

in laboratory studies, manuscript preparations from editing to printing and their general support. Without their selfless assistance, it would not be possible to stay in Roorkee and conduct research for six years of life. I cherish all the light moments shared with **Ojha, Asit, Rajesh, Ratna, Jagannath**, **Dr. B.P, Dr. Behera, Dr. Ajit Behera , Dr, Ajit Sahoo and Dr. Khuntia** during my stay in Hostel.

Many thanks are owed to my parents and family who have given me life and made me what I am today.

Finally, I acknowledge MHRD for providing research fellowship, which financially helped to manage all my research expenditures.

Contents

Abstract i

Acknowledgment v

Contents vii

List of figures ix

List of Tables xiii

Chapter 1 INTRODUCTION 1

1.1 GENERAL DESCRIPTION OF THE STUDY AREA 1

1.1.1 Overview 1

1.1.2 Tectonic history 3

1.1.3 Climate 4

1.2 LITERATURE REVIEW 5

1.3 RESEARCH OBJECTIVES 10

1.4 SCOPE OF THE STUDY 12

Chapter 2 FLUVIAL RESPONSE TO QUATERNARY SEA LEVEL CHANGES ALONG THE MAHANADI DELTA, EAST COAST OF INDIA 15

2.1 INTRODUCTION 15

2.2 METHODOLOGY 25

2.2.1 Drainage morphology and Paleochannel identification; a remote sensing approach 26

2.2.2 Palaeochannels for OSL dating 27

2.2.3 OSL sample processing 28

2.2.4 Ground penetrating radar study 29

2.3 RESULTS 33

2.3.1 Fluvial response to sea-level changes 33

2.3.2 Litho-sections and OSL chronology of Holocene paleochannels 37

2.3.3 Paleo-coastal structures in GPR profiles 44

2.4 DISCUSSION 45

2.4.1 Fluvio-geomorphic changes along paleo-strandlines of Mahanadi delts 45

2.4.2 The anastomosing channels and its relation to sea-level change 46

2.4.3 River mouth shifts along transgressive coastlines 48

2.4.4 Dendritic channels along paleo-coastlines 49

2.4.5 Implications for coastal research 50

2.5 Summary 51

Chapter 3 PALEOCLIMATIC RECONSTRUCTION FROM LAKE SEDIMENTS ALONG MAHANADI DELTA **53**

3.1 INTRODUCTION 53

3.2 METHODS 56

3.2.1 Core collection 56

3.2.2 14C dating 57

3.2.3 Mineral Magnetic measurements 58

3.2.4 CHNS analysis 62

3.2.5 Carbon Isotope analysis 63

3.2.6 Spectral Analysis 63

3.3 PALEOCLIMATIC RECONSTRUCTION FROM ANSHUPA LAKE 64

3.3.1 Study Area 64

3.3.2 Results 65

3.3.3 Discussion 74

3.3.4 Summary 78

3.4 PALEOCLIMATIC RECONSTRUCTION FROM CHILKA LAKE 79

3.4.1 Study Area 79

3.4.2 Results 80

3.4.3 Discussion 85

3.4.4 Summary 88

Chapter 4 CONCLUSIONS **89**

References **93**

Appendix I **119**

List of figures

Figure 1.1 *Geomorphic belts in Mahanadi delta (modified after Mahalik, 2006).....2*
Figure 1.2 *Map showing drainage, landforms, and paleo-strandlines in the Mahanadi delta (modified after Mahalik, 2006). 3*
Figure 1.3 *Map showing distribution of basement faults in Mahanadi basin (Dasgupta et al., 2000). 4*
Figure 1.4 *Mean monthly precipitation data recorded at Naraj (India Water Portal, 1990-2002). 5*
Figure 2.1 *Fluvial response to base-level changes along the coast. (a) When base level increases, river bed aggrades and mouth shifts its position (b) Anastomosing and dendritic channels at the transgressive coastline. With regression, the anastomosing channels merge and form a single channel. The dendritic channels become abandoned at the coast (Modified after Schumm, 1993). 16*
Figure 2.2 *Examples of modern anastomosing rivers with cohesive vegetated banks. Aerial photographs from Google Earth (a) The Six Mile Creek in Alaska, USA (b) The Mississippi River near Keithburg in Illinois, USA (c) The Marmaris River in SW Turkey (d) The Ganga-Brahmaputra delta India. 17*
Figure 2.3 *Examples of modern dendritic channels at present-day coasts. Aerial photographs from Google Earth (a) West coast of North Korea (b) elongate dendritic networks reaching from the tidal flats onto the vegetated marsh, Wash (UK) (c) highly meandering dendritic network, Norfolk (UK) (d) a complex dendritic morphology, Tollesbury Marsh (UK) (d) Interconnected meandering dendritic channels, Santee River delta (e) elongated dendritic channels, Essex Marsh, Massachusetts (USA). ...18*
Figure 2.4 *Recent avulsion and flow direction change of the Yellow River mouth (Google Earth Images) (a) 1960 flow direction, (b) Present flow direction. 19*
Figure 2.5 *Incision of the river valley due to coastline regression followed by channel avulsion during transgression as shown in 3 stages a, b and c. 20*
Figure 2.6 *Fluvio-geomorphic features of Mahanadi delta. The paleo-strandlines are modified after Mahalik (2006). 21*
Figure 2.7 *Lithological cross-section from borehole cuttings, showing marine transgression and regression events in Mahanadi delta (after Mahalik, 2006). 21*
Figure 2.8 *(a) Sea-level changes during the Late Quaternary global oxygen isotopic stage. Adapted from Hope (2005) and Martinson et al. (1987). (b) Relative sea-level curve along Bay of Bengal coast of Bangladesh (adopted from Rashid, 2014) (c) illustration of relative sea-level change of east coast of India during Middle to Late Holocene (adopted from (Banerjee, 2000). 24*
Figure 2.9 *LANDSAT (TM) FCC (R:4 G:3 B:2) image of the Mahanadi delta, showing major rivers and paleo-swamps. 27*
Figure 2.10 *Anastomosing-meandering transition across the paleo-strandlines of Mahanadi delta. The channels show anastomosing pattern at transgressive strandlines and meandering patterns during a subsequent regressional phase. 34*
Figure 2.11 *River mouth shift of Bhargavi, Kuakhai, Brahmani and Baitarani rivers. The NW-SE flowing Bhargavi River flows E-W by shifting its mouth along the Late Holocene strandline. The paleo- and the present courses of Kushabhadra River have shifted 4 km in N-S direction, parallel to the Early Holocene strandline. The Brahmani*

and Baitarani rivers also show river mouth shift up to 7 km along the early Holocene strandline. 35
***Figure 2.12** Dendritic drainage patterns along the Holocene strandlines of Mahanadi delta. Different series of dendritic networks are developed in early and late Holocene strandlines.....37*
***Figure 2.13** Sampling sites for OSL dating. L1 (Bhailpur section), L2 (Brahmagiri section) and L3 (Purushottampur section) are from paleo-dendritic systems to SW of Chilka Lagoon; L4 (Alanda section) and L5 (Popora section) are from paleochannel of Kushabhadra River (see fig.7). L6 and L7 are from paleo-dendritic branches along Ersama swamp (see fig 4 and 6); L8 (Fakirdandy), L9 (Debichhaka), L10 (Olaghar) are from paleo meander scars of Brahmani and Baitarani rivers.....38*
***Figure 2.14** Lithosections at paleochannel trenching sites.....39*
***Figure 2.15** Plot of Sand, silt and clay percentage in the paleochannel sections.....40*
***Figure 2.16** (a) Plotted graph shows typical growth curves for (i) Alanda section and (ii) Popora section. (b) The distribution of equivalent doses (De) values for all samples presented with probability distribution curves. 41*
***Figure 2.17** GPR profile showing onlap and downlap structures between Early and Late Holocene strandline aalong Kushabhadra River. 44*
***Figure 2.18** Block diagrams showing representative anastomosing Meandering transition along Mio-Pliocene strandline. (a) The Mio-Pliocene coastline was transgressive and anastomosing channels developed at the interface of sea (b) with regression during Early to Up. Pleistocene times the anastomosing branches became abandoned and the Mahanadi River migrated towards the Early Pleistocene coastline (c) The present coastline position.....47*
***Figure 2.19** Anastomosing channels at paleo-coastlines observed in different deltas (images from Google Earth). (a) Danube Delta showing anastomosing meandering transition across Holocene coastline, paleocoastline redrawn after Panin, 2003; (b) Mississipi delta, paleocoastline redrawn after((Chamberlain et al., 2018; (c) Mekong Delta, paleocoastline redrawn after Thi Kim Oanh et al., 2002; (d) Krishna delta, paleocoastline interpreted from position of paleo-barrier spits (e) Mahakam delta, paleocoastline redrawn after Husein & J, Joseph, 2013; (f) Rhine delta, paleocoastline redrawn after Tornqvist, 1993.....48*
***Figure 2.20** Dendritic paleochannel systems along paleo-coastlines Yingee sea basin. Buried paleo-channels indicate that sea level remained for some time at the -50m (longest time here), -100m, and -130 to -140 m(lowest level) water depths, and that corresponding paleo-coastlines were formed at the respective depths (redrawn from Fan et al., 1990).....50*
***Figure 3.1 (a)** Locations of Anshupa and Chilka Lake along the Mahanadi delta, (b) and (c) field works during core collection with PVC pipe.....57*
***Figure 3.2** Automated Graphitisation Equipment at IUAC New Delhi.....58*
***Figure 3.3** Instrumentation for mineral magnetic measurements (a) Bartington Susceptibility Meter (b) Molspin pulse magnetizer (c) alternating field (AF) demagnetiser and an ARM attached (d) Molspin spinner fluxgate magnetometer. 60*
***Figure 3.4** Plot showing elemental and carbon isotopic composition of organic matter from marine algae, lacustrine algae, C3 and C4 land plants ((Meyers, 1994; Meyers and Lallier-vergés, 1999).....63*

Figure 3.5 *Geological map and coring site for Anshupa Lake . Redrawn after Sadangi and Mishra (2015).* *64*
Figure 3.6 *Bayesian Age model of Anshupa Lake core.* *66*
Figure 3.7 *Sedimentation rate in Anshupa Lake.Maximum sedimentation rate is found in post LIA (Little Ice Age) period and minimum sedimentation rate is found during LIA period.* *67*
Figure 3.8 *Mineral magnetic measurements of Anshupa Lake core.* *68*
Figure 3.9 *(a) χARM/SIRM vs Age plot showing dominance of bacterial magnetite towards lower end of core (b) χlf values plotted against date and (c) Corg (%) variation with age.* *69*
Figure 3.10 *(a) Bi-logarithmic plot of χARM/χlf and χARM/χfd. The samples with bacterial magnetite plots towards the upper right corner, while those with pedogenic origin plots towards the lower left corner of the graph. (b) The plot shows wide distribution of grainsize values, ranging from coarse SSD to SP grains.* *70*
Figure 3.11 *Down core variations of δ13C, C/N ratio, C%, and N %.* *71*
Figure 3.12 *Plot showing relation between χlf and d-TSI with at different periods. The variation trend in both the data sets show a positive correlation.* *71*
Figure 3.13 *(a) Various detrending curves applied to raw χlf data. (b) χlf values after detrended with r-LOWESS.* *72*
Figure 3.14 *Acycle screenshots showing application of Multi Taper Method.* *72*
Figure 3.15 *Results of spectral analysis showing periodicities in χlf values.* *73*
Figure 3.16 *Bi-logarithmic plot of χARM/χlf and χARM/χfd distinguishing between various sources of fine grained magnetite (after Oldfield, 2007).* *76*
Figure 3.17 *Study area and core location of Chilka Lake (Modified after Pandey et al., 2014).* *80*
Figure 3.18 *Radiocarbon Age modeling using BACON. Lightly shaded region represents likelihood, the dark shade represents more likely hood and the red line represents median age. Blue balloons indicate calibrated age with error bars.* *81*
Figure 3.19 *Sedimentation rate of Chilka Lake core.* *81*
Figure 3.20 *Mineral magnetic parameters of Chilka Lake sediments.* *82*
Figure 3.21 *Various detrending methods for spectral analysis.* *83*
Figure 3.22 *r-LOESS detrending on χlf values.* *83*
Figure 3.23 *Spectral analysis of χlf showing climate periodicities.* *84*
Figure 3.24 *Paleomonsoonal changes inferred from present study compared with regional paleoclimatic records during Holocene. After 1) Chauhan et al. (2004); 2)Chauhan and Vogelsang (2006); 3) Chauhan and Suneethi (2001); 4) Mathien and Bassinot (2008); 5) Chauhan et al. (2000a); Chauhan et al.,(2000); 6) Rashid et al. (2007); 7) Laskar et al. (2013); 8) Lückge et al. (2001); 9) Sarkar et al, (2000); 10)Thamban et al. (2002); 11) Sharma et al. (2006); 12) Saxena et al. (2013); 13) Alam et al. (2009); 14) Singh et al. (2007); 15) Enzel et al. (1999) 16) Patnaik et al. (2012) 17) Kuppusamy and Ghosh (2012); 18) Thamban et al. (2007); 19, 20, 21) Achyuthan et al. (.2014).* *86*
Figure 3.25 *Comparison of Magnetic susceptibility data with Historical settlements. (Historical settlement data obtained from (Giosan et al., 2017).* *87*

List of Tables

Table 1.1 Genetic landforms in the Mahanadi delta 1
Table 1.2 Generalised stratigraphy of Mahanadi delta (after Radhakrishnan, 2001) ...4
Table 2.1 Lithology from four representative boreholes to SW Mahanadi delta (Mahalik, 2000; 2006) 23
Table 2.2 OSL ages of paleochannel sections.....29
Table 3.1 Various mineral magnetic parameters and their use 60
Table 3.2 Radiocarbon dates for Anshupa core 66
Table 3.3 Radiocarbon dates used for age modeling 80

Chapter 1 INTRODUCTION

1.1 GENERAL DESCRIPTION OF THE STUDY AREA

1.1.1 Overview

The Mahanadi Delta is formed by the Mahanadi River and its distributaries at the interface of the Bay of Bengal, extending from Paradip in the East to Chilka Lake in the West (Fig. 1.1). This arcuate-shaped delta (Nayak et al., 2006) was developed along the Mio-Pliocene Sea due to the vast amount of sediments eroded from the Mahanadi-Gondwana basin (Mahalik, 2006). Radiocarbon dates reveal that the oldest fluvial deposits date back to 35,000 yrs BP (Mahalik, 2006). The continuous sedimentation since upper Pleistocene (>35,000 yrs BP) has modified the paleogeography and paleo-environments of the delta. Both marine and fluvial processes contribute substantially to redistributing the deltaic sediments. The delta prograded several times during the Pleistocene and Holocene (Mahalik, 2006, 1984) concealing paleo-landforms (i.e., paleochannels, paleo-beach ridges, dunes, and paleo-strandlines). Various types of fluvial, marine and aeolian landforms constitute the present-day delta morphology. These genetic landforms studied by Mahalik et al. (1996) based on satellite images are summarized in the Table 1.1.

Table 1.1 Genetic landforms in the Mahanadi delta

Agents	Features
1. Subaerial weathering	1. Laterites (i.e., Eastern-Ghats laterites and residual hillocks)
2. Fluvial	2. Braid bars, point bars, river terraces, flood plains, paleo drainage networks, swamps and bogs, ox-bow lakes
3. Marine and coastal processes	3. Beach, barrier spits, barrier islands, dunes, tidal flats and lagoons

The delta can be divided into two major parts, i.e. the upper deltaic plain and the lower deltaic plain, based on the fluvio-geomorphic features (Fig.1.1). The upper deltaic plain is predominantly evolved under a fluvial environment and formed in Early-Pleistocene time whereas the lower deltaic plain has several paleo-marine landforms indicative of marine transgressive and regressive events. Borehole cuttings reveal that sediments of marine origin underlie the lower deltaic plain (Mahalik, 2006).

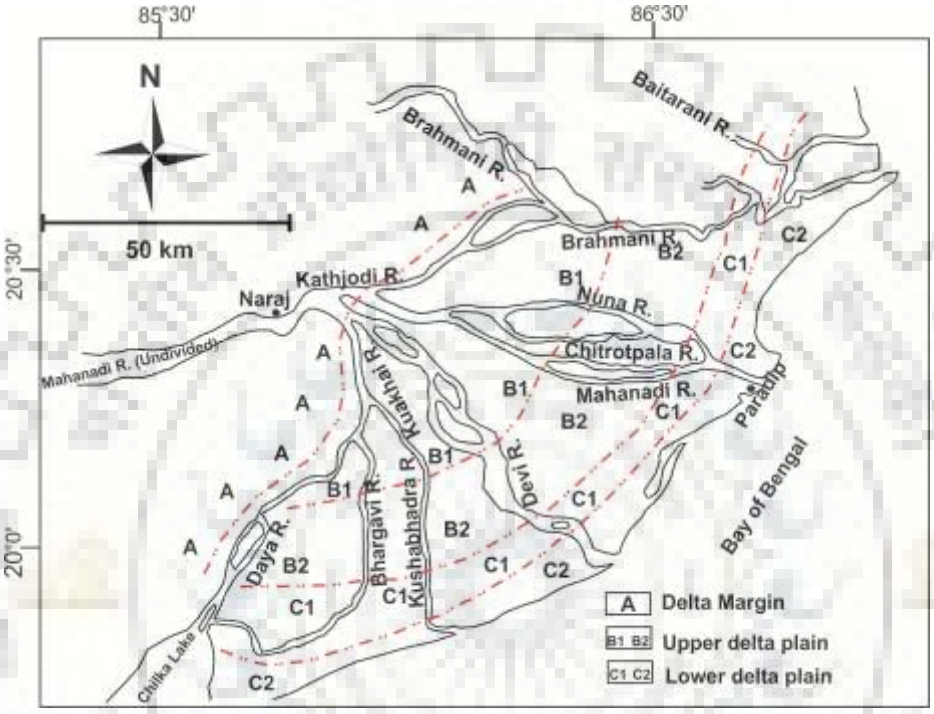

Figure 1.1 *Geomorphic belts in Mahanadi delta (modified after Mahalik, 2006).*

The upper deltaic plain is characterized by fanning distributary systems consisting of major rivers, namely Birupa, Mahanadi, Kathjodi, Debi, Brahmani, Bhargavi, Daya and Kuakhai.

The lower deltaic plain can be divided into two parts- (i) marginal part, which has many fluvio-marine features developed due to sediment redistribution by sea waves i.e. spits, barrier islands and ridges, and (ii) inland part, which is characterized by swamps, paleo-beach ridges, paleochannels, and aeolian dunes. Mahalik (2006) has suggested four stages of delta development owing to Pleistocene (> 30,000 to 10, 000 yrs BP) and Holocene (10,000 yrs BP to 5,000 yrs BP) transgression–regression events based on the distribution of paleochannels, paleo-beach ridges and borehole studies (Fig. 1.2).

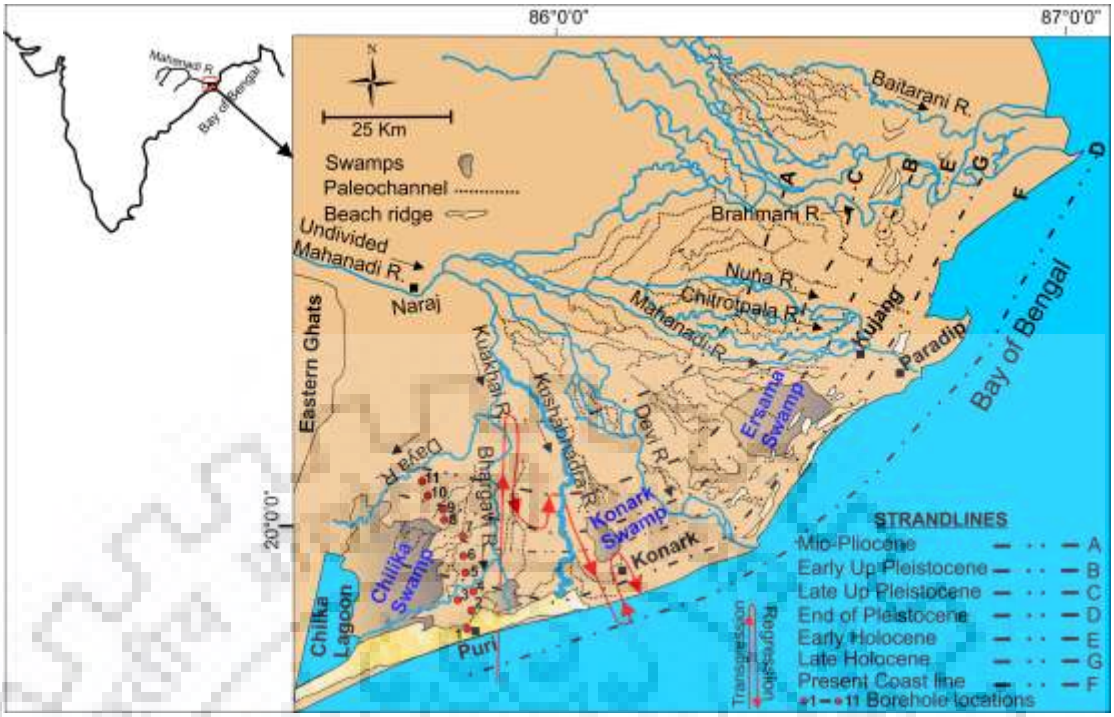

Figure 1.2 *Map showing drainage, landforms, and paleo-strandlines in the Mahanadi delta (modified after Mahalik, 2006).*

1.1.2 Tectonic history

The Mahanadi basin was initially developed from a graben, which is believed to be a failed arm of a triple junction resulting from the tectonic down wrap of the Gondwana plate (Burke and Dewey, 1973; Jagannathan et al., 1983). The plate containing India, Antarctica, and Australia drifted from the rest of the Gondwanaland during the Jurassic (Kaila et al., 1987; Larson, 1977, 1975; Markl, 1978; Ridd, 1971). Burke and Dewey (1973) suggested mantle plume type triple junctions, along which continents get separated. Four paleo-triple junctions have been identified along the east coast of India (Mahalik, 2000). The Bengal triple junction along the Ganga basin, the Cuttack triple junction along the Mahanadi basin, the Guntur triple junction along the Godavari basin and the Palk triple junction along the Cauvery basin. During the northward movement of the Indian plate, the east coast of India remained a passive margin, favoring stable-shelf sedimentation. Following the rifting of the Indian plate, pull apart basins developed along the eastern margin of India. Basement rocks of these basins have been characterized by several sets of faults (Dasgupta et al., 2000) (Fig. 1.3). As revealed from seismic surveys the coastal part of the Mahanadi basin shows sediment thickness of about 2400 m, implying continuous subsidence by the activity of growth faults (Mohanti and Swain, 2003). Throughout Quaternary, the shoreline has

moved seawards covering those growth faults (Bharali et al., 1991). The deltaic sediments of the basin range in age from Late Jurassic/Early Cretaceous to Recent (Radhakrishna, 2001). The general stratigraphy of Mahanadi delta has been summarised in Table 1.2.

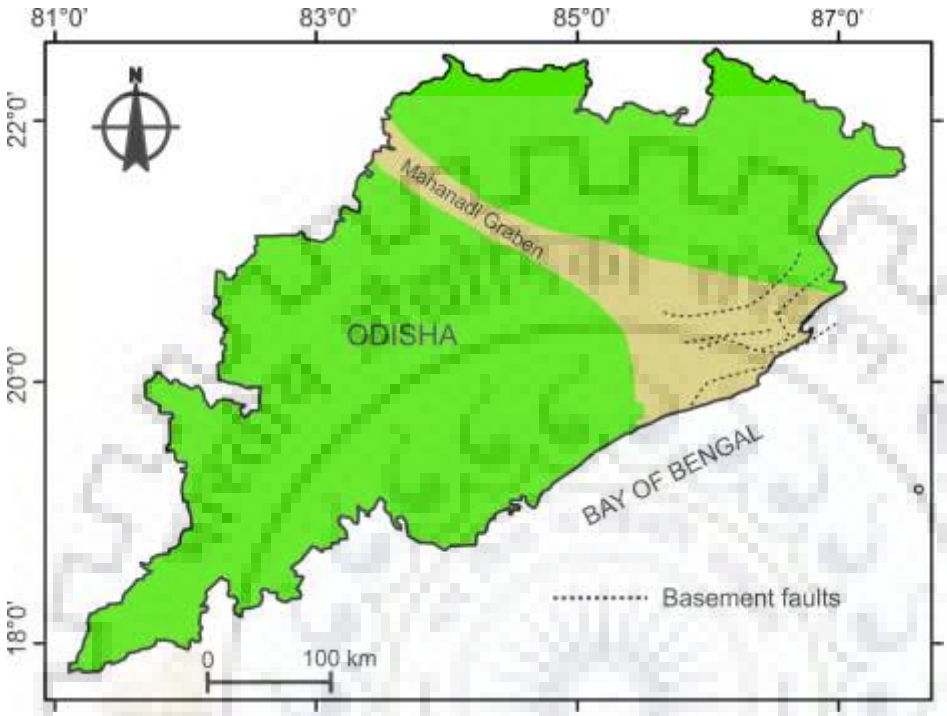

Figure 1.3 *Map showing the distribution of basement faults in Mahanadi basin (Dasgupta et al., 2000).*

Table 1.2 Generalised stratigraphy of Mahanadi delta (after Radhakrishnan, 2001)

Stratigraphy	***Lithology***
Iron ore series, Eastern Ghat series (basement rocks)	Amphibolites, quartzites, phyllites, feldspathic gneisses and charnockites
Jurassic	**Sandstones, grits, and conglomerates**
Plio-Miocene and Miocene	Bluish and brownish-gray clays, Grey sandy gravels with limestones
Alluvium and laterite	**Well-sorted sands, gravels, and clays with brown colorations**

1.1.3 Climate

The delta experiences a hot and humid tropical monsoonal climate. The average annual rainfall of the region is 1572 mm, and the sediment yield of the catchment varies from 200-400 tons/km (Meijerink, 1982). Nearly 70% of the precipitation occurs during Mid. June to Mid. October (Fig.1.4) by the southwest monsoon. An average annual

discharge of 48,691 million cubic meters of water has been recorded near the starting point of the delta at Naraj, mostly with a dominant monsoonal component of 41,000 million cubic meters. A monthly record of water discharge depicts a clear picture of the monsoonal/meteorological impact on water flow in the deltaic region (Fig. 1.4). The deltaic coast is micro-tidal with a mean tidal range of 1.29 m and experiences a semi-diurnal tidal cycle. During SW monsoonal time, the deltaic coast becomes wave-dominated, while in non-monsoonal seasons, it is mixed wave and tide-dominated. The northeast monsoon (between Decembers - early January) is much milder in its dynamic activity. Southwest monsoon winds generate high waves ~ 3m high or more and waves striking the shore obliquely induces a littoral / longshore drift of sands from southwest to northeast along this coast, which annually moves ~ 1.5 million cubic meters of sand in the nearshore regime.

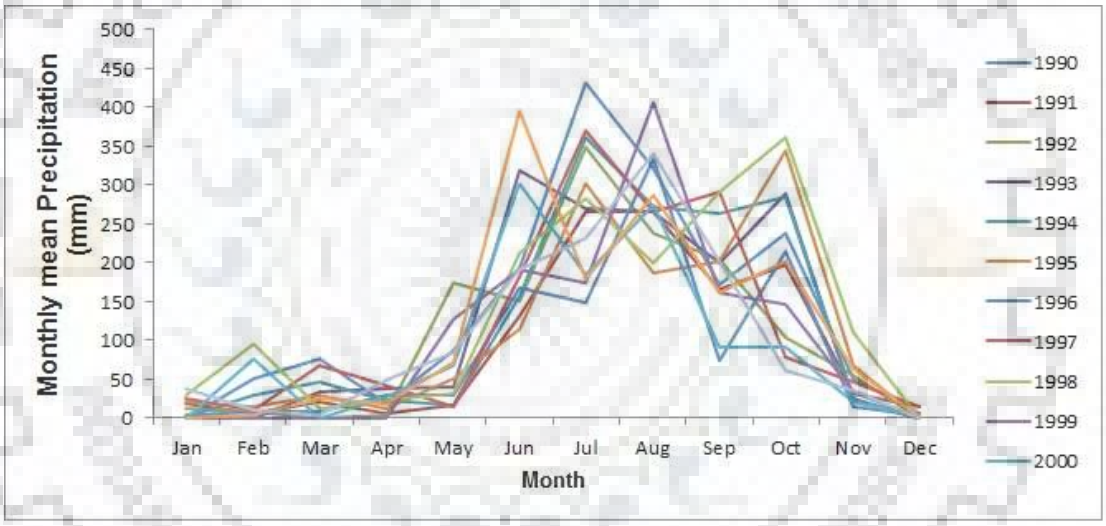

Figure 1.4 *Mean monthly precipitation data recorded at Naraj (India Water Portal, 1990-2002).*

1.2 LITERATURE REVIEW

Fluvial landscapes and deposits are important indicators of Quaternary paleo-geomorphic changes, and the associated alluvial strata provide information about sedimentary successions in changing environmental conditions. River deltas are formed at the interaction zone of multiple geomorphic agents, like fluvial, marine, aeolian, and sub-surface tectonism. Hence the deltaic landforms are prone to dynamic surface and sub-surface processes. Moreover, the study of long-term fluvial successions in deltaic environments is important to understand the control of external or 'allogenic' agents in shaping the delta. The present study area of Mahanadi delta is situated in the passive

eastern margin of the Indian subcontinent; hence tectonic activities have less role in modifying the delta geomorphology. Along all the other major deltas of India, no previous studies have reported any tectonic activity controlling the fluvial geomorphology. The eastern continental margin has remained passive since Quaternary; hence we rule out any major tectonic disturbances controlling the geomorphology of the coast. The dominant forces controlling geomorphology of peninsular India, especially the coastal India, are fluvial, marine and the climatic. Several concepts on fluvial response to climate and sea-level change from the early 1900s have provided a key role in understanding fluvial morphology in deltaic environments. Powell (1875) defined the concept of base-level as the lower limit to which rivers can erode, equivalent to the mean sea level. Penck and Brückner (1909) linked incision of the river valley to interglacial periods and sediment aggradation to glacial periods. Fisk (1945) suggested that during sea-level regression valley incision, terrace formation and abandonment of flood plain occurs in the fluvial systems, while during transgression, river valley aggradation takes place. Upstream agents mainly control fluvial morphology in continental interiors (Butzer, 1980; Coleman, 1988; Leopold and Maddock, 1953; Schumm, 1968; Schumm, 1985; Schumm and Schumm, 1998). Many of these studies reflected that climate-induced sediment discharge controlled river morphology in continental interiors. At the continental margins, fluvial discharge is dominated by eustatic sea-level changes, which is an indirect outcome of climate change. Fisk (1945) investigated the Lower Mississippi valley and correlated changes in stream gradients to glacio-eustatic changes. According to Fisk, the Mississippi River valley was deeply eroded and incised during the lower sea level. Braided channels developed during the interglacials, the period of higher sea levels. Apart from Fisk's model, many conceptual and experimental models were developed during the 1990's to characterize fluvial response to base-level changes at continental margins. Along continental margin environments, upstream controls on fluvial morphology are negligible with comparison to sea-level changes (Begin, 1988; Begin et al., 1981; Leopold and Bull, 1979; Leopold and Maddock, 1953). Brown et al. 1988 and Leckie (1994), studied the Canterbury plains and correlated river gradient to sea-level changes. Aggradation or degradation of the river profile depends on the direction of base-level change. Apart from the direction of change, the rate of change is also important. If base level change is fast, vertical erosion will be greater than lateral erosion. Whereas when the change is slow, lateral erosion is more than vertical erosion

(Wood et al., 2009; Yoxall, 1969). The duration of base-level change is more important than magnitude and the rate of change. The rate of base-level change is slow if the duration is long and vice versa. Examples of effects of sea-level change on fluvial morphometry in coastal zones are further discussed and illustrated in chapter 2.

The second objective of the present study is to investigate paleoclimatic signatures from Mahanadi delta sediments. Mahanadi delta is situated in the core monsoon zone of India, affected by SW Indian monsoon. Though Quaternary climatic reconstruction has been carried out along many lakes and sediment profiles of the Indian subcontinent, no significant study has been carried out yet along the Mahanadi basin. Previous studies have been mainly carried out along the continental margins of India i.e. from Bay of Bengal or Arabian Sea sediments. Investigation of Inland lakes has been mainly restricted to the Himalayan terrain. The climatic condition of Mahanadi delta is mainly affected by fluctuation in SW Indian monsoon. During SW summer, monsoon winds drive intense upwelling along the coasts of Somalia and Oman, and sporadic upwelling along the western coast of India (Wyrtki, 1973). The upwelling rates are related to the strength and intensity of SW Indian monsoon. The abundance of specific flora and fauna depends upon the upwelling rate along the continental boundaries, which are eventually settled with the sediments and preserve records of paleoclimate. Increased upwelling rate around 12 ka BP indicates an intensification of SW Indian monsoon and, this is correlated with increased discharge of glacial meltwater in the northern hemisphere (Fairbanks, 1989) and increase in solar insolation (Berger, 1978). The paleo-monsoon in South East Asian region was weakest about 15 ka BP. During the post LGM period (17ka – 13ka) the Asian region showed a strengthening of Indian Summer Monsoon.

The period from 13 ka to 8 ka had intensified monsoon with maximum upwelling during Holocene, and this period coincides with highest lake levels in Africa, India and other Asian continents (Bera and Farooqui, 2000; Divakar Naidu, 1995; Naidu and Malmgren, 1996; Rajagopalan et al., 1997; Sandeep et al., 2015; Street and Grove, 1979). The Nilgiri hills show a dominance of C3 type of vegetation during 9 ka BP, which supports a high precipitation phase during the early Holocene period (Rajagopalan et al., 1997). Sandeep et al. (2015) showed high magnetic parameters and low carbonate content during the early Holocene, supporting the view of intense precipitation during Early Holocene. Weakening of SW Indian monsoon started after 5

ka BP, with the weakest phase around 3.5 ka to 1 ka BP (Gasse and Van Campo, 1994; Nigam, 1993; Nigam and Khare, 1992). Others recorded the weakest monsoon phase during 4 ka BP (Anoop et al., 2013; Prasad et al., 1997, 2014; Saxena et al., 2015; Saxena and Singh, 2017). The onset of the arid phase at about 3.5 ka BP had two major impacts on the Indian subcontinent, one was the adverse impact on Indus valley civilization and the other was the drying of Saraswati River. Paleoclimatic records for the past 2 ka years in peninsular India indicate moderate to high rainfall, with intermittent dry phases. Yadava and Ramesh (1999) recorded an intense monsoon phase during 1666 AD. Warrier et al. (2017) studied magnetic susceptibility of lake sediments and found periodic cyclicity of ISM during LIA. Comparison of climatic fluctuations in high and low latitude areas of Africa, Asia, and Australia indicates that common factors have controlled the climatic changes during Holocene (Fairbanks, 1989). Milankovitch (1930) proposed that the Quaternary glacial and interglacials are associated with solar insolation and suggested that comparison of paleoclimatic records showed climatic periodicities at 100 ka, 41 ka, and 23 ka, which are related to changes in Earths eccentricity, obliquity, and precession.

So far, paleogeographic and paleoclimatic studies on Indian deltas are concerned few studies have been carried out to date along the Eastern coast of India. A brief discussion of past studies on Indian deltas is presented below.

Bengal Delta: The evolution of Modern Bengal delta has been studied in many previous works based on channel morphology, geomorphic features in LANDSAT images, and lithological changes (Curray and Moore, 1971; Ganju et al., 1982; Morgan and McINTIRE, 1959; Vaidyanadhan, 1991). Initial phases of delta formation started during the low sea level phase during Wisconsin sea level lowering. During the low sea stand, the rivers eroded their valleys to reach the exposed shelf region. The second phase of delta development occurred during the Flandrian transgression phase. The river valleys were drowned and branching of river channels occurred due to riverbank instability. Estuarine type environments developed at river mouths. The River Ganga gradually shifted eastward, leaving behind the abandoned delta plains to the west. The older deltaic plains are marked with abandoned channels, paleo ridges, and point bars.

Subarnarekha Delta: Between macrotidal Hoogly estuary and compound deltas of Mahanadi River, the mesotidal Subarnarekha delta is situated along the

Balasore coastal plain of Odisha. The delta plain has successive rows of sandy paleo-beach ridges, separated by intervening clayey deposits. These sandy paleo beach ridges are indicative of punctuations in Holocene sea-level regression (Niyogi, 1971, 1970). 14C dating of dune sediments shows that Holocene strandline was around 6 ka B.P. and the next regression punctuation was around 3 ka B.P. The 6 ka transgression corroborates with Flandrian transgression phase (Selby, 1985).

Godavari Delta: Four stages of delta evolution have been studied in previous works (Babu, 1973; Krishna Rao, 1990; Mahadevan, 1958; Rao, 1979; Sambasiva Rao, 1987, 1979). Based on fluvial morphology and paleo-marine features, authors have classified the delta into several progradational sequences. Krishna Rao (1990) dated the four paleo-sand ridges of Krishna delta, which are a continuation of Godavari delta ridges. The ages were 6500, 4500, 3250, and 2450-2150 years BP respectively, with youngest towards present-day coast. Paleo-distributaries characterize the paleo-lobes of the delta with sand at the bottom of clay deposits, which indicate that the channels were exhumed with successive phases of delta development. Massive sand deposits characterize the progradational boundaries of delta beneath the clay, which are indicative of paleo-coastline. Based on ages and paleo-morphologic features, it can be concluded that the delta prograded throughout the Holocene towards the present coast.

Krishna Delta: The geological evolution of Krishna delta took place in five stages, continuously with falling sea level during Quaternary (Babu, 1973, 1975; Krishna Rao, 1990; Nageswara Rao, 1987; Rao, 1985). Paleo-beach ridges and tidal flat deposits mark the paleo-strandline positions. These paleo-fluviomarine features show a parallel trend, indicating migrating shoreline. Paleo-deltaic lobes presently represented by paleochannels end abruptly along the paleo beach ridges. These distributary lobes formed as the delta debouched sediments into the sea. The relative quantity of lobes varied between the starting and debouching points of the delta. The oldest beach ridge dated was ~7 ka BP. This indicates that the delta prograded continuously during the Holocene.

Cauvery Delta: The entire delta of the Cauvery River is abandoned except the northern lobe (Ramasamy et al., 1987). The southern lobe of the delta has paleochannels, which show continuous shifting towards the north. This indicates that the Cauvery River mouth has shifted northward, leaving behind its paleo-distributaries.

Lineaments trending N-S, NE-SW and NNE-SSW dissect the deltaic plain into many geomorphic zones (Raiverman et al., 1966; Ramasamy, 1992). The Cauvery delta also has many ENE-WSW trending magnetic lows, which indicate the presence of many grabens/depressions. The sediment thickness along these depressions is much greater than in other parts of the delta.

Other studies along the coastal zones of India indicate a similar phenomenon of fluvial channel evolution with changing sea levels during Holocene. Many small deltas along the eastern coast have migrated their deltaic lobes with continuous progradation of the delta due to falling sea level during Holocene (Vaidyanadhan, 1991; Vaidyanadhan and Ghosh, 1993).

1.3 RESEARCH OBJECTIVES

Though Mahanadi delta is situated in the core monsoon zone of India and the delta building activity is governed by dynamic geomorphic processes, very little attention has been given to understand past sedimentological and climatic records from its sedimentary architecture. Previous studies have focused on past marine transgression and regression records, while other major geomorphic attributes have not been taken into account. Drainage morphological changes, paleo-marine features, and fluvial-marine interaction zone facies changes have not been studied in detail. Also, past climatological studies in the delta are lacking. The present study deals with understanding two major aspects of delta geology i.e. the paleo-geomorphological changes in response to fluvio-marine interaction and the paleo-climatological studies to understand high-resolution paleo-monsoonal variations in central monsoon zone of India.

Previous studies on fluvial response to base-level changes are mostly laboratory-based and very few investigations in deltaic areas have been carried out till now (Begin et al., 1981; Koss et al., 1994; Makaske, 2001; Nelson and Maldonado, 1988; Schumm, 1993; Wood et al., 2009; Xue, 1993). The Mahanadi delta is developed by the contribution of several tributaries and distributaries of Mahanadi River, which have been modified by different fluvio-marine geomorphic processes since the inception of the delta. The present fluvial morphological features of the Mahanadi delta region are the result of past environmental settings to which the delta was exposed. Mahalik (2006) has studied multiple transgression and regression phases in the

Mahanadi delta. During transgression, the delta prograded, while during regression, the delta retreated. The transgression and regression events not only change the sediment delivery of the fluvial systems but also change the fluvial channel morphology (Makaske, 2001; Torbjorn E Tornqvist, 1993a). Evidence of these changes is preserved in the inner deltaic region as paleo-geomorphic features. The present study aims to correlate these paleo-fluviogeomorphological evidences with transgression and regression events. To understand paleo-geomorphological processes, detailed channel morphological and chronological studies are to be carried out in the present study. Previous studies indicate that drainage morphologic changes like anastomosing-meandering transitions, river mouth shifts, the occurrence of dendritic drainage patterns and paleo-river cut-offs are some of the fluvio-geomorphic features indicative of base-level change (Dominguez et al., 1987; Schumm, 1993; Torbjorn E. Tornqvist, 1993). These geomorphic features owe their individual genetic history and give insight into delta evolution in spatial and temporal scales. The present study aims to correlate the paleo-channel morphological changes with transgressive and regressive events along the Mahanadi River delta. An integrated approach combining remote sensing, field-based fluvio-marine facies study, and chronological studies would help in understanding the processes that controlled paleo-fluvial geomorphology of the Mahanadi delta.

The second objective of the study is to reconstruct the paleoclimatic history of the Mahanadi delta region. As the Mahanadi delta is situated in the core monsoon region of the Indian subcontinent and is directly influenced by Indian Summer Monsoon, a high-resolution paleoclimatic study will reveal past monsoonal fluctuations in the Indian subcontinent. Since the Mahanadi delta region is influenced by both marine and fluvial processes, the present study aims at understanding the influence of ISM on sediment depositional environment of both fluvial and marine-influenced systems. To fulfill above objective sediment cores from a freshwater lake (Anshupa Lake) and a brackish water lake (Chilka Lake) along Mahanadi delta has been used for paleoclimatic reconstruction. Further, paleoclimate of the Mahanadi delta region would be correlated with paleogeography and paleogeomorphology. Various paleoclimatic proxies like environmental magnetism, stable isotopic records, and organic carbon variations are to be used to infer past monsoonal changes. Environmental magnetism is a great tool for paleo-monsoonal reconstruction as the measurement process is rapid

and non-destructive. These environmental parameters can be directly related to paleo-precipitation (Shankar, 2006; Warrier et al., 2017). The elemental and isotopic record of organic carbon fluctuations indicates vegetation dynamics, which in turn depends upon monsoonal changes. A stable isotopic record of organic carbon and carbon to nitrogen ratio is to be used for the present study to infer past monsoonal dynamics. The ^{13}C record in combination with C/N ratio has been used as a climatic proxy in various past investigations around the world. Indian east coast encompasses good vegetation dynamics which have been studied in many previous investigations (Das and Samal, 1998; Pandey et al., 2014). These vegetational ecosystems are monsoon-fed and proliferation or decline in the vegetation history is subject to larger/ smaller monsoonal fluctuations.

1.4 SCOPE OF THE STUDY

The present study deals with two broad research objectives in the Mahanadi delta region, i.e. to study fluvial response to Quaternary sea-level changes and paleoclimatic reconstruction from Mahanadi delta sediments. Previous studies on fluvial response to sea-level changes were mostly based on laboratory experiments, and only a few field studies have been carried out. The laboratory experiments have not been applied to field-based observations. The present study is mostly focused on the application of past fluvio-geomorphic concepts at land-ocean interaction zones. The Mahanadi delta owes its unique position to study fluvial geomorphology as it is influenced by various geomorphic agents such as fluvial, marine and aeolian. Application of geomorphic concepts to study channel morphologic changes in such multi-environmental regions would add to a better understanding of the impact of different geomorphic agents and the dominant force. Past studies on the evolution of Indian deltas are mostly based on satellite imagery and do not encompass any field-based observations, nor any detailed sequence of events controlling evolutionary history have been carried out. The present study on the fluvial channel morphology of the Mahanadi delta region would be first of its kind on Indian deltas and will have a deeper understanding of geomorphic processes in the deltaic environment.

The second objective deals with the paleoclimatic reconstruction of the Mahanadi delta region. The Mahanadi delta is situated in the core monsoonal region of India, affected by SW Indian monsoon. The delta is composed of many geomorphic

features that record past climatic signatures. However, no past studies on paleoclimatic reconstruction have been carried out in this region. Two major lakes in the Mahanadi delta region, i.e. Chilka Lake (brackish water lake, connected to sea) and Anshupa Lake (a freshwater lake), are suitable sites to study paleoclimatology. This study will differentiate the preservation potential of paleoclimatic records in marine and freshwater environments. The Chilka Lake is one of the largest brackish water lakes in Asia, influenced by the southwest Indian Monsoon and derives its sediments from Eastern Ghat rocks. The lake has been affected by several episodes of sea-level changes due to its position marginal to coast. Hence, the sediment profile of the Chilka Lake will provide evidence of past episodes of sea-level fluctuations and the influence of ISM on sedimentation history. Anshupa Lake is one of the largest freshwater lakes in the Odisha state. It is situated in the upper deltaic region and its horseshoe shape indicates an oxbow lake type origin. Further, it is bounded by Athgarh hills, limiting its catchment area to a few kilometers surrounding the lake. Hence, the Anshupa Lake sediments will give evidence of the only catchment derived sedimentation history and associated condition that led to its separation from the Mahanadi River.

Chapter 2

FLUVIAL RESPONSE TO QUATERNARY SEA LEVEL CHANGES ALONG THE MAHANADI DELTA, EAST COAST OF INDIA

2.1 INTRODUCTION

Studies around the globe have documented several fluvio-geomorphic modifications in response to base-level changes; such as transformation of single-channel to anastomosing channels (David Knighton and Nanson, 1993; Tornqvist, 1993b; Makaske, 1998; 2001), generation of dendritic drainage pattern (Ren and Shunan, 1990; Schumm, 1993; Xue, 1993) and lateral shift of river mouth at sea-land interface (Eisma, 1998; Hughes, 2012; Schumm, 1993). These channel morphological changes are preserved in the sedimentary record as paleochannels, and their morphology indicates the associated environmental condition. Transgressive coastlines cause river anastomosis due to aggradations at the river mouth and these anastomosing branches coalesce to form straight/meandering channels at the lower slope when sea level retreats (Makaske, 1998; McIntosh, 1983; Walker and Coleman, 1987). River mouth shifts are the result of avulsion like processes nearer to coast. Rise in relative sea-level drowns the river mouth, diminishing its sediment transporting efficiency. The streams adjust to the increased sediment load through avulsion (Ren and Shunan, 1990; Schumm, 1993; Xue, 1993). Dendritic drainage networks are formed when flow concentrates near coastal areas due to lower slope (Schumm, 1993); hence paleo-dendritic branches along different strandlines are indicative of paleo- coastline position (Fig. 2.1).

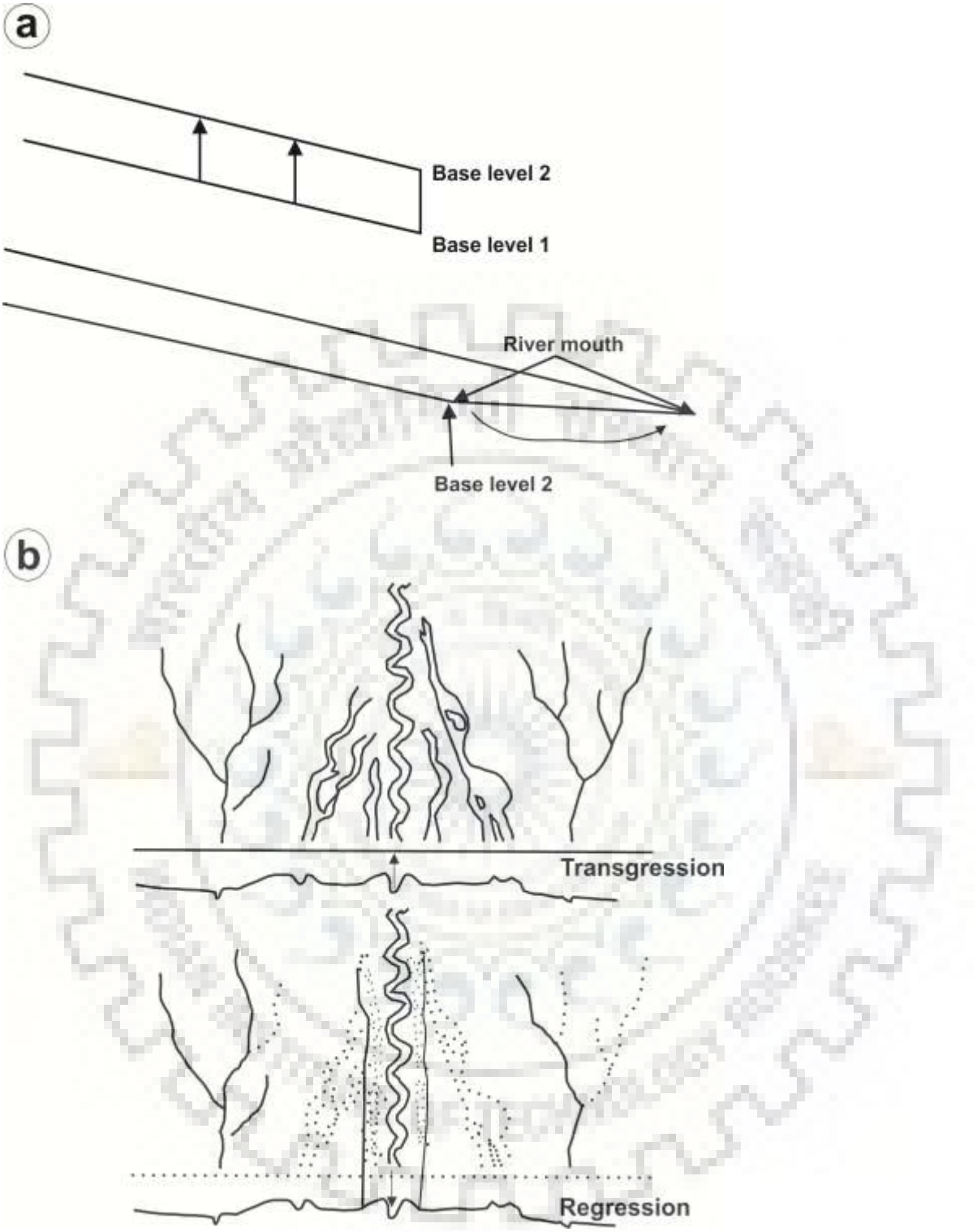

Figure 2.1 *Fluvial response to base-level changes along the coast. (a) When base level increases, river bed aggrades and mouth shifts its position (b) Anastomosing and dendritic channels at the transgressive coastline. With regression, the anastomosing channels merge and form a single channel. The dendritic channels become abandoned at the coast (Modified after Schumm, 1993).*

Near to present-day coastlines, due to the high sedimentation rate and sea-level rise, many such channel modifications are observed worldwide. Anastomosing

channels developed due to channel aggradation are found in the vicinity of many present-day coastal environments (Fig. 2.2).

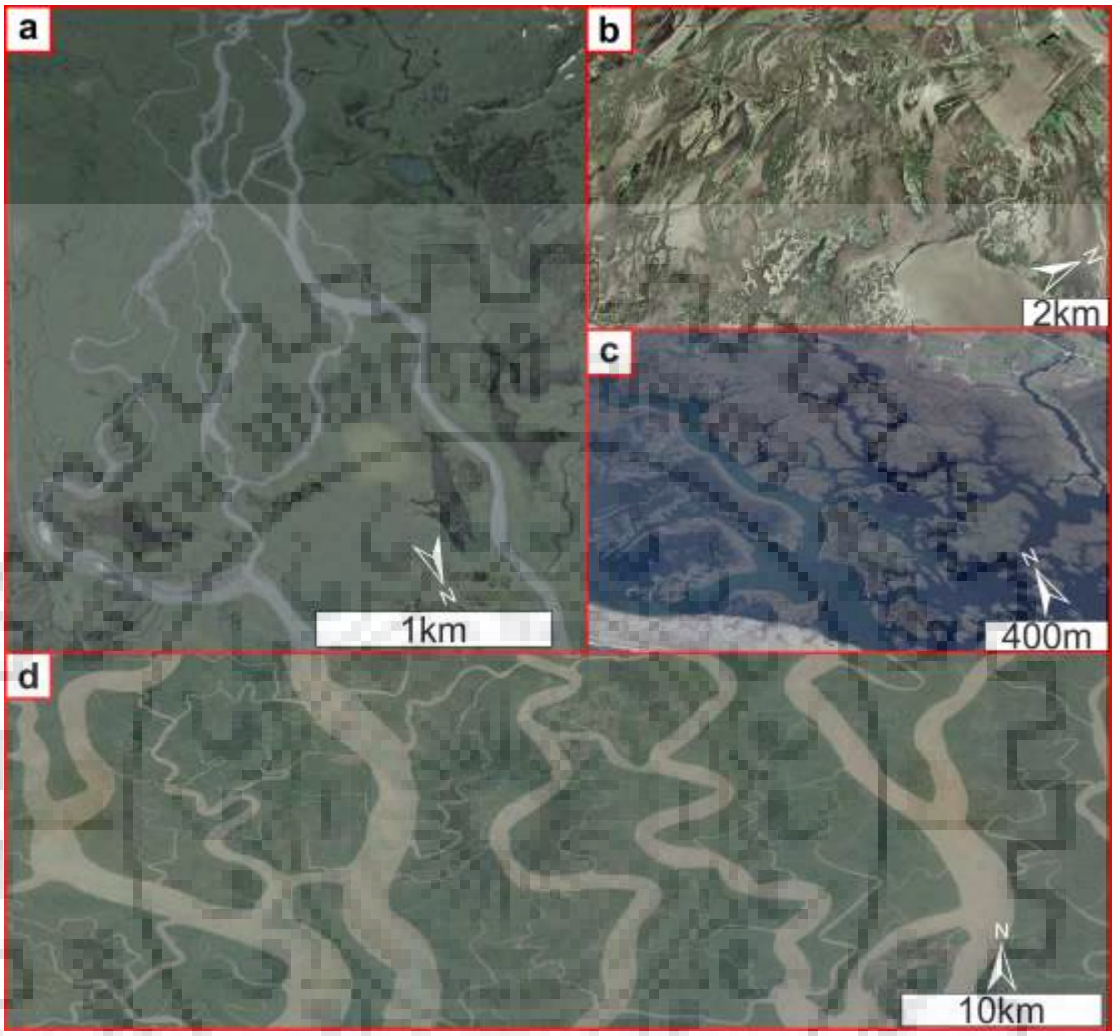

Figure 2.2 *Examples of modern anastomosing rivers with cohesive vegetated banks. Aerial photographs from Google Earth (a) The Six Mile Creek in Alaska, USA (b) The Mississippi River near Keithburg in Illinois, USA (c) The Marmaris River in SW Turkey (d) The Ganga-Brahmaputra delta India.*

Occurrence of coastal zone dendritic channels and river mouth shifts associated with marine transgressional events are common fluvio-geomorphic features observed along major deltaic systems. Dendritic channel networks are commonly observed along tidal flats and salt marshes (Fig. 2.3).

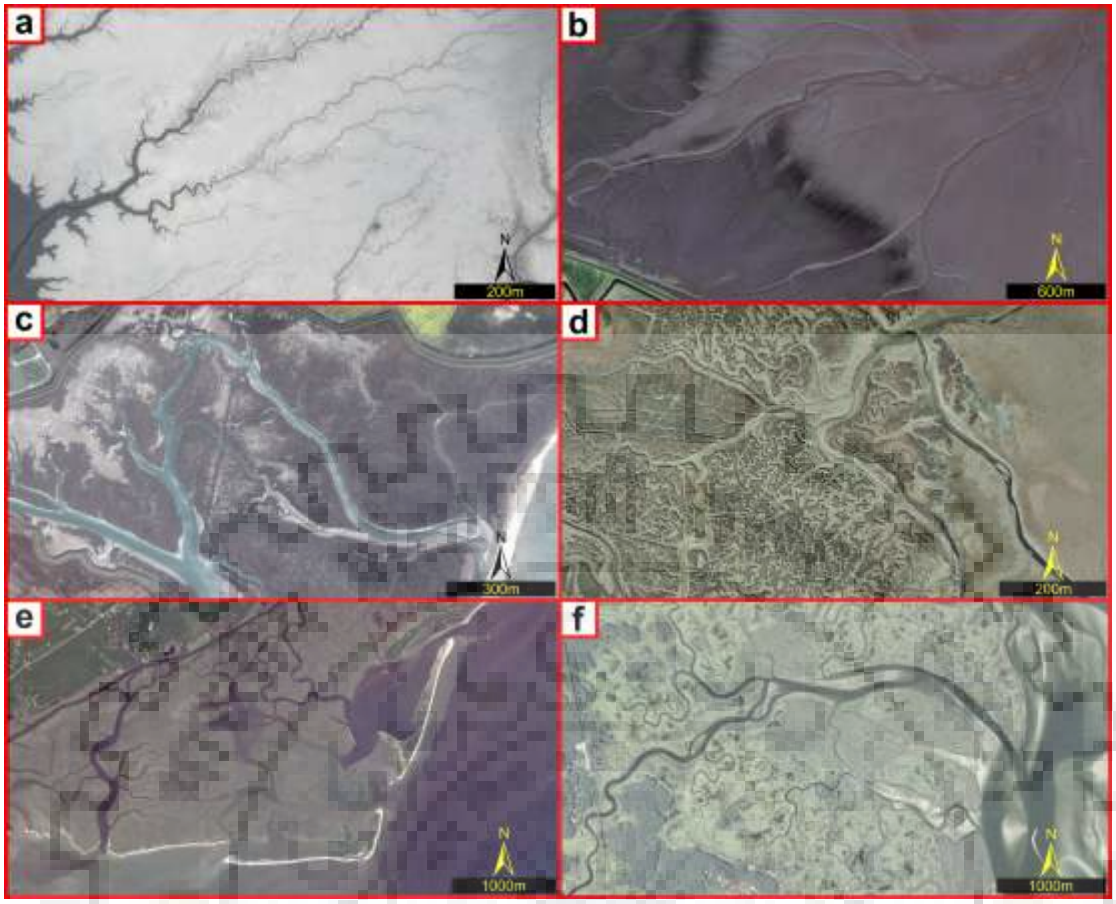

Figure 2.3 *Examples of modern dendritic channels at present-day coasts. Aerial photographs from Google Earth (a) West coast of North Korea (b) elongate dendritic networks reaching from the tidal flats onto the vegetated marsh, Wash (UK) (c) highly meandering dendritic network, Norfolk (UK) (d) a complex dendritic morphology, Tollesbury Marsh (UK) (d) Interconnected meandering dendritic channels, Santee River delta (e) elongated dendritic channels, Essex Marsh, Massachusetts (USA).*

One of the major examples of river mouth shift is the Yellow River mouth, which has shifted SW-NE from the past NW-SE direction due to avulsion at present-day coastline (Fig. 2.4).

Figure 2.4 *Recent avulsion and flow direction change of the Yellow River mouth (Google Earth Images) (a) 1960 flow direction, (b) Present flow direction.*

These morphological changes near to the present-day coasts are examples of fluvio-geomorphic modifications at sea-land interaction zone. Paleochannels showing such fluvio-geomorphic features are indicative of the paleo-coastline position. With retreat in sea level, larger channels incise through the bed-rock to adjust slope change. Smaller channels along the coast are either captured by large rivers or become abandoned, as they have very low incision capacity to adjust the slope change (Fig. 2.5) (Colman and Mixon, 1988; Leigh and Feeney, 1995; Mixon, 1985; Reineck and Singh, 2012). Thus, a chronology of paleochannels showing morphological features indicative of sea-level changes is useful in deciphering the paleo-coastline position. Previous studies (Barnhardt et al., 1997; Colman and Mixon, 1988; Koss et al., 1994; Leigh and Feeney, 1995) have mentioned Spatio-temporal correlation between coastal zone paleochannels and sea-level changes.

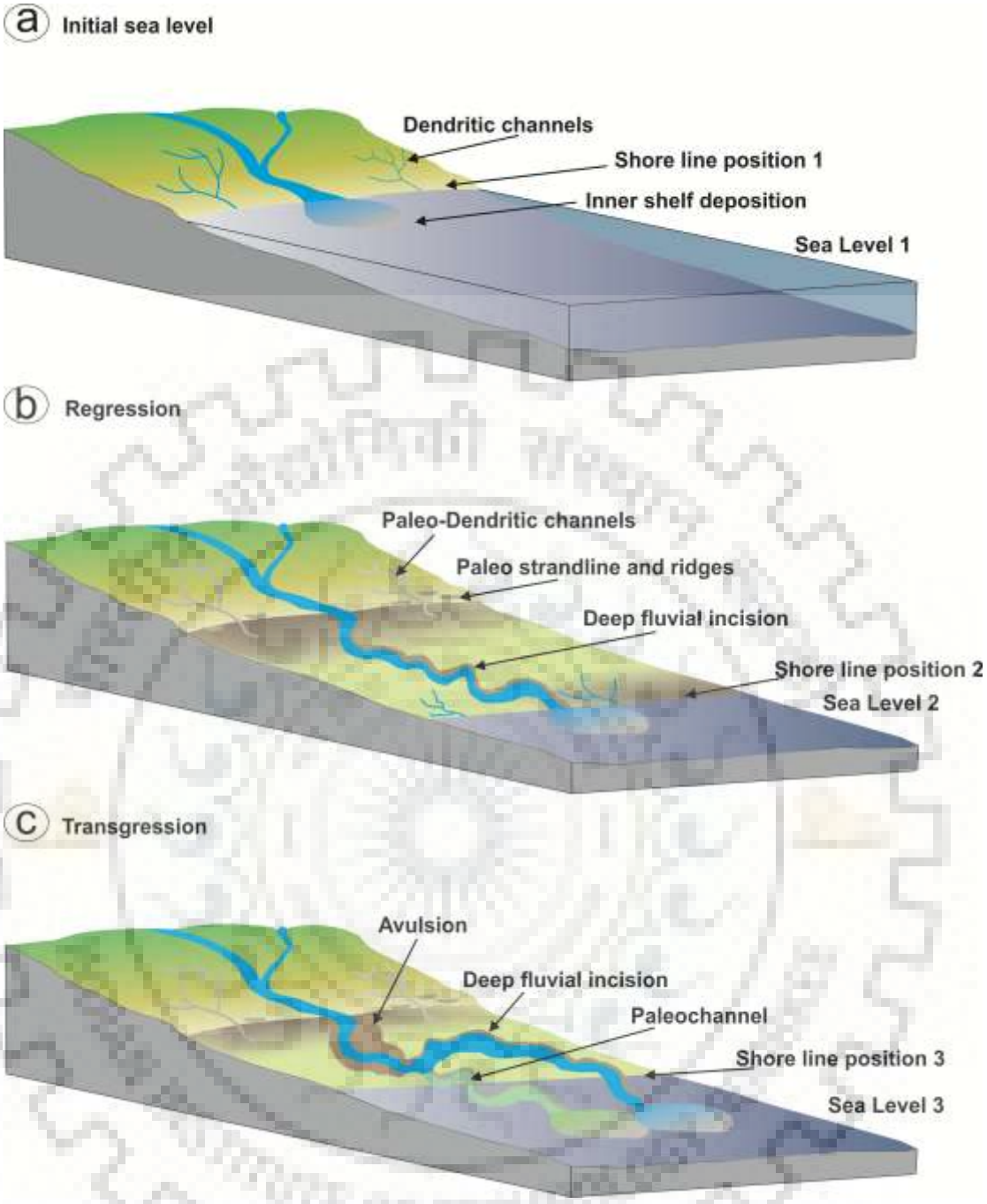

Figure 2.5 *Incision of the river valley due to coastline regression followed by channel avulsion during transgression as shown in 3 stages a, b and c.*

Mahalik (2000;2006) suggests four stages of Mahanadi delta development and strandline positions, using facies variations and fossils assemblage from borehole cuttings (Fig. 2.6 and 2.7).

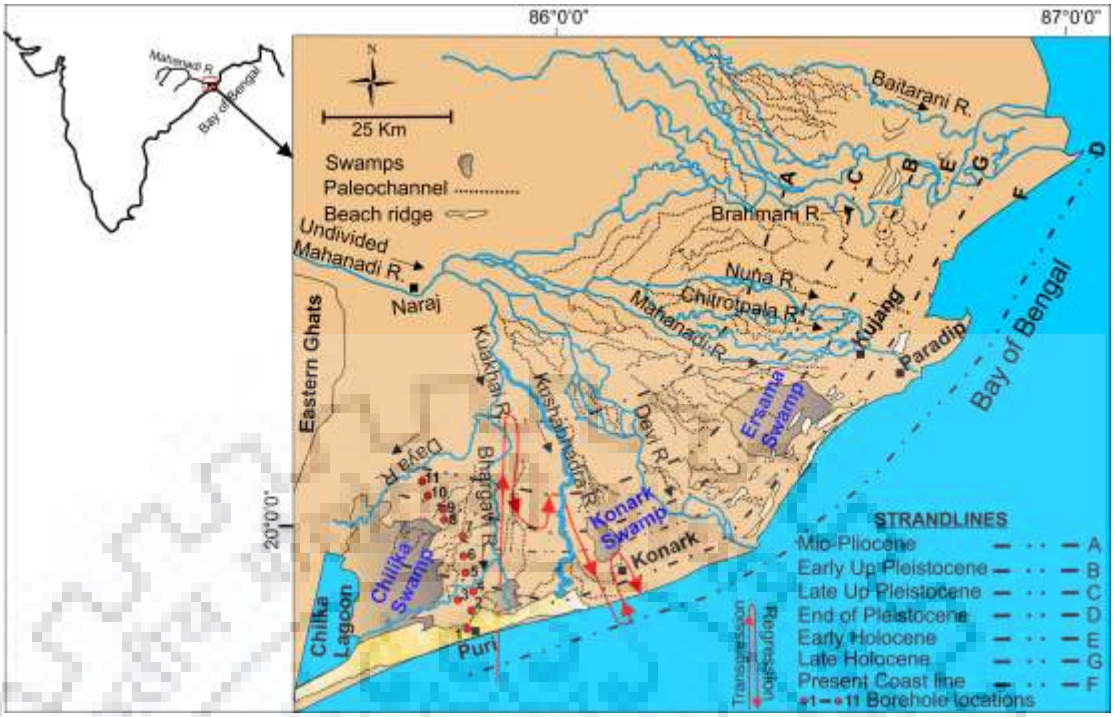

Figure 2.6 *Fluvio-geomorphic features of Mahanadi delta. The paleo-strandlines are modified after Mahalik (2006).*

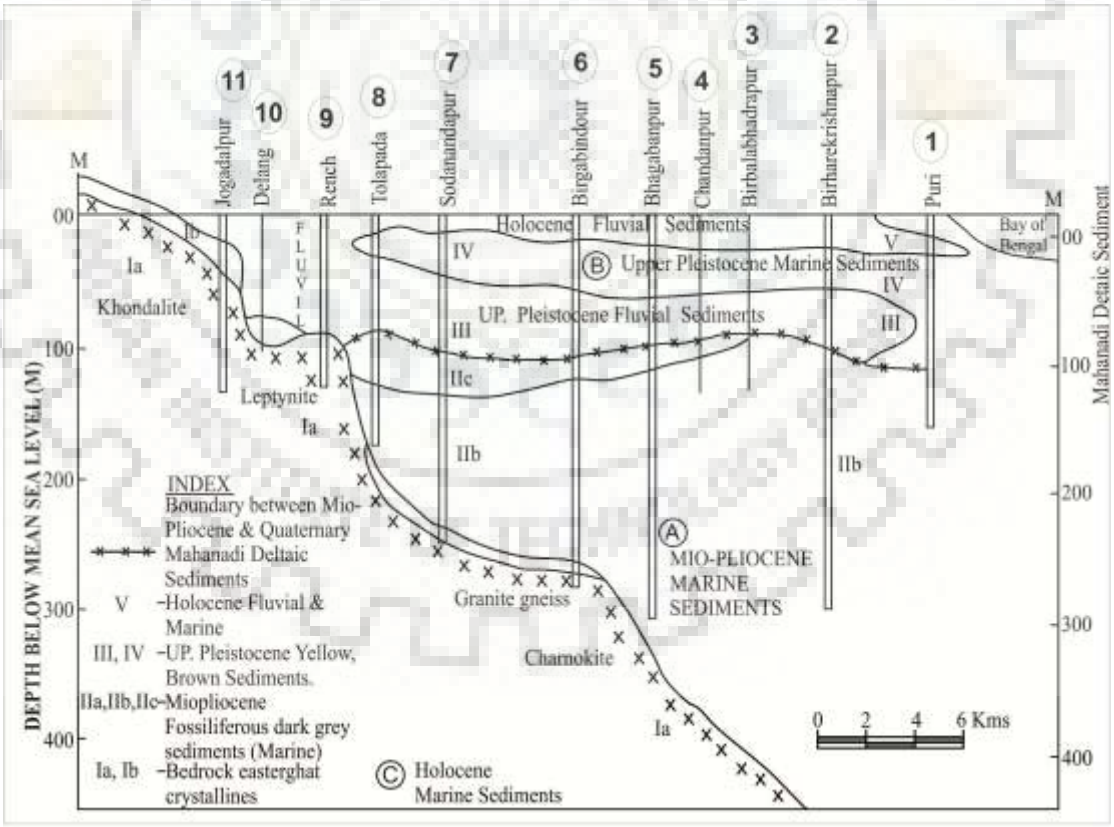

Figure 2.7 *Lithological cross-section from borehole cuttings, showing marine transgression and regression events in Mahanadi delta (after Mahalik, 2006).*

Borehole cuttings from four representative locations are presented in Table 2.1. Several other studies on fluvial and marine sediments (Banerjee, 2000, 1993; Vaz and Banerjee, 1997; Woodroffe and Horton, 2005) also have documented similar Quaternary sea-level changes along the Bay of Bengal coast. White (2011) has correlated the global Quaternary sea-level changes to glacial and inter-glacial events (Fig. 2.8a). The interglacial periods are associated with increased relative sea-level (RSL), and the glacial periods are associated with decreased RSL. Rashid (2014) has documented relative high stand during Early to Mid and Mid to Late Holocene periods (~2 m and 5 m respectively above the present-day mean sea level) along the Bangladesh coast of Bay of Bengal (Fig. 2.8b). Using near coastal facies changes Banerjee (2000) has documented an increase in relative sea level (~ 3 m above present low tide level) during early and mid-Holocene periods, along the Bay of Bengal coast of India (Fig. 2.8c).

Table 2.1 Lithology from four representative boreholes to SW Mahanadi delta (Mahalik, 2000; 2006)

Depth (m)	Bore hole lithology	Environment of deposition	Remarks
	Delang Bore Hole		
0-46	Yellow sand and clay	Subaerial, fluviatile deposits under oxidizing conditions (Quaternary deposits) Possible marine influence	Mahanadi river deposits of Quaternary period
46-80	Brownish clay and sand		
80-93	Lavender blue, reddish brown and blue sand, clay (Radiocarbon Age: 35,000 yrs BP)		
93-106	Basement rocks (khondalite and charnockite)	Basement rock	Archean age
	Tolapada Bore Hole		
0-26	Yellow clay	Flood plain deposits	Mahanadi river deposits on land
26-60	Light yellow coarse sand and gravel deposits	River bed deposits	
60-80	Blue clay	Possible marine influence	Mahanadi river deposits in sea
80-90	Light brown gravelly sand	River bed deposits	Mahanadi river deposits on land
90-197	Black to greyish black sediments with organic shells (Radiocarbon age 35,000 yrs BP)	Marine Tertiary deposits	Not related to Mahanadi sediments
	Bhagabanpur Bore Hole		
0-10	Dark grey	Flood plain deposits	Mahanadi river sediments during Quaternary period
10-55	Yellow sediments with limestone and invertebrate shells (20,000 yrs BP)	Marine deposits under oxdising condition	
55-80	Yellow sand and clay without shells and limestone	Subaerial deposits	
80-153	Dark grey to black sediments with oolites and marine shell remains	Tertiary marine sediments	Not related to Mahanadi river
	Puri Bore Hole		
0-38	Shallow marine sediments with shells and laterite gravel (5000-8000 yrs BP)	Shallow marine	Mahanadi river sediments during Quaternary period (5000 -8000 yrs BP)
38-89	Yellow clay	Subaerial deposits	
89-103	Yellow sand	Marine deposits	
103-146	Dark grey sediments with shells and oolites	Tertiary marine deposits	Not related to Mahanadi river

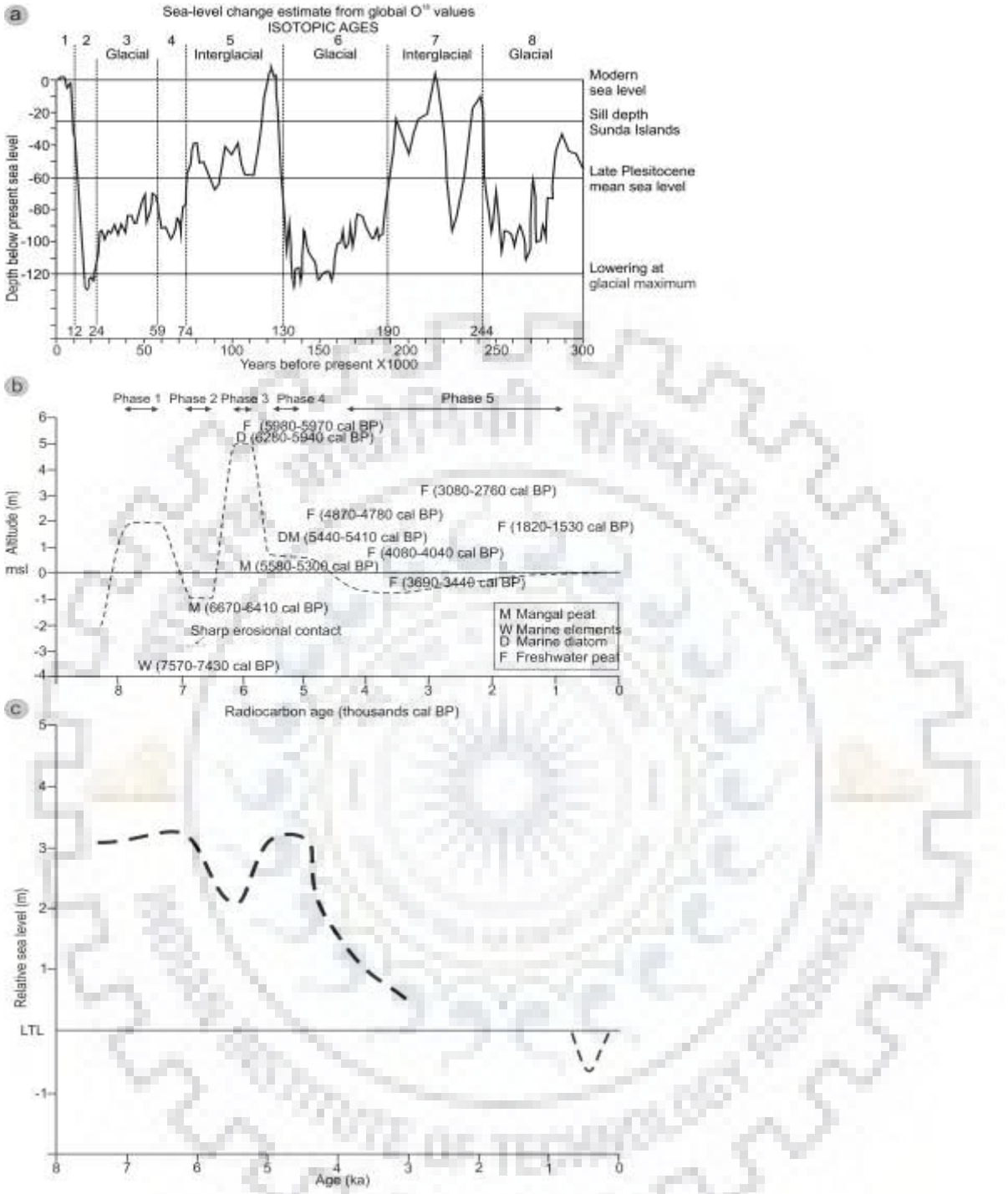

Figure 2.8 *(a) Sea-level changes during the Late Quaternary global oxygen isotopic stage (Redrawn from White, 2011) (b) Relative sea-level curve along Bay of Bengal coast of Bangladesh (Redrawn from Rashid, 2014) (c) illustration of relative sea-level change of east coast of India during Middle to Late Holocene (adopted from (Banerjee, 2000).*

Similar events of Holocene sea-level changes have been recorded worldwide in many previous studies. Woodroffe and Horton (2005) have shown that despite geographical differences, the nature of Holocene sea-level changes has been similar

throughout the world. The Early Holocene strandline in Mahanadi delta region extends from Kujang to Konark, and the Late Holocene strandline is in between the Early Holocene strandline and the present-day coast, extending from Paradip to Puri (Mahalik, 2006). Though Quaternary sea-level changes have been reported in many parts of the eastern Indian coast, limited studies on the response of fluvial system to eustatic sea-level changes have been carried out. Therefore, the occurrence of fluvio-geomorphic features along paleo-strandlines in a spatial and temporal scale has been ignored or poorly understood so far. In the present study, various fluvial geomorphic features associated with paleo-strandlines in the Mahanadi delta have been identified and correlated with the marine transgression and regression events.

Satellite imageries and topographic maps over the entire Mahanadi delta plain yield a distinct picture of Spatio-temporal variations of various geomorphologic features associated with the delta formation and subsequent modifications (Bharali et al., 1991; Dash, 2000; Maejima and Mahalik, 2001; Mahalik, 2000, 1995; Mahalik et al., 1996). The paleo-strandlines on the delta are marked by the presence of paleochannels, paleo-beach ridges, remnant spits, and elongated dune deposits. In the present study, the response of coastal rivers to shoreline changes have been documented based on drainage morphology and optically stimulated luminescence (OSL) chronology.

2.2 METHODOLOGY

To correlate different fluvio-geomorphological features with marine transgression/regression events, an integrated study using remote sensing and chronology of paleochannels along paleo-strandlines has been carried out. This integrated approach brings out different generations of paleochannels and their spatial distribution concerning the paleo-strandlines. Paleochannels representing different river morphological behavior, which are indicative of marine transgressional and regressional events, were demarcated on LANDSAT imagery. Chronological studies of these paleochannels were carried out using OSL dating.

2.2.1 Drainage morphology and Paleochannel identification; a remote sensing approach

Remote sensing is being increasingly used in study of regional geomorphology (Weng, 2002; Chu et al., 2006; Grosse et al., 2006; Pavelsky and Smith, 2009) and paleochannels mapping (Mantelli et al., 2009; Paillou et al., 2009; Rossetti, 2010; Samadder et al., 2011; Zani et al., 2012). In the present study, the LANDSAT Thematic Mapper (TM) image (Path-139, Row-46) has been used for identifying fluvio-geomorphic features (Fig. 2.9). Geomorphic characteristics indicative of marine transgression and regression events, such as anastomosing-meandering transition, river mouth shift, and dendritic channel patterns at paleo-coastlines, were identified on the LANDSAT imagery. Since the study area is a deltaic plain affected by monsoonal floods, surficial evidence of paleochannels is rarely available. Contrasting dark tone, high reflectance of Near-Infra-Red (NIR) bands, association of water bodies, well-defined connectivity to the main channel were some of the parameters taken into consideration for paleochannel identification. Drainage morphology of the presently active/paleo-channels was identified from the false-color composite (FCC) of TM image and the anomalous zones were precisely marked for correlation with paleo-strandlines. A color composite image of bands 4, 3 and 2 was used. Band 4 with wavelength ranging around the infrared region (NIR) targets water bodies. Since moisture/water strongly absorbs NIR, it makes it suitable to distinguish between dry and moist soil. Hence swamps and paleochannels in the Mahanadi delta region could be targeted using this FCC composite. Since the paleochannels in the Mahanadi delta region are densely covered with vegetation (Mahalik, 2006), targeting the vegetation cover would help in distinguishing paleochannels from surrounding barren land. In the NIR band agricultural lands, grasslands and show brighter tone than thickly vegetated zones, like forest lands. This band can separate thickly vegetated areas from surrounding barren lands. The band 3 has a wavelength ranging in the visible red region, and it senses a strong chlorophyll region and shows higher reflectance from barren soils. The band 2 having a wavelength ranging in the visible green region, targets green reflectance from forests. Hence this band is useful in separating thickly vegetated areas from the surrounding barren soil. In addition to channel mapping, geomorphic features indicating present/paleo-coast line positions such as beach ridges, dunes, and barrier spits were also identified. Similar results can be obtained using other combinations,

such as 7, 4 and 2 in LANDSAT ETM+ images. The TM image and the Survey of India topographic maps were geo-referenced in the same coordinate system to check geomorphic features in their exact geographic locations during fieldwork.

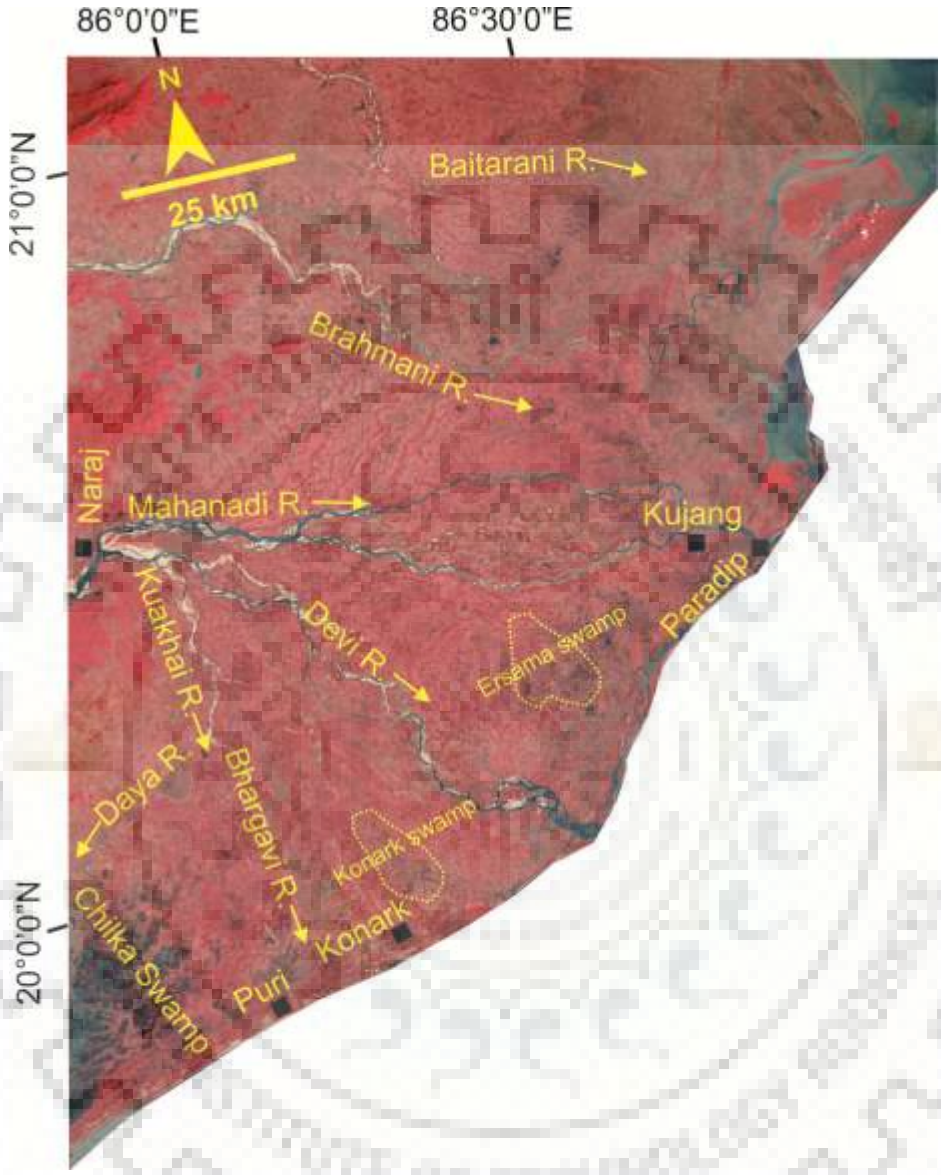

Figure 2.9 *LANDSAT (TM) FCC (R:4 G:3 B:2) image of the Mahanadi delta, showing major rivers and paleo-swamps.*

2.2.2 Palaeochannels for OSL dating

To correlate fluvial activity with the timing of sea-level changes, paleochannels indicative of paleo-sea level changes were demarcated along paleo-strandlines and their chronology was studied by using OSL dating technique. The paleochannels identified through remote sensing were examined in the field. Samples for litho-stratigraphic study and OSL dating were collected by trenching. The Mio-Pliocene paleochannels

exist at a deeper depth (up to 100 m) (Mahalik, 2006), hence examining their litho-sections by trenching becomes a difficult task. Only Holocene paleochannels were selected for OSL dating and lithostratigraphy study, as these are located at a shallower depth. The paleochannels indicating Holocene coastline positions such as abandoned channels due to river mouth shift, paleo-meander scars, and the paleo-branches of dendritic channels were marked on the map with the help of georeferenced satellite images to collect samples for OSL dating.

Sand at the base of the paleochannel is generally deposited when bed-load transportation stops, as the channel flow ceases. Clay is deposited from suspended sediments immediately above the bed-load in the stagnant water phase. Abandoned paleochannels develop topsoil when the channel sediments are exposed to pedogenic processes. Previous studies have used chronology of paleochannel sand/clay deposits to ascertain last riverine activities (Hall, 1990; Leigh and Feeney, 1995; Ramasamy et al., 2006, 2005; Rotnicki, 1991). In the present study, narrow width paleo-channels were selected for trenching and sample collection, as the bed sediments of these channels are accessible at a shallower level.

2.2.3 OSL sample processing

Samples for OSL dating were collected in galvanized iron pipes to avoid any exposure to sunlight during sampling. From both sides of the sample-tube; 5 cm of the sample were removed in the laboratory to avoid any potential contamination. Sample preparation for OSL dating was carried out using the standard protocols used in previous studies (Bateman et al., 2004; Jaiswal et al., 2009; Murray and Wintle, 2000, 2003; Wasson et al., 2013; Wintle and Murray, 2006, 1998). Carbonate and organic matters were removed with 1N HCL and H_2O_2 (30%) treatment, respectively. The samples were then sieved to get required grain size fractions of 90 to 150 µm. Quartz and feldspar were separated using density separation method, with a heavy liquid Sodium Polytungstate (2.58 g/cc). The quartz grains obtained were etched using 40% hydrofluoric acid (HF) for 80 min and then followed by an HCL (35%) treatment for 30 minutes to remove alpha irradiated outermost layer of approximately 10 µm, feldspar contamination present if any and fluorides formed at the time of HF treatment. Using silko-spray silicone oil a monolayer of quartz grains was spread over stainless steel discs of 10 mm diameter. Small aliquots (2mm) diameter were used to spread the

quartz grains. Luminescence measurements were carried out on a Freiberg Lexsyg Smart TL-OSL reader with a blue light-emitting diode (LED) source (λ=458±10 nm), delivering a 100 mW/cm^2 power to the quartz grains. The equivalent dose was estimated using a single aliquot regenerative dose (SAR) technique following Murray and Wintle (2000, 2003) by preheating at 300°C for 20 seconds. For dose rate estimation, the elemental concentration of Uranium and Thorium were measured using ICPMS and the concentration of Potassium was measured using XRF (Table 2.2). A brief description of OSL dating procedure is given in APPENDIX-I.

Table 2.2 OSL ages of paleochannel sections

Location	U (ppm)	Err U (ppm)	Th (ppm)	Err Th (ppm)	K (%)	Err K (%)	De (Gy)	Err De (Gy)	Age (ka)	Err Age (ka)
L1 (Bhailpur)	0.934	0.033	10.747	0.045	2.85	0.036	12.11	0.46	3.713	0.205
L2 (Brahmagiri)	1.127	0.022	15.28	0.044	2.83	0.023	13.91	0.47	3.907	0.201
L3(Purushottampur)	0.985	0.041	12.422	0.051	2.57	0.027	5.87	0.15	1.871	0.087
L4 (Alanda)	0.792	0.005	10.523	0.067	2.1	0.056	17.94	0.76	6.945	0.411
L5 (Popora)	1.28	0.014	9.567	0.084	1.61	0.015	17.56	0.35	7.938	0.343
L6 (Dobala)	0.84	0.011	10.15	0.077	1.91	0.016	6.57	0.21	2.726	0.137
L7 (Padmapur)	1.15	0.006	9.87	0.061	2.11	0.021	7.15	0.08	2.722	0.11
L8 (Fakirdandy)	0.917	0.021	10.22	0.055	2.41	0.018	11.88	0.41	5.29	0.38
L9 (Debichhaka)	1.18	0.045	11.14	0.049	1.78	0.051	13.56	0.99	5.578	0.466
L10 (Olaghar)	0.88	0.007	9.55	0.068	1.89	0.022	18.38	0.57	7.773	0.388

2.2.4 Ground penetrating radar study

Ground-penetrating radar (GPR) study has been proved to be a well-established technique to study shallow subsurface features (Bristow and Jol, 2003). To study subsurface sediment architecture, concealed structures underlying surface sediments, high-resolution imagery of deformation structures and depositional boundaries, GPR study has been proved to be useful (Bristow and Jol, 2003; Gawthorpe et al., 1993). GPR study has been used to study depositional environments in many geological settings such as fluvial, lacustrine, near coastal and aeolian. (Jol and Smith, 1991). Ground-penetrating radar has wide range of applications for solving environmental problems i.e. estimating groundwater potential and recharge zones measuring ice thickness, estimating soil stratigraphy, reservoir modeling, archaeological studies etc.

(Bhatt and Bhonde, 2003; Davis and ANNAN, 1989; Dolphin et al., 1978; Jol and Smith, 1991; Knight and Endres, 1990; Maurya et al., 2013; Prizomwala et al., 2016; Sharma et al., 2017; Shukla et al., 2013; Thompson et al., 1995) GPR works within frequency of 20 MHz to 2.5 GHz, using electromagnetic radiation for subsurface imaging. Different sub-surface lithology/sediment layers are distinguished on the basis of dielectric constant. The vertical or horizontal image resolution depends on differences in dielectric constant (Martinez and Brynes, 2001). GPR is widely used in fluvial environments due to ease of access, heterolithic character of sediments and varied depositional architecture (Bristow and Jol, 2003; Ékes and Friele, 2003). In past decades GPR has been widely used to characterize Holocene coastal sediments. As opposed to studying using sediment cores, GPR has been a more cost-effective method in visualizing subsurface features in two/three-dimensional profiles. GPR has been widely used by past geomorphologists/ geologists to study past depositional environments in coastal areas. A compressive review of previous studies in different environments has been discussed by Neal (2004). GPR study has been widely used in coastal environments especially to characterize Hurricane and Tsunami deposits (De Lange and Moon, 2007; Horwitz and Wang, 2005; Horwitz, 2008; Switzer et al., 2006; Wang and Horwitz, 2007), barrier islands and beach ridges (Bennett et al., 2009; Bristow et al., 2000; Bristow and Pucillo, 2006; Costas et al., 2006; Dougherty et al., 2004; Fitzgerald and Buynevich, 2002; Fitzgerald and Van Heteren, 1999; Grant et al., 1998; Heteren et al., 1998; Hodgkinson et al., 2008; Jol et al., 2003, 1997, 1996; Jol and Bristow, 2003; Neal et al., 2003, 2002a, 2002b; Tamura et al., 2008; van Heteren et al., 1996; Van Heteren et al., 1997; Van Overmeeren, 1998), coastal evolution and stratigraphic analysis (Barboza et al., 2018, 2014; E G Barboza et al., 2011; Eduardo Guimarães Barboza et al., 2011; Barboza et al., 2013, 2009; da Silva et al., 2014; Dillenburg et al., 2009, 2006, 2017, 2014, 2011; Dillenburg and Barboza, 2014, 2009; Leal et al., 2016; Oliveira Jr and Medeiros, 2008; Rockett et al., 2016; Rosa et al., 2016, 2011).

GPR uses the wave nature of Electromagnetic radiation and exploits electrically conducting band of EM radiation. Discrete pulses of EM radiation are used to detect subsurface discontinuities typically up to 50m depth (Neal, 2004). The control unit in GPR has the functions to control gain, range, basic filtering, and display during a survey. An antenna transmits or receives electromagnetic waves. The penetration depth

of the signal depends upon the frequency, lower the frequency higher the penetration depth and vice versa. When signals meet boundaries between layers of different conductivity reflections are produced. When the contrast between layers is greater, stronger reflections are produced. All the signals that are transmitted are not reflected; some are attenuated into the layers itself. The presence of underground water which has high dielectric value slows down the waves, and hence the true signal gets distorted. For the present study to identify subsurface structures indicative of paleo-coastal structures, 100MHz antennae were used. GPR profile study was carried out across paleo marine coastlines. Electronic devices, electric poles and hypertension lines which are sources of electromagnetic waves were avoided in the vicinity of the study area. Heavy traffic areas and railway lines were avoided to reduce any noise effect on the signals. GPR was best possibly moved over smooth surfaces to avoid any undulations while surveying.

The survey was carried out across Holocene strandlines, as the Holocene marine structures were expected to be found within the penetration limit of GPR. RADAN software of Geophysical Survey System Instruments (GSSI) was used to process the data using various filters, as suggested by Fisher et al. (1996). Various filters used for the present study are as described below. A high pass and low pass filter of 40/50 and 150/180 MHz respectively, were used throughout the study.

Stacking: Stacking uses a running average method to stack adjacent scan lines, thereby omitting occasional high-frequency noises.

Skipping: This function is used to specify the number of scans to be skipped in between specified scans.

Stretching: To expand horizontal scaling of the simple dataset average between two nearest scan lines is calculated and an average scan is placed in-between them.

Infinite Impulse Response (IIR) filters: This function allows us to define definite high and low pass vertical as well as horizontal filters and the time interval for which it will be processed. IIR filters are asymmetrical and cause minor phase shifts in the data.

Finite Impulse Response (FIR) filters: FIR filters produce a finite filtered version of encountered feature and produce symmetrical results, without shifting reflections. Two

sub-functions of FIR filters are available for data processing i.e. Triangular and Boxcar filters.

Horizontal High Pass (Background Removal) Filter: Flat lying ringing system noise is usually most prevalent when the range (the time window in nanoseconds that the instrument will record from a single pulse) is set near the maximum limits for the antenna. It is characterized by flat-lying or horizontal bands usually of a vertical frequency lower (shown by wider bands) than that of real reflections in the data set. This type of noise can obscure or mask real reflections at greater depths. This type of low-frequency noise is removed by using the Background Removal Filter. When a non-zero value is used, thigh pass filtering will occur in the horizontal direction. Low-frequency features in the data will be removed, such as antenna ringing. This filter will also remove the surface reflection (direct coupling) pulse.

Low Pass filters: High-frequency noise is usually most prevalent when the range is set near the limits for the antenna in use, and large amounts of gain are used. It is characterized by "snow-like" noise in the data at depth. This type of noise can make it difficult to map real reflections at depth. Both Vertical and Horizontal Low Pass Filters are effective for removing high-frequency noise. A Vertical Low Pass Filter will reject frequencies above an established threshold. When a non-zero value of Horizontal Low Pass Filter is used, low pass filtering will occur in the horizontal direction and reduce the "snow" noise and smooth the data. A number of scans on either side of the center are averaged and the results placed in the center scan.

Spatial Fast Fourier Transform (FFT) Filter: The spatial FFT filter, which is a two-dimensional frequency filter, takes place in the time-space domain. It is often called a frequency-wave number, or F-K, domain. This approach generates a two-dimensional matrix, the complex element of which represent the phase and amplitude of various spatial waves present in the radar data. It allows developing a two-dimensional filter to attenuate the noise. Performing the inverse Fourier transformation of the product matrix from the transformed data and the filter yields data with reduced noise. Technically, at this stage, the frequency domain data is reconstructed back to the time domain. The advantage of F-K filtering over successive vertical and horizontal one-dimensional frequency filtering is that it enables a better distinction to be made between the signal

and the noise. The signal and noise spectra may overlap in one-dimension, which makes their separation impossible, but this is less likely in the F-K domain.

Deconvolution: Multiples or "ringing" occur when the radar signal bounces back and forth between an object (such as a piece of metal or a layer of wet clay) and the antenna, causing repetitive reflection patterns throughout the data and obscuring information at lower depths. Multiple reflections may also be observed when mapping the water bottom, bedrock, or voids. Deconvolution is the filtering method used to remove this type of noise. The earth behaves as a filter by removing high-frequency information from the data. Deconvolution can also be used to restore the vertical resolution of the radar wave before it underwent this filtering process by compressing the reflected wavelets. Hence, in addition to removing unwanted multiples, deconvolution can be used to resolve closely spaced layers.

2.3 RESULTS

2.3.1 Fluvial response to sea-level changes

Paleochannels and other geomorphic features were identified from LANDSAT thematic mapper (TM) image. The paleochannel maps were cross verified with some of the available paleochannel maps in the study area (Mahalik, 2006). Several generations of paleochannels are found in the Mahanadi delta (Fig. 2.6), corresponding to different stages of delta development with sea-level fluctuation. The anastomosing-meandering transition is clearly observed along strandlines. All the major rivers of the Mahanadi deltaic system show similar trends in the anastomosing-meandering pattern along the strandlines (Fig.2.10). River mouth shifts (Fig.2.11) and different series of dendritic channels (Fig. 2.12) are observed along Early and Mid-Holocene strandlines.

2.3.1.1 Anastomosing-meandering transition

River anastomosis is observed along the Mio-Pliocene, Pleistocene and Holocene transgressive coastlines and shifts to meandering pattern with subsequent regressional intervals (Fig. 2.10). Three major distributaries of the undivided Mahanadi River i.e., Mahanadi, Devi, and Nuna Rivers follow episodic anastomosing to meandering transition along paleo-strandlines. The Devi River shows anastomosing pattern at the Mio-Pliocene, Pleistocene and Early Holocene strandlines, which were

transgressive coastlines, and it changes to meandering pattern during subsequent regression events. Similarly, the Brahmani and Baitarani rivers also show anastomosing patterns at the transgressive strandlines. Anastomosis is observed at the river mouth as channel aggrades with marine transgression and later turned to meandering pattern with sea-level fall (Aslan and Blum, 2009; Gallais, 1967; Leigh et al., 2004; Makaske, 1998; McIntosh, 1983; Walker and Coleman, 1987). Along the paleo-strandlines of the Mahanadi delta region, a similar pattern of anastomosing-meandering channel transition in all the major rivers indicates that sea-level change had a significant impact on sediment delivery and channel morphology of the rivers.

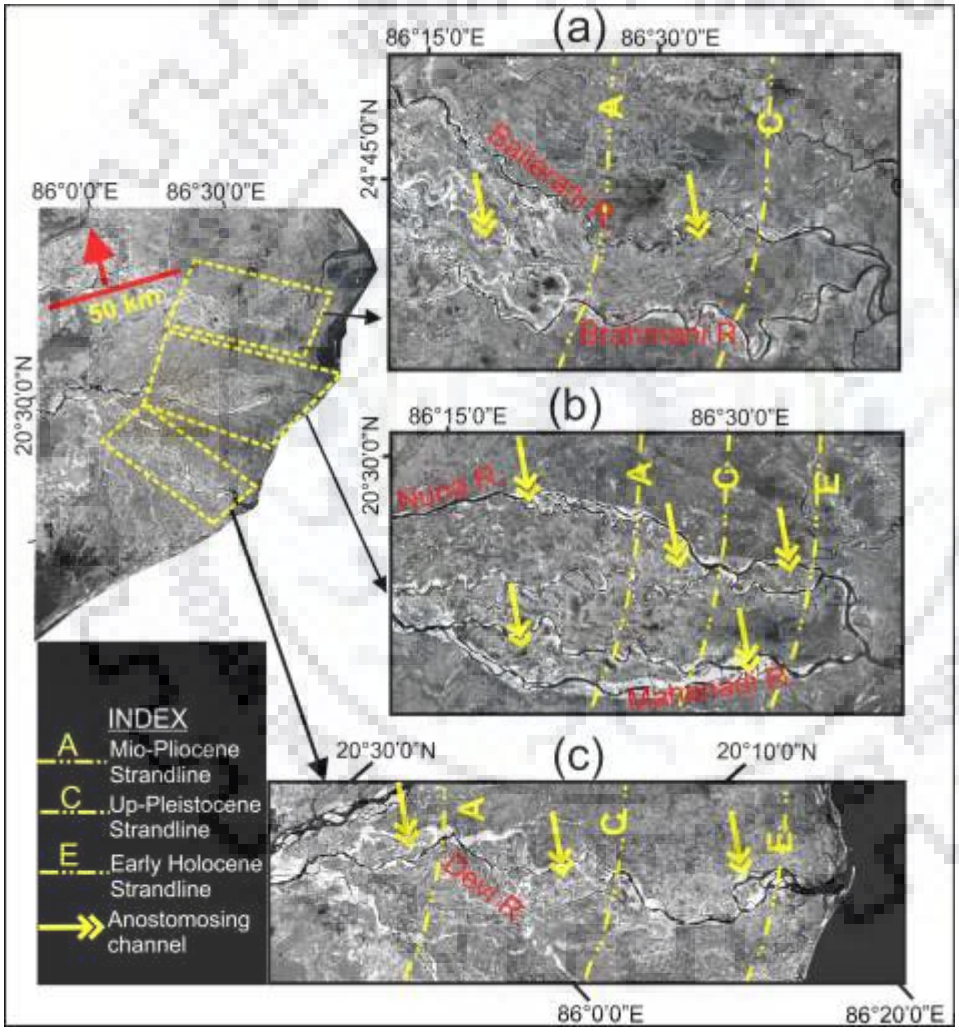

Figure 2.10 *Anastomosing-meandering transition across the paleo-strandlines of Mahanadi delta. The channels show anastomosing pattern at transgressive strandlines and meandering patterns during a subsequent regressional phase.*

2.3.1.2 River mouth shift

Parallel to Holocene strandlines, major shifting of river mouths has been observed along the lower deltaic plains (Fig. 2.11). The NW-SE flowing Bhargavi River flows N-W by shifting its mouth along the Late Holocene strandline. The present course of Kushabhadra River has shifted 4 km in E-W direction, parallel to the Early Holocene strandline. The Brahmani and Baitarani rivers also show river mouth shifts up to 7 km along the early Holocene strandline. Paleo-meander scars of Brahmani and Baitarani

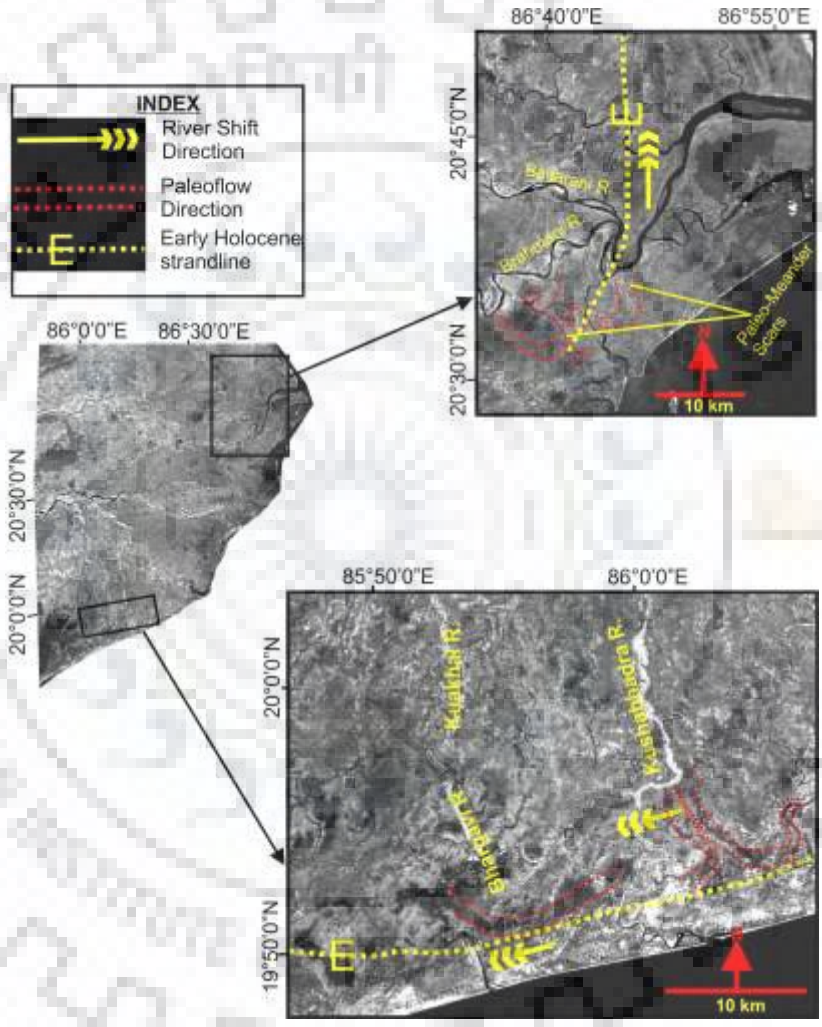

Figure 2.11 *River mouth shift of Bhargavi, Kuakhai, Brahmani and Baitarani rivers. The NW-SE flowing Bhargavi River flows E-W by shifting its mouth along the Late Holocene strandline. The paleo- and the present courses of Kushabhadra River have shifted 4 km in N-S direction, parallel to the Early Holocene strandline. The Brahmani and Baitarani rivers also show river mouth shift up to 7 km along the early Holocene strandline.*

rivers observed in the LANDSAT imagery are indicative of avulsion processes and river mouth shifts. These river mouth shifts indicate that the Holocene strandlines were

transgressive, which caused channel avulsion and hence the mouth shift (Ren and Shunan, 1990; Schumm, 1993; Xue, 1993).

2.3.1.3 Dendritic channels along strandlines

Dendritic drainage patterns are observed near to present-day coast (Fig. 2.12), along the Holocene strandlines. The dendritic channels converge to single-channel before advancing to the sea. The Early Holocene dendritic channels have their dendritic branches concentrated near the Early Holocene strandline between Kujanga and Konark. The Late Holocene dendritic channels are found within Late Holocene and the Early Holocene strandline, between Paradip and Puri. Swamps along the Holocene strandlines (Fig. 2.6 and 2.9) are identified by their dark tone in the satellite imagery. Mahalik (2006) defined these swamps as tidal flats along paleo-coastlines. Near coastal swamps/tidal flats provide favorable conditions for dendritic channel development (Choi et al., 2013; Hughes, 2012). Paleochannels abruptly terminating along paleo-swamps are indicative of paleo-coastline position. The paleochannels to SW of the Mahanadi delta terminate along the Chilka swamp (paleo-extension of the Chilka Lagoon) (Fig. 2.6 and 2.9). The paleo-extension of the Chilka Lagoon marks the Late Holocene strandline (Mahalik, 2006), as evident from coast parallel paleo-beach ridges bounding the Chilka swamp. Similarly, the Konark and Ersama swamps along Holocene strandlines also shows abruptly terminating dendritic paleochannels (Fig. 2.9). Dendritic channels form in coastal swamps/flat tidal regions, as the runoff is concentrated due to the lower slope. These channels have low base level erosion capacity, hence cannot adjust to regressional slope change and become abandoned when sea level retreats (Schumm, 1993). The dendritic channels near the Mio-Pliocene and Pleistocene paleo-strandlines have either been buried or captured by major rivers.

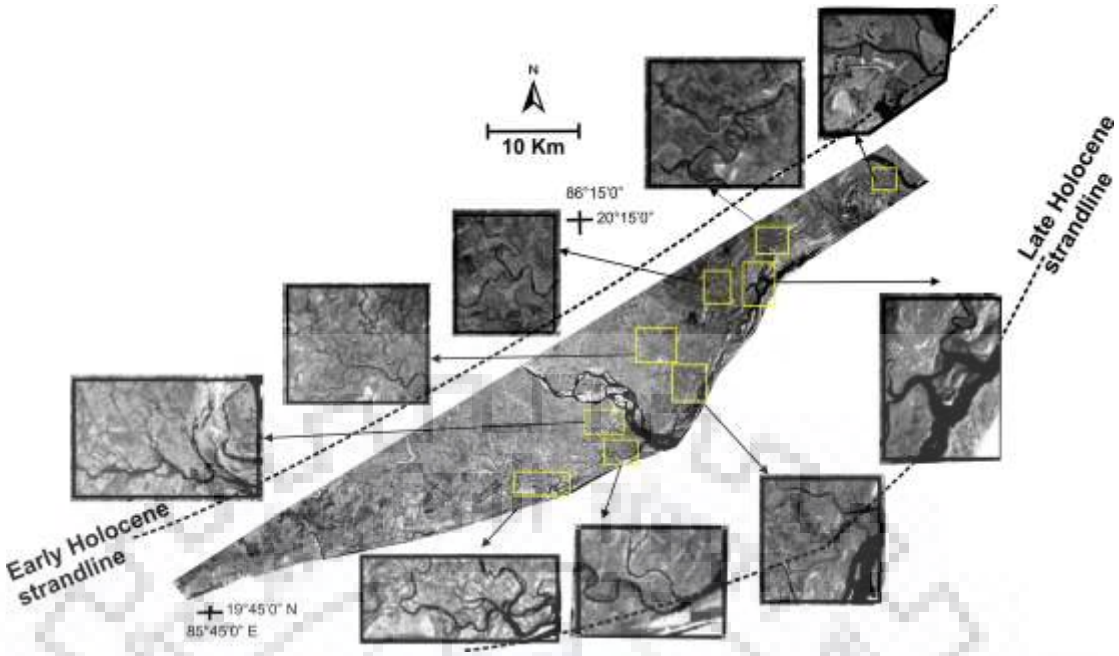

Figure 2.12 *Dendritic drainage patterns along the Holocene strandlines of Mahanadi delta. Different series of dendritic networks are developed in early and late Holocene strandlines.*

2.3.2 Litho-sections and OSL chronology of Holocene paleochannels

Sampling was carried out at ten locations from the paleochannels along early and late Holocene strandlines (Fig. 2.13). Detailed lithologs at the trenching sites were prepared (Fig. 2.14 and 2.15), and channel deposits were dated to know the timing of last riverine activity. General stratigraphy of the paleochannel deposits is channel-sand at the bottom, followed by sandy-clay, clay, and topsoil. Vertical profiles of paleochannels show fining sedimentation (Fig. 2.14) upward, indicating decreasing channel strength. The chronology of the paleochannels was established with OSL dating of the basal litho-sections (Fig. 2.16 and Table 2.2). Suitable disc for OSL dating was selected based on (i) recycling ratio within 10%, (ii) error less than 10% and recuperation below 5%. The estimated doses show a good distribution around average value (Fig. 2.16). Heterogeneous bleaching was not found as shown by well-constricted paleo does distribution and overdispersion was found to be less than 10%. Hence average Paleodose was taken for age calculation.

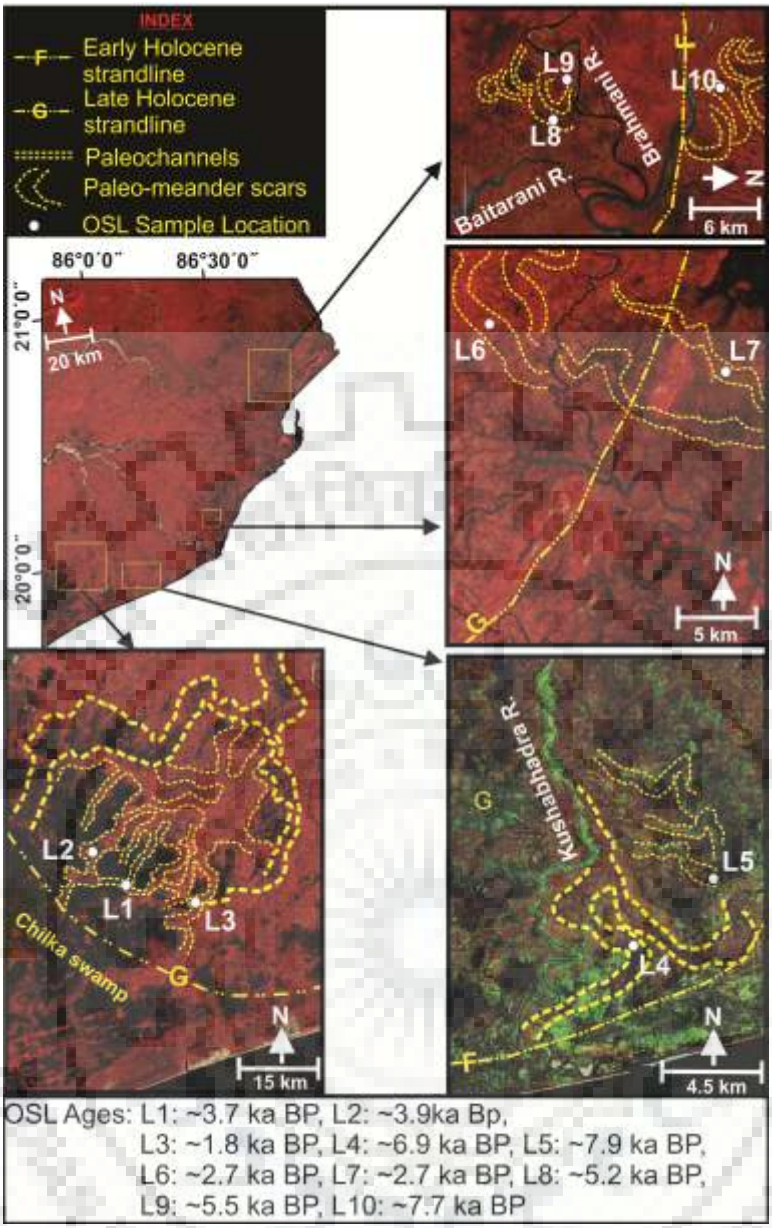

Figure 2.13 *Sampling sites for OSL dating. L1 (Bhailpur section), L2 (Brahmagiri section) and L3 (Purushottampur section) are from paleo-dendritic systems to SW of Chilka Lagoon; L4 (Alanda section) and L5 (Popora section) are from paleochannel of Kushabhadra River (see fig.7). L6 and L7 are from paleo-dendritic branches along Ersama swamp (see fig 4 and 6); L8 (Fakirdandy), L9 (Debichhaka), L10 (Olaghar) are from paleo meander scars of Brahmani and Baitarani rivers.*

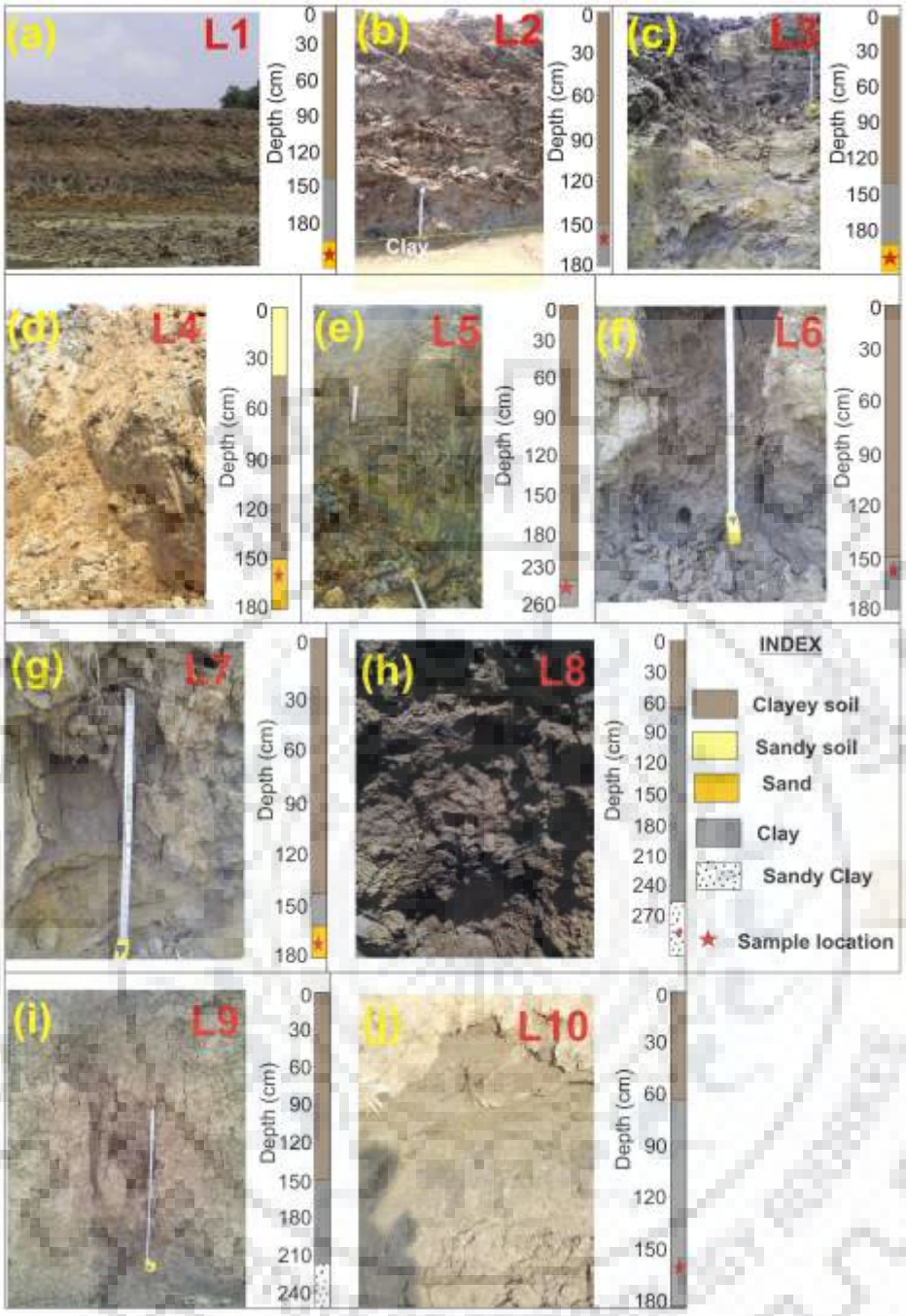

Figure 2.14 *Lithosections at paleochannel trenching sites.*

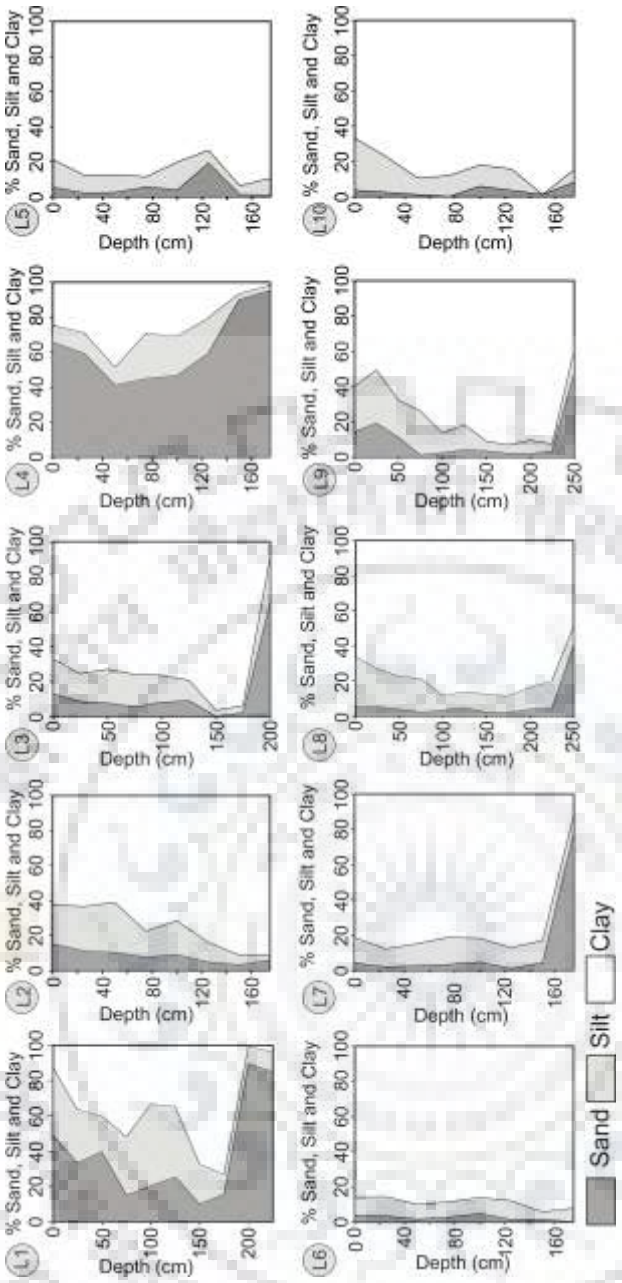

Figure 2.15 *Plot of Sand, silt and clay percentage in the paleochannel sections.*

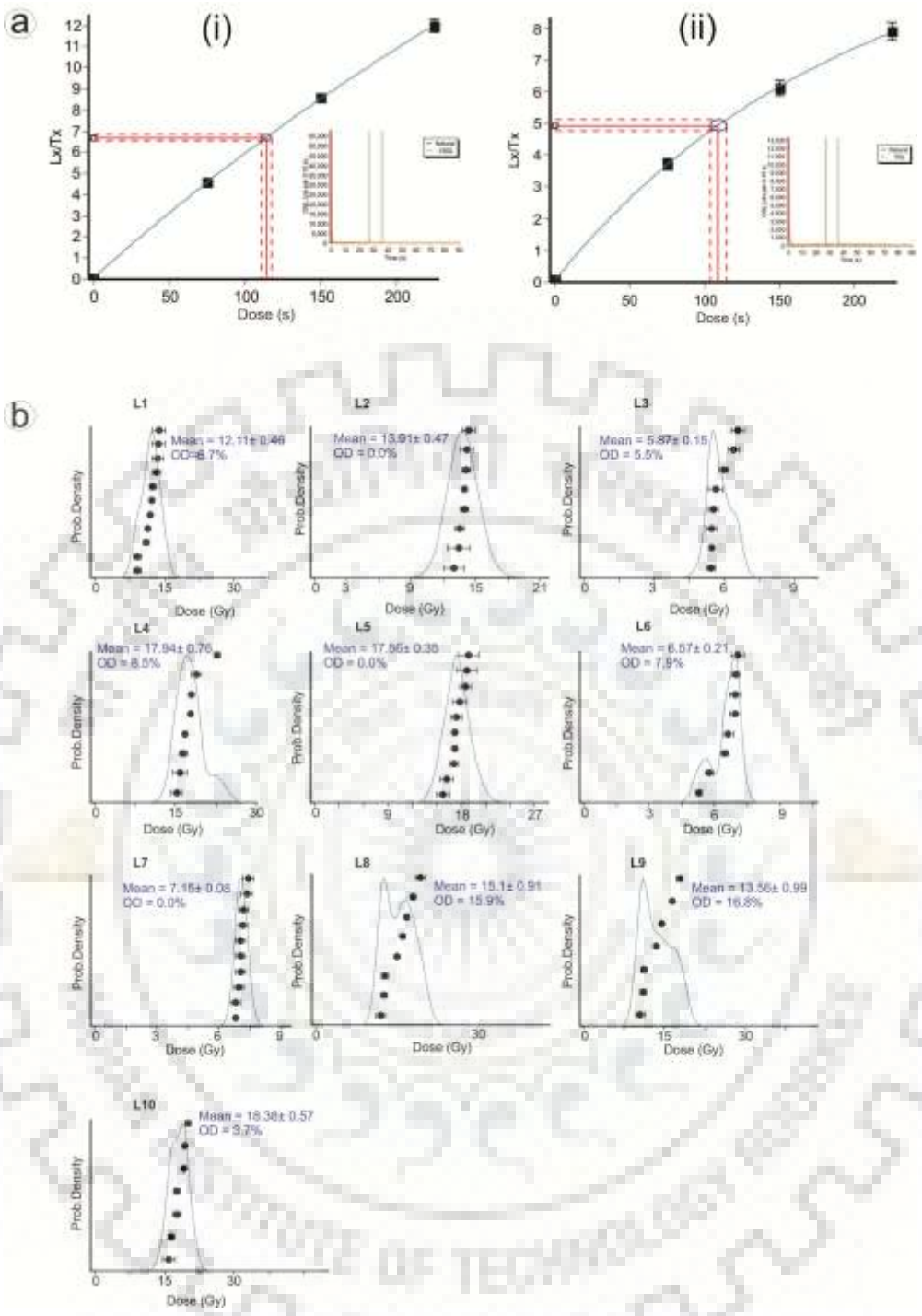

Figure 2.16 *(a) Plotted graph shows typical growth curves for (i) Alanda section and (ii) Popora section. (b) The distribution of equivalent doses (De) values for all samples presented with probability distribution curves*.

To the SW of Mahanadi delta, three locations were chosen from a series of dendritic paleochannels terminating abruptly along the Mid-Holocene strandline (Fig. 2.13). These channels end along the Chilka swamp towards the NW of present-day Chilka lagoon. Mahalik (2006) has stated that the swamp to NW of Chilka lagoon is

the due to Mid-Late Holocene transgression event, which led the salt marshes to transgress inland and invade the low laying areas. These paleochannels became defunct due to lack of base-level erosion capacity to adjust the regressional slope change, following the Mid- to Late Holocene high stand. The chronology of these paleochannels would indicate the timing of their last fluvial activity along the Mid-Holocene coastline. Vertical sections of paleochannels at Late-Holocene strandline to the SW of the Mahanadi delta were studied at three localities i.e. at Bhailpur, Brahmagiri and Purushotampur (L1, L2 and L3 respectively, in Fig. 2.13 and 2.14) and sampling was carried out for OSL dating. Lithostratigraphy of the Bhailpur section consists of a massive sand deposit at the bottom (>2 m thick), followed by 1 m greyish black clay and the topsoil horizon. The boundaries between successive litho units are gradational, indicating that the channel abandonment was gradual. The bottom sand dates back to 3.7 ka BP. The soil horizon overlying the clay has a thick "B" horizon. At the Brahmagiri section, the bottom layer consists of a clayey horizon overlain by clayey soil. The bottom clay layer dates back to 3.9 Ka BP. The Purushotampur section has a coarse sand horizon at about a depth of 2 m below the surface, overlain by thick sandy soil horizon. The bottom sand dates back to 1.8 Ka BP. The ages of these paleochannels indicate that the dendritic channels to SW of Chilka Lagoon were active during Mid to Late Holocene period and later were abandoned when sea level retreated to the position of present-day coastline.

Prominent paleo-flow paths of Kushabhadra River are observed in the LANDSAT imagery (Fig. 2.13). The river mouth shifts are observed along the Early Holocene strandline. The chronology of these paleo-flow paths will indicate the timing of the avulsion process and the associated marine transgression event. Paleochannel section of river Kushabhadra at Alanda (location L4, in figure 2.13 and 2.14) was studied for lithostratigraphy and OSL dating. The Paleochannel section at Alanda has massive coarse sand below a depth of 1.5 m from the surface, which extends further below. It is overlain by 1 m thick clay and about 50 cm thick sandy soil horizon at the top. The bottom sand dates back to 6.9 ka BP. A series of paleo-dendritic channels are observed in the Konark swamp adjoining to Kushabhadra paleochannels. These paleo-dendritic channels indicate that Konark swamp was dominated by dendritic channel systems, which were abandoned due to the Holocene sea-level retreat. The Popora paleochannel

section (location L5, in figure 2.13 and 2.14) represents a paleo-dendritic system of Konark swamp.

The bottom of this section has thick black clay overlain by clayey soil horizon. The clay bed dates back to 7.9 ka BP. Early to Mid-Holocene ages of these paleochannels indicate that the mouth shift occurred during the Early-Mid Holocene transgression event and the dendritic channels in the Konark swamp were dried up along the Mid-Late Holocene coast.

A series of dendritic paleochannels between the Mahanadi and Devi rivers terminate at Late Holocene strandline, along the Ersama swamp. Paleochannel sections at Dobala and Padmapur (locations L6 and L7, in figure 2.13 and 2.14) are branches of a paleo-dendritic system. Abandonment of these dendritic channels may have occurred because of low base level erosion capacity to adjust the slope change, due to Holocene regressional intervals. Paleochannel section studied at Dobala consists of 50 cm thick clayey sand horizon at the bottom, followed by a massive clay horizon at the top. The bottom layer dates back to 2.7 Ka BP. The Padmapur section has coarse sand at the bottom, followed by clay and well-developed soil horizon at the top. The bottom sand dates back to 2.7 ka BP. Late Holocene ages of these paleochannels indicate that the channels were active at the Mid-Holocene coastline and later became abandoned due to sea level regression.

The Fakiradandi, Devichhaka, and Olaghar paleochannel sections (L8, L9 and L10 respectively, in fig. 2.13 and 2.14) are from paleo-meander scars of Brahmani and Baitarani rivers, developed along Early Holocene strandline. These meander scars were developed as a result of river mouth shifts in Brahmani and Baitarani rivers. The Early Holocene river transgression event might have caused favorable conditions for avulsion and river mouth shifts. Chronology of these meander scars will represent the timing of river mouth shift and associated Early Holocene transgression event. These meander scars are represented by sandy clay at the bottom and clay at the top of the channel. The basal section of these paleochannels was used for OSL dating. The Fakirdandy section dates back to 5.2 ka, the Debechhaka section dates back to 5.57 ka and the Olaghar section dates back to 7.7 ka BP.

2.3.3 Paleo-coastal structures in GPR profiles

The GPR study was carried between Early and Late Holocene strandlines along Kushabhadra River. Shallow subsurface structures were studied up to a depth of 25 meters. These features are identified as onlap and downlap depositional structures in the sub-surface strata (Fig.2.17).

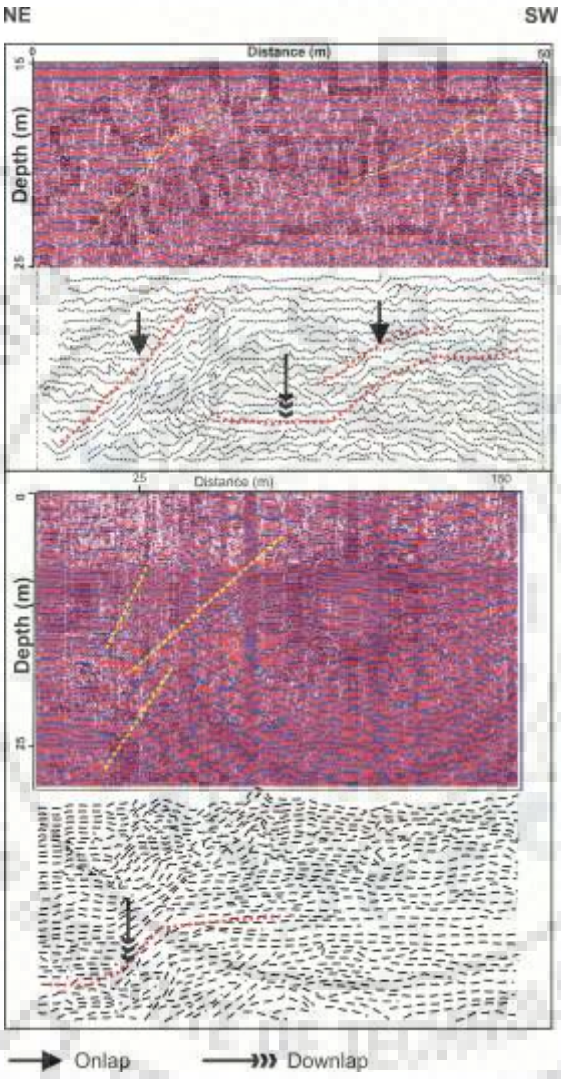

Figure 2.17 *GPR profile showing onlap and downlap structures between Early and Late Holocene strandline aalong Kushabhadra River.*

2.4 DISCUSSION

2.4.1 Fluvio-geomorphic changes along paleo-strandlines of Mahanadi delts

Paleochannels along the paleo-strandlines of Mahanadi delta indicates that Quaternary sea-level changes control the channel morphology. The pre-Holocene strandlines are well distinguished by a transition from anastomosing channels to meandering channels, while they lack relict paleo-coastal features like paleo-beach ridges, spits, and marshes. Relict paleo-coastal features at pre-Holocene strandlines could have been modified/buried by later fluvio-geomorphic changes. Holocene witnessed two major sea-level fluctuations along the Bay of Bengal coast. The Late Holocene strandline extends from Paradip to Puri, as indicated by paleo-beach ridges/spits. The Early Holocene strandline extends from Kujanga to Konark and is marked by Konark and Ersama swamps. GPR study along the Holocene strandlines further adds evidence to the presence of paleo-coastline around Early –Mid Holocene times. The Early to Mid-Holocene age of Kushabhadra river paleochannels indicate that river avulsion occurred at the Early-Mid Holocene coastline. Dendritic paleochannels towards SW of the Mahanadi delta terminate at paleo-extension of Chilka Lagoon. OSL ages of these channels date back to Late Holocene time, indicating their development along the Late Holocene strandline. The dark tone in the LANDSAT image to SW of Chilka Lagoon represents the paleo-swamp of Chika Lagoon. This indicates that the lagoon was present farther landwards during the Late Holocene and retreated to present location with sea level retreat. The dendritic channels near to the present-day coast (Dobala and Padmapur sections) terminate at the Ersama swamp and are of Late Holocene age. This indicates that the Ersama swamp was developed near the Mid-Late Holocene coastline and the paleo-dendritic channels along the Ersama swamp were terminated following retreat of coastline to the present position. Paleo-meander scars of Brahmani and Baitarani rivers are of Early-Mid Holocene age. These meander scars were developed due to a shift in flow paths of these rivers. Early-Mid Holocene age of the meander scars indicate that the channel shift might have occurred due to the avulsion process associated with Early to Mid- Holocene marine transgression.

2.4.2 The anastomosing channels and its relation to sea-level change

Past investigations on anastomosing rivers have revealed climate change as a prompting factor for instability, causing stream anastomosis. The transition from arid to humid climate often leads to increase in sediment and water discharge of the river, which subsequently induces channel avulsion (Bakker et al., 1989; Bowler et al., 1978; Gallais, 1967; Garner, 1959; Makaske, 1998; McIntosh, 1983). The Pleistocene and Holocene sea-level changes are indirect outcomes of climate change (Fairbanks, 1989; Galbraith et al., 2002; Hoegh-Guldberg and Bruno, 2010; Lambeck, 2001; Raper and Braithwaite, 2006). Quick sea-level change causes favorable conditions for river anastomosis. In fluvial frameworks connecting marine basins, fast sea level rise may give a downstream control to upstream alluviation and development of channel anastomosis (Mackin, 1948; Smith, 1973). Quick aggradation coming about because of a downstream control is essential in building up the anastomosed frameworks. Anastomosis is observed at the river mouth as channel aggrades with marine transgression and later turned to meandering with sea-level fall. Anastomosing rivers indicating transgressional events have been reported along the marine coast in humid climatic regions of Europe (e.g., Loire River, France, Straffin et al., 1999; Meuse River, northwest Europe, Kasse et al., 1995; Warta River, Poland, Kozarski, 1991). Increased rates of floodplain accretion following Holocene sea level rise have been reported by Russell (1957, 1954), and McCave (1969), recommends comparable circumstances resulting alluviation in a Devonian transitional succession. Base level change aggrades the channel and reduces the gradient, thus, increasing the avulsion frequency. Quick sea level ascent is viewed as a primary factor for the occurrence of numerous distributaries around the mid-Holocene Rhine– Meuse delta (Makaske, 1998; Torbjorn E Tornqvist, 1993b, 1993a). In the Mahanadi Delta region, the episodic nature of transition from anastomosing to meandering drainage pattern along the paleo-strandlines indicates that the anastomosing channels were formed during transgression event and adopted the meandering pattern during the regressional event. During Mio-Pliocene times, the sea transgressed farthest into land, represented by radiocarbon dates of marine shells in Tolapada and Delang boreholes (Fig. 2.7 and Table 1). The inception of the initial phases of Mahanadi delta formation began at the Mio-Pliocene Sea. Rivers showing an anastomosing pattern were formed at the Mio-Pliocene transgressive boundary. Sea level retreated after Mio-Pliocene transgression event, as represented by

gravel and sand deposits of fluvial origin above Mio-Pliocene marine deposits in Delang and Talapada boreholes. With retreat in sea level, the anastomosing channels coalesced to form single meandering channels (Fig.2.18). During the Upper Pleistocene, the second phase of marine transgression occurred.

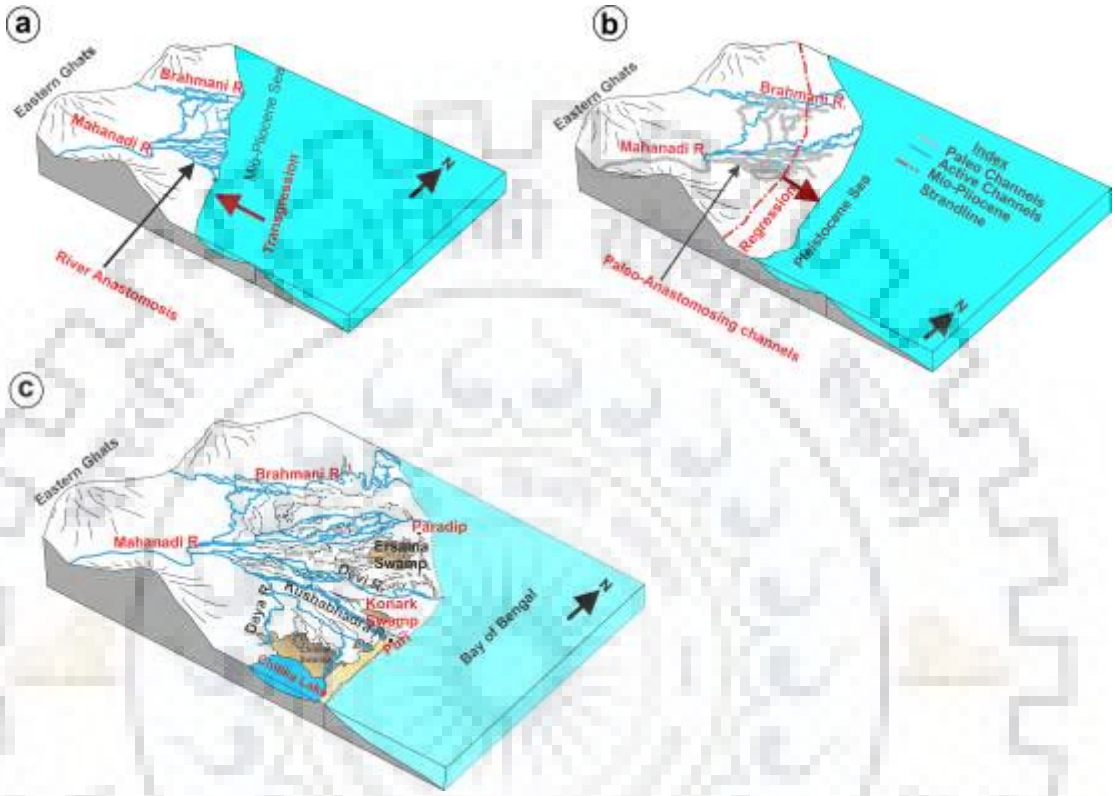

Figure 2.18 *Block diagrams showing representative anastomosing Meandering transition along Mio-Pliocene strandline. (a) The Mio-Pliocene coastline was transgressive and anastomosing channels developed at the interface of sea (b) with regression during Early to Up. Pleistocene times the anastomosing branches became abandoned and the Mahanadi River migrated towards the Early Pleistocene coastline (c) The present coastline position.*

Marine shells above the fluvial sands in Bhagabanpur borehole represent this transgressive event. Towards the end of Pleistocene, sea level retreated near to the present-day coastline. The Upper Pleistocene anastomosing channels formed single meandering channels in response to the regressive event. Holocene witnessed two phases of marine high stands, the Early to Mid and Mid to Late transgressive phases. These Holocene transgressions were separated by a narrow, low stand period, around 6 ka BP. Along with early to Mid-Holocene strandline major rivers of the Mahanadi delta show anastomosing channel pattern, indicating transgressive coastline. Tornqvist,

(1993b) suggests that the principal condition for the development of anastomosing channels is rapid vertical aggradation (caused by rapid sea-level rise) and cohesive sub-soil, consisting of thick clay and organic matter. All the transgressive phases along Mahanadi delta occurred during interglacial warm climatic periods, while the regressive coastlines occurred during glacial periods. The warm interglacials could have provided enough sediments to river channels, favoring the development of an anastomosing pattern. Anastomoising channels present at Mio-Pliocene, Pleistocene and Holocene transgressive strandlines are due to high aggradation at the river mouth and riverbank instability. Shift from anastomosing to meandering pattern occurred in response to pronounced changes in flow velocity and sediment discharge. As base-level falls, the distributaries coalesce at the lower slope and incise the bedrock. Anastomosing fluvial systems along paleo-coastlines may be more abundant than that has been reported. Major deltaic systems throughout the world show distributary channel systems along paleo-coast lines (Fig. 2.19), suggesting that present-day distributary channels may be part of past anastomosing systems.

Figure 2.19 *Anastomosing channels at paleo-coastlines observed in different deltas (images from Google Earth). (a) Danube Delta showing anastomosing meandering transition across Holocene coastline, paleocoastline redrawn after Panin, 2003; (b) Mississipi delta, paleocoastline redrawn after((Chamberlain et al., 2018; (c) Mekong Delta, paleocoastline redrawn after Thi Kim Oanh et al., 2002; (d) Krishna delta, paleocoastline interpreted from position of paleo-barrier spits (e) Mahakam delta, paleocoastline redrawn after Lambiase, 2013; (f) Rhine delta, paleocoastline redrawn after Tornqvist, 1993.*

2.4.3 River mouth shifts along transgressive coastlines

River mouth shifts laterally in response to base level change to compensate for the change in its sediment load. These movements are described by their suddenness and most likely happen through an avulsion like process, which is directly related to imbalance in fluvial dynamics. A fast positive swaying of sea level drowns the waterway's mouth and diminishes the stream's sediment transporting proficiency. The

streams adjust to the increased sediment load through avulsion. At the newly occupied river mouths, progradation resumed during the subsequent regressive events. Major shifting in the river mouth position has been observed along the lower deltaic plains. River mouth shifts of Bhargavi, Kushabhadra, Brahmani and Baitarani rivers along Holocene strandlines indicate that the Holocene strandlines were transgressive. Age of the paleochannels representing river mouth shift indicates that there were two transgressional events during Holocene, conforming earlier observations of sea-level change along the Bay of Bengal coast (Banerjee, 2000; Rashid, 2014).

2.4.4 Dendritic channels along paleo-coastlines

As runoff from sloping surfaces is concentrated near to the coast, small channels form and dendritic drainage networks develop. These channels have low incision capacity due to lower elevation (close to the coast), and hence they are readily captured or shift their mouth laterally (Schumm, 1993). Several Late Holocene dendritic channels terminate at Ersama swamp along the Early Holocene strandline (between Kujang and Konark, (Fig. 2.7). Similarly, a network of dendritic channels is found between the Early Holocene strandline and the present-day coastline. These channels were developed during Late Holocene times, along the Late Holocene strandline between Paradip and Puri. OSL ages of paleochannel sections at Dobala and Padmapur indicate their origin along the Late Holocene coastline. The dendritic channels towards SW of Chilka Lagoon were developed along Mid-Late Holocene strandline, and these channels exhumed during the late Holocene sea-level retreat. This type of channel behavior has been documented for a different environment at the foot of the Book Cliffs (Rich, 1935), the Henry Mountains in Utah (Hunt et al., 1953), and the Beartooth Mountains of Montana (Ritter, 1972), but the general morphologic situation is similar. Fan et al., (1990) have located a series of buried paleochannels along paleo-coastlines of Yingge sea basin continental shelf region (Fig. 2.20). Dendritic channels commonly develop in marshy/tidal flat regions of the coast. These channels are shallow and narrow, with low incision capacity. When sea level retreats, they are either captured by larger rivers or become abandoned, and are preserved as paleochannels in sedimentary records.

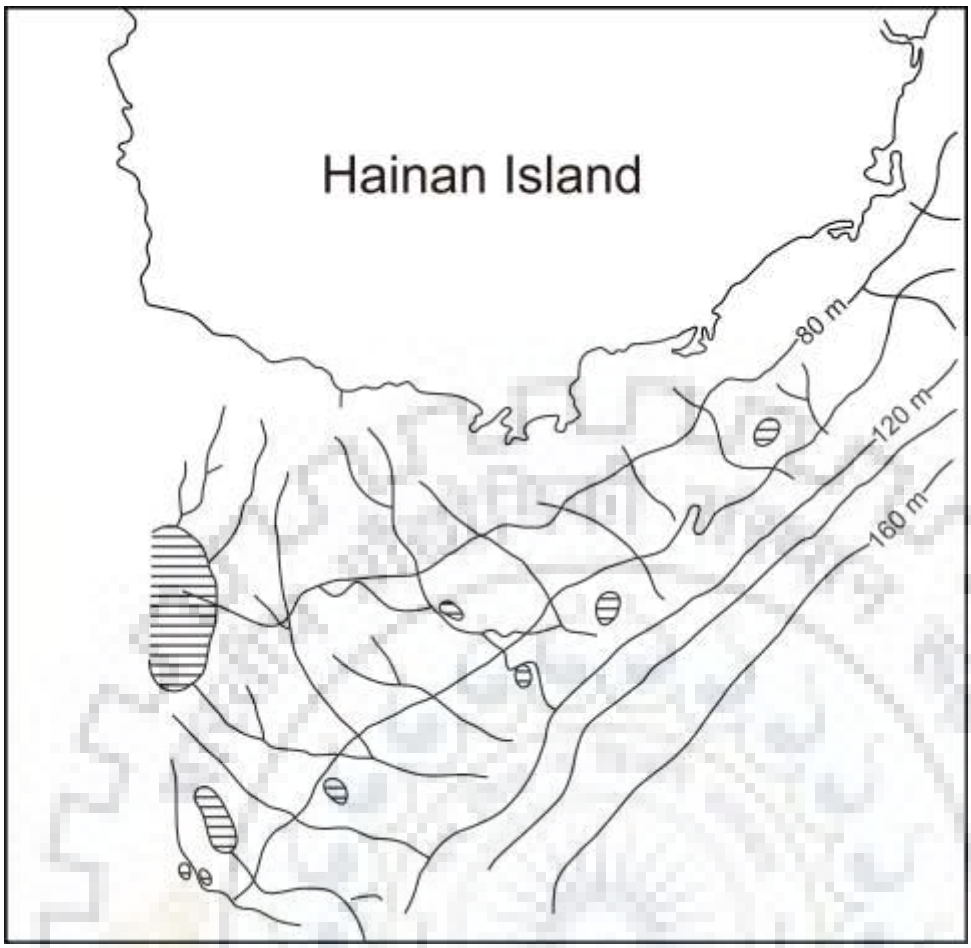

Figure 2.20 *Dendritic paleochannel systems along paleo-coastlines Yingee sea basin. Buried paleo-channels indicate that sea level remained for some time at the -50m (longest time here), -100m, and -130 to -140 m(lowest level) water depths, and that corresponding paleo-coastlines were formed at the respective depths (redrawn from Fan et al., 1990).*

2.4.5 Implications for coastal research

The present study shows that the major rivers have migrated up to the present coastline with base-level adjustments to changing coastline, while the small channels ended abruptly with retreat in sea level. The small channels could not adjust to the base level changes; hence channel aggradation occurred, which promoted termination of the channels. Ages of paleochannels corroborates with the timing of the paleo-strandlines. Similar fluvio-geomorphic features have been observed along all the major deltas of the world. The study of paleo-fluvial features along paleo-coastlines would add to better understanding/prediction of future fluvio-geomorphic changes in relation to rising sea levels. River mouth frameworks are in the focus of environmental research because of the enormous economic significance of the area, so that for sustainable development, management and future modeling of these environmental systems can be possible. As

a large part of human civilization depends on deltaic zones, both present and future infrastructure projects need to be studied in the framework of geomorphic models. These studies allow a better understanding of geomorphic scenarios not only for recent processes but also for the geological development of the area and its future projection. The comparison of coastal and river mouth environments of different marginal seas will lead to a deeper understanding of the processes within the land-ocean transition zones.

2.5 Summary

Remote sensing, chronological and GPR based studies suggest that the drainage morphology of Mahanadi delta is controlled by various stages of sea-level changes since Pleistocene. Various morphological changes representative of sea-level changes indicate that in coastal environments sea-level fluctuations are important contributing agents in modifying the deltaic geomorphology. The anastomosing –meandering transition, river mouth shift and the dendritic channels along the paleo-strandlines are indicative of various stages of marine transgression and regression along the Mahanadi delta. OSL ages reveal that the river mouth shifts along the Holocene strandline were prominent. Most of the river sinusitis along the present-day coast is because of mouth shift along the paleo-coasts. The chronology of dendritic channels supports the position of paleo-strandlines. GPR study along the Holocene strandlines reveal sub-surface shallow marine structures. A comparison with other deltaic systems of the world indicates that similar phenomenon of sea-level control on fluvial geomorphology of deltaic systems are prominent along all the major deltaic systems.

Chapter 3

PALEOCLIMATIC RECONSTRUCTION FROM LAKE SEDIMENTS ALONG MAHANADI DELTA

3.1 INTRODUCTION

Since origin, there have been considerable fluctuations in the Earth's climate due to several internal and external forces. Solar activity, volcanism, and tectonics, etc. are several important factors controlling the climate change (Arthur et al., 2013; Foukal and Lean, 1990; Hoorn et al., 2010; Lean et al., 1995; Patel and Bhatt, 1995; Raymo and Ruddiman, 1992; Sarkar et al., 2003b, 2003a). Over the past century, there has been considerable progress in studying earth's climate fluctuations and its causative factors. There has been a growing number of evidence that over the past 1500 years centennial-scale climate oscillations affected broad areas of the earth. Efforts have been made to extend the understanding of climate variability beyond the instrumental and historical records. Millennial-scale climate periodicities have been recorded from lake sediments, marine sediments and speleothems (Bianchi and McCave, 1999; Bloemendal and deMenocal, 1989; Bolton et al., 1995; Warrier et al., 2017; Yadava and Ramesh, 2007). These climatic oscillations not only affected the high latitude areas of the earth, past studies suggest that they also affected monsoon dominated regions.

Nearly 80 % of South East Asia's annual precipitation is controlled by Indian Summer Monsoon (ISM), which plays a vital role in sustaining agriculture and economy. ISM shows fluctuation over intra-annual, annual, decadal, centennial and millennial to multi-millennial time scales (Singh et al., 2019, 2018, 2012, Tiwari et al., 2009; Wasson et al., 2013). Yearly to decadal-scale variations is archived by meteorological information going back just to 197 years. This restricted information has given a coarse resolution study on the effects of worldwide atmosphere change on ISM. For interpreting low recurrence variations (for longer timescales), many fine-resolution climate proxies are analyzed, for example, tree-rings, corals and ice-cores, which give information of high resolution past climatic variations (1 year or less), and speleothems, ocean sediments, which do likewise, yet with a coarser resolution (yearly to decadal) (D'Arrigo et al., 2001, 1992; Grudd et al., 2002; Lachniet, 2009; Roberts et al., 1998). The process of transforming such proxy information into the important

climatic parameters (for example, precipitation) is generally alluded to as 'reconstruction' in the palaeoclimatic literature. The Arabian Sea and Bay of Bengal offers an incredible chance to examine past variations in ISM with relations to climatic changeability as it encounters exceptional bio-geochemical changes with variation in precipitation, which get recorded in corals and sediments (Madhupratap et al., 2003; Shenoi et al., 2002; Vaz and Banerjee, 1997; Warrick et al., 1993). Of a few studies that attempted to reproduce past ISM variability, longer records demonstrate that it was more pronounced during the interglacial and weak during the glacial time frames (Stefani and Vincenzi, 2005; Yang and Ding, 2008). A few compelling components hypothesized to clarify the monsoon inconstancy on various timescales (decadal to millennial) incorporate both internal (for example, variations in ocean-atmospheric framework, changes in green-house gases, volcanism, glaciation and vegetation spread) and external causes (insolation changes due to Milankovitch cycles and changes in the sunspot activity). High-resolution studies have uncovered that much the same as climatic oscillations appeared during Pleistocene glaciation and interglacial stages, large variations during present interglacial times is also observed in many of the past climatic studies. The present interglacial period, the Holocene (11,700 years), however, viewed as a time of moderately warm period, was punctuated by interims of short and long term changes, for example, the 8.2 kyr cold event and Holocene Climate Optimum (Alley et al., 1997; Dean et al., 2002; Mischke and Zhang, 2010; WANG et al., 2002). The Holocene is the main interim in the geological time-scale whose limit (the Pleistocene–Holocene limit) is characterized climate-stratigraphically as opposed to other Phanerozoic age limits which have been characterized bio-stratigraphically. The base of the Holocene is fixed in the North Greenland Ice Core Project (NGRIP) (Walker et al., 2009) record at the boundary demonstrating the most clear sign of climatic warming, an event that denotes the end of the last cold period (Younger Dryas) of the Pleistocene. Even though the International Stratigraphic Commission has yet proposed no formal subdivisions of the Holocene age, most researchers freely use the terms 'early Holocene', 'mid-Holocene' or 'late Holocene' when alluding to climatic changes seen during different time interims over the most recent 11,700 years. Holocene climatic changes would thus be able to be considered as perturbations in the general hotter period which started ~ 11,700 yrs BP after the short spell of the colder Younger Dryas interim. The rare record of Younger Dryas in numerous parts of the world itself puts imperatives on perceiving the Pleistocene–Holocene limit. When a standard Global

Boundary Stratotype Section and Point (GSSP) is proposed, it depends on some characteristic facies, which frequently varies with locality. On account of Holocene, the facies of GSSP is ice. Along these lines, for denoting the base of the Holocene in the Indian region is the end of Younger Dryas or gets a radiocarbon date near 10,000 yrs BP (chronometrically). The division of the Holocene for any marine sedimentary or lake sediment records in tropical regions would be founded on chronometrically decided dimension rather than a solid sign of the end of the Younger Dryas.

Apart from the broad Holocene climate changes, instrumental records reveal that there has been strong inter-annual to inter-decadal variability of ISM for the last 150 years. Throughout the world, periods of severe drought causing a million deaths have been recorded during the 14^{th} and 15^{th} centuries due to decadal-scale climate variability. Several historical records show that there were periods of severe drought-induced famines and large scale deaths during 14^{th} and 15^{th} centuries, which was the period of solar minima (Sporer minimum)(Beer et al., 1998; Camenisch et al., 2016; Eddy, 1983; Jiang and Xu, 1986; Miyahara et al., 2006; Schröder, 1994). Several draught induced famines are also recorded during periods of Munder and Wolf minimums. Mishra et al. (2019) have reported six major draughts from 1870 to 2016, linked with the positive phase of El Niño–Southern Oscillation. As reported by the Center for Research on the Epidemiology of Disasters (2005) during the 1960s failure of ISM for three consecutive years caused the death of about 1.3 million people in the Asian subcontinent. This large scale Spatio-temporal variability of ISM warrants the necessity of determining longer records of climate periodicities (Berger et al., 2002) and its projection to the future. Millennial-scale periodicities are deciphered from marine records (Bond et al., 1997), while decadal-to century-scale periodicities are analyzed through detailed examinations of different paleoclimatic records from lacustrine environments (Chen et al., 2015; Grudd et al., 2002; Liu et al., 2009; Ojala et al., 2015) and speleothems (Muñoz et al., 2015; Yadava and Ramesh, 2007). To recognize the millennial, centennial and decadal-scale periodicities, spectral analysis is carried out on various climatic proxies. A clear understanding of this will enable future understanding of the rainfall variability in the Indian subcontinent. Periodicities in the ISM have been recorded for the past few years from instrumental data. However to ascertain long-term periodicities past records of rainfall variability are required. An

important aspect of Lake Sediment record is it preserves a good temporal resolution of local and regional climate.

For this study, we present high-resolution sediment records from an inland freshwater lake (Anshupa Lake) and a brackish water lake (Chilka Lake) along Mahanadi delta to understand Quaternary climatic history. Multiproxy studies including environmental magnetism, C/N ratio and stable isotopes have been carried out to understand the impact of local and regional climate changes on the temporal variability of ISM. Environmental magnetism along with other supportive proxies has been widely used as an important tool in reconstructing past rainfall variability. Several workers have attempted to reproduce past monsoonal precipitation utilizing: I) wind speed related variables like lithogenic grain size (Clemens and Prell, 1990; Sirocko et al., 1991), ii) upwelling-and productivity-related variables like *G. bulloides plenitude*, δ15N and natural carbon content (Altabet et al., 2002; Clemens et al., 1996; Naidu and Shankar, 1999; Naidu and Malmgren, 1996; Prabhu and Shankar, 2005), iii) monsoonal precipitation related variables like ocean surface salinity (Chodankar et al., 2005; Prabhu et al., 2004), and iv) chemical weathering and pedogenesis related fluctuations like magnetic grain size and Ti/Al ratios (Colin et al., 1998; Shimmield et al., 1990). It might be noted that the above parameters are indirect and do not give a direct record of the precipitation. Paleoclimatic investigation of sediment cores from Southern Indian lakes (Bhattacharyya et al., 2015; Sandeep et al., 2017; Shankar and Pandarinath, 2008; Warrier et al., 2017) had proposed that high-resolution magnetic susceptibility (χlf) might be utilized as an important tool for past monsoonal reconstructions. A positive relationship between χlf and instrumental precipitation has been recorded by Shankar (2006), for a duration of 130 years.

3.2 METHODS

3.2.1 Core collection

Two cores (~2.3 m and ~1.3 m core from Chilka and Anshupa Lake respectively, Fig, 3.1) were recovered from the middle of the lake using PVC pipe. The cores were immediately subsampled at 0.5 cm intervals and stored in a freezer. An integrated approach using mineral magnetism, CHNS, and stable isotope analysis was carried out to study the climatic impacts on depositional environments of the lake

sediments. Chronology was obtained from 14C dating of bulk organic matter and intact shells.

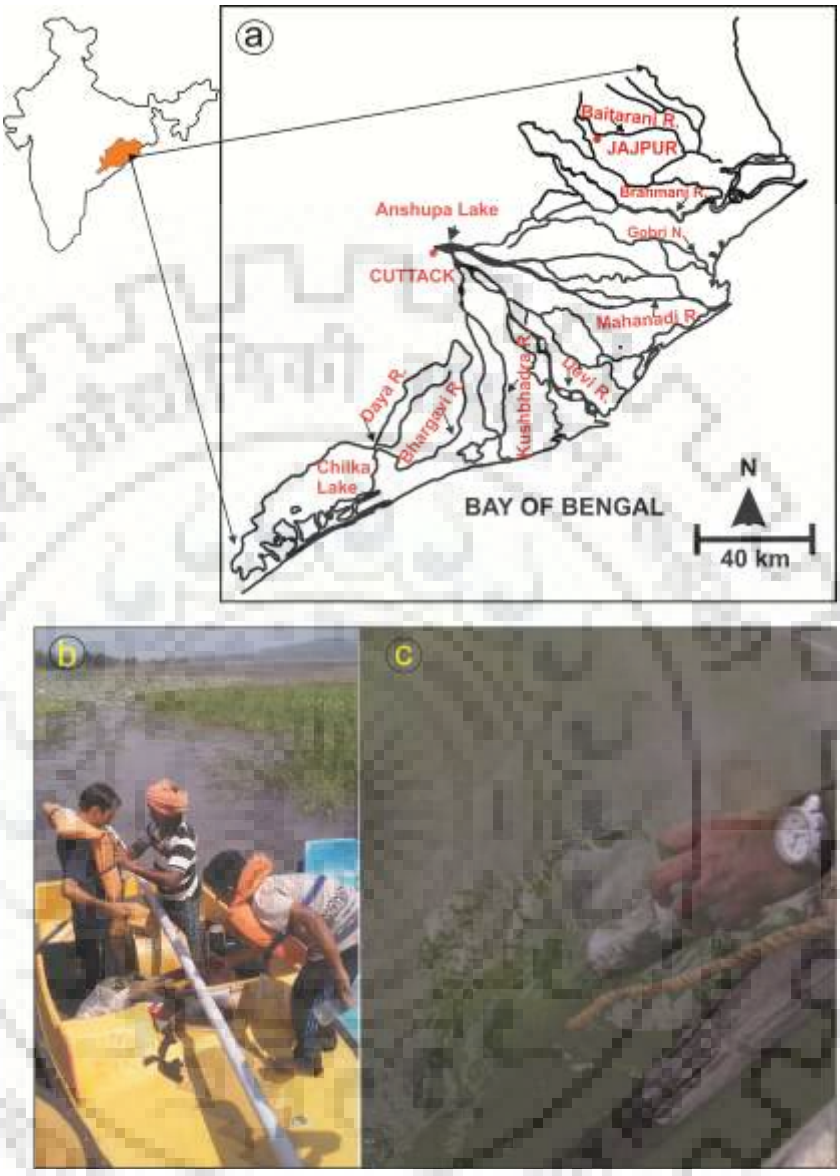

Figure 3.1 (a) *Locations of Anshupa and Chilka Lake along the Mahanadi delta, (b) and (c) field works during core collection with PVC pipe.*

3.2.2 14C dating

Air-dried samples were powdered, homogenized and studied under a microscope to ascertain the presence of any modern impurities like roots, etc. Samples (~1g) were weighed and transferred to centrifuge tubes for pretreatment. ABA (acid-base acid) protocol was followed according to Brock et al. (2010). First, sediment samples were treated with 1N HCL for about 3h at about 60° C. Subsequently, samples

were washed with 0.5 N NaOH and further with 1N HCL to remove humic acids and CO_2 formed during previous steps. Sediments were washed repeatedly after each pretreatment step at about 750 rpm till the pH reached 7. Samples were freeze-dried overnight to remove water content and were packed in tin capsules for graphitization using the IonPlus automated graphitization equipment (AGE) (Fig.3.2) (Němec et al., 2010; L Wacker et al., 2010; L. Wacker et al., 2010). Samples were combusted at 900 °C in the presence of O_2 in the elemental analyzer (EA) of the AGE system and the CO_2 from this combustion was transferred to a glass tube, where it reacted with H_2 gas and reduced into graphite powder in the presence of Fe as a catalyst:

$$CO_{2(pure)} + H_{2(gas)} \xrightarrow{Fe(S)} C_{(graphite)} + H_2O_{(vapors)}$$

Following this, graphite was pressed into cathode capsules and placed into a cathode wheel of AMS for radiocarbon measurements.

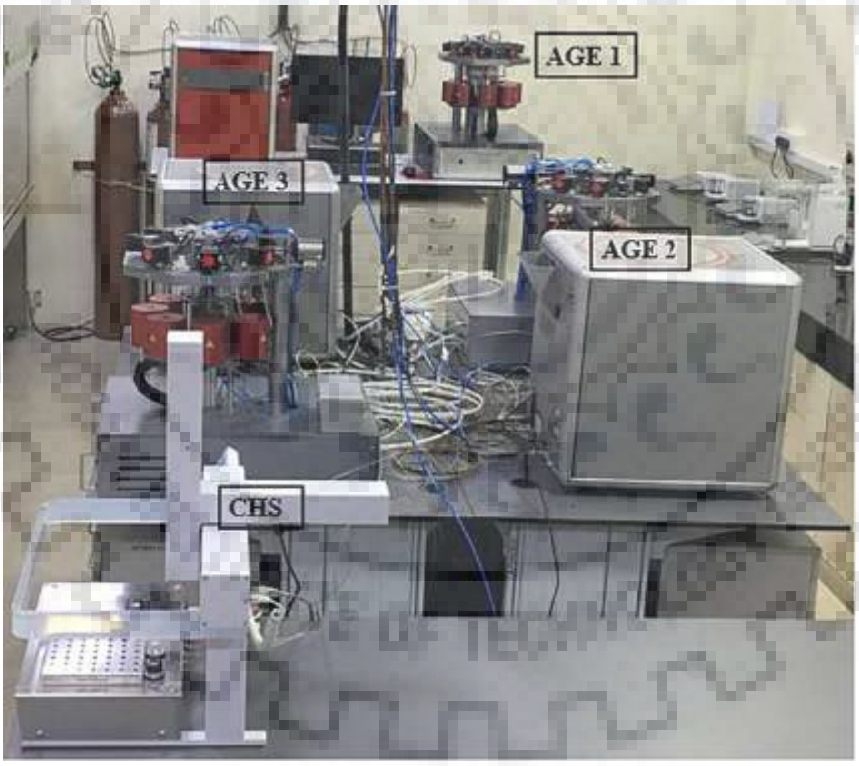

Figure 3.2 *Automated Graphitisation Equipment at IUAC New Delhi*

3.2.3 Mineral Magnetic measurements

Sediment samples were tightly packed in 10 cc plastic bottles for rock magnetic measurements. Bartington Susceptibility Meter (Fig. 3.3a) (Model: MS2B) was used to measure the magnetic susceptibility at both low and high frequencies (0.465 and 4.65

kHz; χlf and χhf respectively). Before measurement instrument was calibrated with 1 % Fe_3O_4 standard. Frequency-dependent susceptibility (χfd) and percentage χfd was calculated using χlf and χhf:

$$\chi fd = \chi lf - \chi hf$$

$$\chi fd(\%) = (\chi lf - \chi hf)/\chi lf$$

Anhysteretic remnant magnetization (ARM) was applied to the samples with an alternating field (AF) demagnetizer and an ARM attached (Fig.3.2 c). The ARM was grown steadily and was measured on a Molspin spinner fluxgate magnetometer (Fig. 3.2 d).

Mass-specific ARM was calculated according to (Walden et al., 1999) :

$$Mass\ specific\ ARM\ (Am^2kg^{-1}) = \frac{Total\ Combined\ Vector\ (10^{-3}Am^{-1}) \times 12.9(10^{-6}m^3)}{Sample\ Weight\ (kg)}$$

Where 12.9 x 10-6 m^3 is the volume of the calibration-sample.

Mass-specific susceptibility of ARM (χARM) was obtained with the ratio of mass-specific ARM and size of the biasing field (0.04 mT = 31.84 Am^{-1}; Walden et al., 1999):

$$\chi ARM\ (10^{-5}m^3kg^{-1}) = \frac{Mass\ specific\ ARM\ (10^{-5}Am^2kg^{-1})}{Steady\ biasing\ field\ (Am^{-1})}$$

Figure 3.3 *Instrumentation for mineral magnetic measurements (a) Bartington Susceptibility Meter (b) Molspin pulse magnetizer (c) alternating field (AF) demagnetiser and an ARM attached (d) Molspin spinner fluxgate magnetometer.*

Isothermal remanent magnetization (IRM) was grown sequentially at intervals 20, 40, 60, 100, 300, 500, 600 and 1,000-mT field strengths using a Molspin pulse magnetizer (Fig.3.3 b) (the maximum field attainable in the Environmental Magnetism Laboratory at Mangalore University), hence 1000-mT was considered as the saturation isothermal remanent magnetization (SIRM). IRMs and SIRM were measured using the Molspin spinner fluxgate magnetometer. Hard isothermal remanent magnetization (HIRM) was calculated as:

$$HIRM=SIRM-IRM300MT$$

To determine mineralogy and magnetic grain size Intra-parametric ratios ($\chi ARM/\chi lf$, $\chi ARM/\chi fd$, $\chi ARM/SIRM$, $SIRM/\chi lf$) were calculated (Oldfield, 2013a, 2007; Walden et al., 1999; Sangode and Bloemendal, 2004; Snowball, 1991). Common interpretations of mineral magnetic analysis are presented in the following table:

Table 3.1 Various mineral magnetic parameters and their use

Parameter or Ratio	Units	Indicative of
Mass-specific low- and high-frequency magnetic susceptibility (χlf and χhf)	(10^{-8} m^3kg^{-1})	Concentration of ferrimagnetic minerals.

Frequency-dependent susceptibility (χfd)	(10^{-8} m^3kg^{-1})	Concentration of ultra-fine grained superparamagnetic (SP) minerals.
Percentage frequency-dependent susceptibility (χfd %)	(%)	Proportion of SP grains.
Susceptibility of anhysteretic remanent magnetization (χARM)	(10^{-5} m^3kg^{-1})	Concentration of single domain (SD) ferrimagnetic minerals.
Isothermal remanent magnetization (IRM) and saturation IRM (SIRM)	(10^{-5} Am^2kg^{-1})	Concentration and grain size of remanence carrying Minerals.
Hard isothermal remanent magnetization (HIRM)	(10^{-5} Am^2kg^{-1})	Concentration and grain size of magnetically "hard" minerals like hematite and goethite.
SIRM/χlf (Wm^{-1})	10^3 Am-1	Grain size and mineralogy. The higher the ratio, the coarser the grain size.
χARM/SIRM	10^{-5} mA^{-1}	Grain size and proportion of SD remanence carrying Minerals. The higher the ratio, the finer the grain size.
χARM/χlf	Dimensionless	Grain size and mineralogy; the higher the ratio, the finer the grain size. Values > 40 indicate bacterial magnetite.
χARM/χfd	Dimensionless	Grain size and mineralogy; the higher the ratio, the finer the

		grain size. Values > 1000 indicate bacterial magnetite.
S-ratio = IRM300mT/SIRM	Dimensionless	Mineralogy (Relative proportions of ferrimagnetic vs. anti-ferromagnetic Minerals).
Oxidation Index (HIRM/IRM300mT)	Dimensionless	Relative proportion of haematite to magnetite, as a result of oxidation.
Reduction Index (χARM/HIRM)	mA^{-1}	Relative proportion of magnetite to haematite.

3.2.4 CHNS analysis

C/N ratio along with other climatic proxies, gives a better understanding of paleo-environment and paleoclimate (Meyers, 1994; Meyers and Lallier-vergés, 1999). Lake's nutrient dynamics indicate the processes involved in catchment landscape and changes in these processes are associated with a change in the regional climate. In lake sediments OM and C: N ratios alter as a consequence of changes in terrestrial export related to climatic fluctuations. Similarly, change in isotope ratios indicates a change in watershed vegetation from C4 to C3 plants (fig.3.4). Thus, analyzing changes in the dynamics of C: N ratio and OM percentage is important for understanding the multitude of processes operating within the ecosystem. Carbon to Nitrogen (C/N) ratio and Total Organic Carbon (TOC) was analyzed using an elemental analyzer (CHNSO-2000).

Samples were powdered using an agate mortar and sieved through ASTM-230 sieve. About 10 mg sample was packed in tin capsules and positioned in the autosampler for analyses. Blank tin capsules and standard BBOT (2.5-Bis (5-tert-butyl-2-benzo-oxazol-2-yl) thiophene) with known elemental composition were used to assure the blank composition. The standard deviation of analytical precision ranged from 3 to 5 %. In the TOC calculation process, all samples were acidified with a 1 M solution of hydrochloric acid to remove inorganic carbon (IC) (Hedges and Stern, 1984). Later, all samples were washed using distilled water and allowed to dry in the oven at a temperature of 40°C, and further analyzed using the CHNSO-2000 analyzer at a combustion temperature of 950 °C.

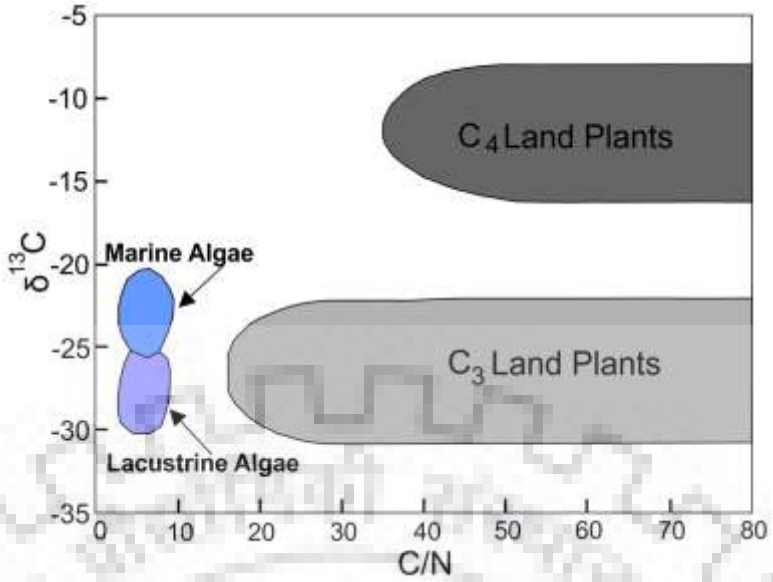

Figure 3.4 *Plot showing elemental and carbon isotopic composition of organic matter from marine algae, lacustrine algae, C3 and C4 land plants (*(Meyers, 1994; Meyers and Lallier-vergés, 1999).

3.2.5 Carbon Isotope analysis

To analyze the δ13C of natural carbon, a small fraction (~ 1 g) of bulk sediment was treated with 10% HCl for a few hours, dried and warmed at 900 °C with CuO powder and silver foil (Northfelt et al., 1981). The CO_2 developed was purified cryogenically before infusing it into the mass spectrometer. The isotopic content is expressed as δ13C in parts per thousand (‰) in respect to the Vienna-Pee Dee Belemnite (V-PDB) standard. (δ = ((Rsam) − (Rstd) − 1) × 1000, where Rsam and Rstd are 13C/12C proportion in the sample and the standard separately). The accuracy of the lab standard was ± 0.12‰ for δ13C. For reproducibility check, a couple of duplicates were run and they indicated no critical contrasts.

3.2.6 Spectral Analysis

Spectral analysis was carried out using the Acycle MATLAB extension package (Li et al., 2019). Spectral analysis was carried out on magnetic susceptibility values obtained at 0.5 cm intervals from the entire section of the core. Before spectral analysis, the magnetic susceptibility (χlf) values were sorted and resampled with median value. The data was then detrended using LOWESS (Locally Weighted Scatterplot Smoothing). Locally weighted smoothing is a popular tool used in regression analysis

that creates a smooth line through a time plot (Howarth and McArthur, 1997; McGuire et al., 1997). Spectral analysis was carried out using a robust Multi Taper Method.

3.3 PALEOCLIMATIC RECONSTRUCTION FROM ANSHUPA LAKE

3.3.1 Study Area

Anshupa Lake (Fig. 3.5) (85°86'E and 20°32'N) is one of the largest inland freshwater lakes in the state of Odisha, Eastern coast of India. The lake covers an area of 385 acres and is bounded by upper Gondwana Athgarh sandstones. The lake is situated in the upper part of Mahanadi delta at an elevation of 16 m above MSL. The catchments carry sediments from the Saranda and Bishnupur hills of Athgarh sandstone formation. The Athgarh sandstones are the northernmost expansion of the Upper Gondwana basin of India. The Athgarh Formation is a clastic succession of 700m thick, comprising conglomerates, sandstones, and shales as major litho units. Petrographic investigations of Athgarh sandstones (Sadangi and Mishra, 2015) reveal quartz dominantly with minor feldspar and rock fragments (QFL: 96.63:1.56:1.81), indicating quartz arenite type sandstones.

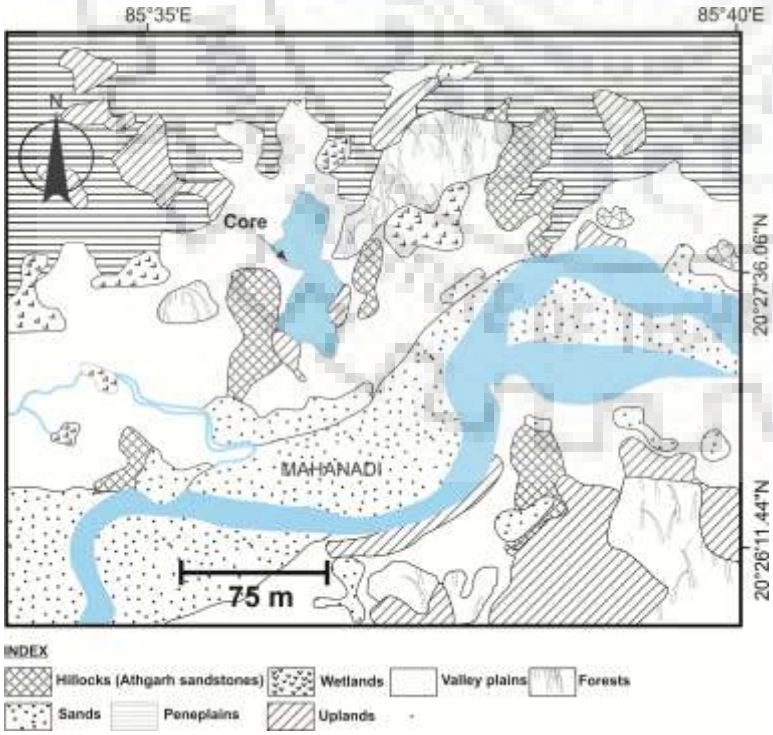

Figure 3.5 *Geological map and coring site for Anshupa Lake . Redrawn after Sadangi and Mishra (2015).*

More prominent monocrystalline quartz over polycrystalline grains proposes the source area to be of granitic/pegmatitic. The substantial minerals like zircon, ilmenite, rutile, tourmaline, brookite, kyanite, hornblende, sillimanite, monazite, and staurolite indicate plutonic and low to high-grade metamorphic rocks. Geochemical analysis with high CIA and CIW values (74.55 to 98.82 and 83.22 to 98.98, respectively) indicate prolonged weathering in the source area. The petrographic and geochemical values indicate that the sandstones were formed under warm climatic environments.

There are records of large scale deforestation in the catchment area in the recent past. The settlement report of 1920 uncovers that the lake territory was accepting a normal yearly precipitation between 53" to 57" (Das and Mohanty, 2008). With continuous denudation of forest spread, the normal precipitation has now got diminished to 48"-50" a year. The area receives around 73 rainy days and the temperature shifts from 55°F to 104°F. The humidity varies from 72% to 80% during south-west and post-monsoon periods, respectively. The area is surrounded by valleys and peneplains (Fig. 3.5). The valleys cut across the steep hills and are catchments to the lake. This lake is totally occupied with hydrophytes, particularly *Potamogeton pectinatus*. The sediments contain high silica (Das et al., 2005), and the pH changes somewhere in the range of 7.1 and 8.5. The water at times is totally without oxygen because of minimal uncovered surface and higher microbial action. The Dissolved Oxygen extends from 6.1 to 10.3 mg/L with the lowest values during pre-monsoonal months, while the BOD varied from 3.3 and 9.0 mg/L with higher values during the same period.

3.3.2 Results

3.3.2.1 Chronology

The chronology of the sediment core is obtained by AMS 14C dates. The radiocarbon ages (Table 3.2) were calibrated using CALIB 7.1 software (Stuiver and Reimer, 1993) against the IntCal 13 calibration curve (Fig.3.6). The calibrated age ranges at 95% certainty interval (2σ), and their weighted median is given in Table 3.2. Age depth modeling was carried out using OxCal online programming. The age varies from 1406 AD to recent. Sedimentation rate fluctuates from 0.09 cm/year to 0.4

cm/year (Fig. 3.7). The minimum sedimentation rate is encountered from ~1450 to ~1800 AD. The average sedimentation rate is ~0.2cm/Yr.

Table 3.2 Radiocarbon dates for Anshupa core

Sample Id	Depth (cm)	Age (BP)	Calibrated Age (BP)
IUACD#18C1810	34	181 ± 25	1943
IUACD#17C1233	77.5	159±39	1838.5
IUACD#17C1223	102	330±37	1579.4
IUACD#17C1237	124.5	434±40	1440
IUACD#17C1225	131.5	518±39	1406.3

Due to this high sedimentation rate, sampling at a 0.5 cm interval would provide fine resolution climatological information. A conceivable explanation behind this high sedimentation rate is that the lake is spread to a smaller areal extent and is supplied by a large number of watersheds running from Athgarh sandstone hills. Nevertheless, the core temporally covers the entire Little Ice Age period (1400 AD to 1800 AD) to the present day, hence would provide insight into recent paleorainfall fluctuations in the Indian subcontinent during LIA.

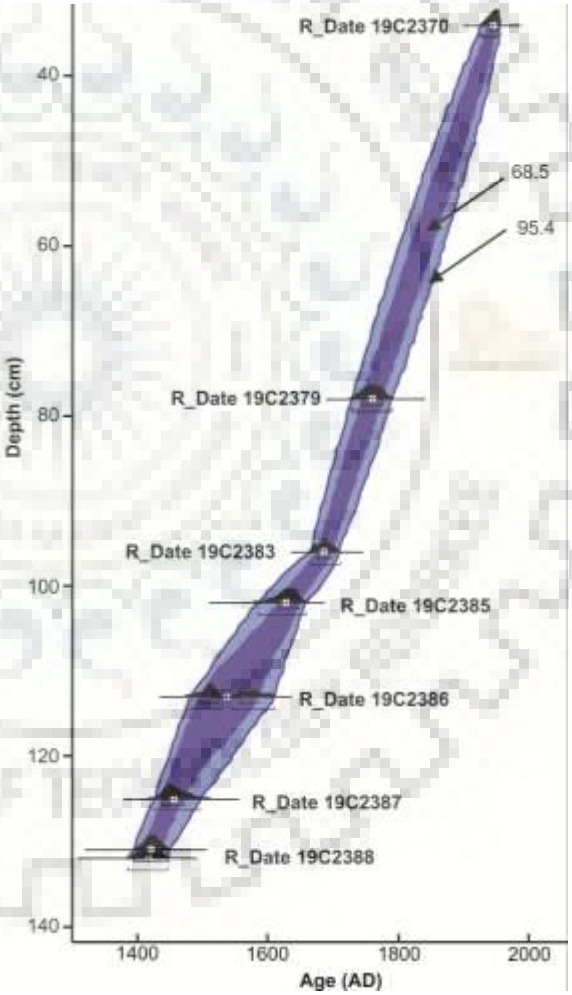

Figure 3.6 *Bayesian Age model of Anshupa Lake core.*

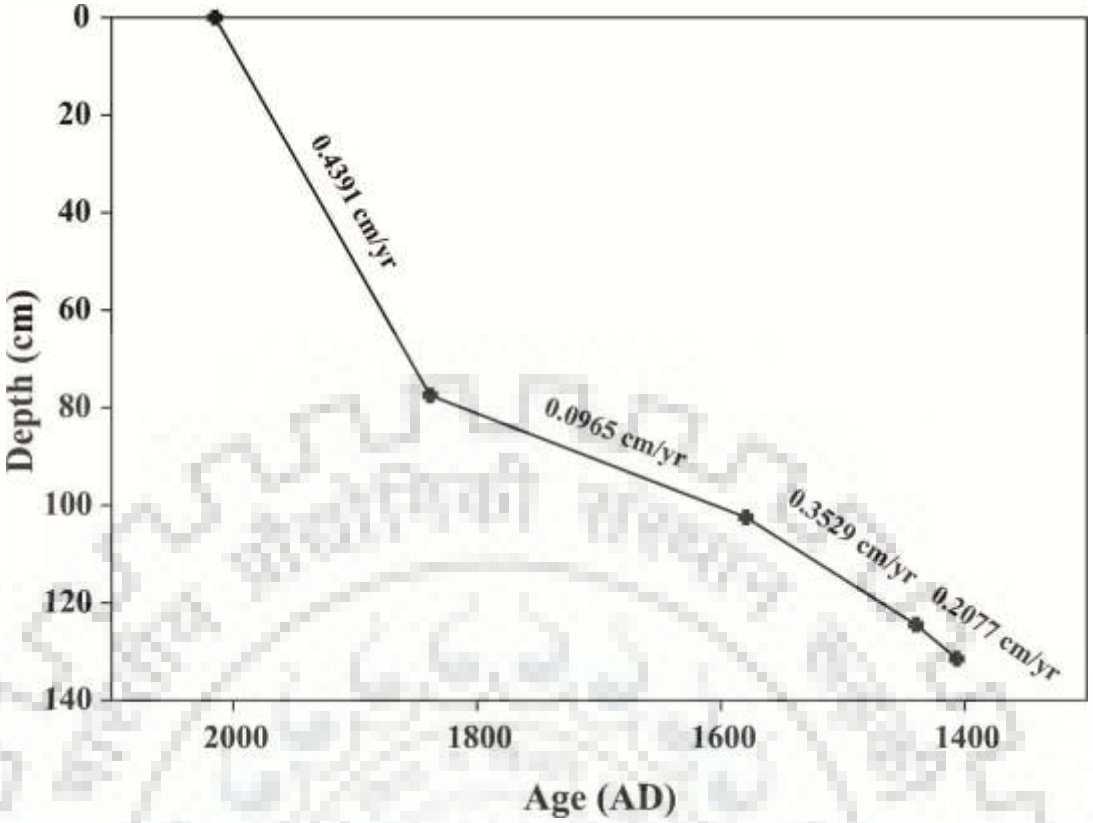

Figure 3.7 *Sedimentation rate in Anshupa Lake.Maximum sedimentation rate is found in post LIA (Little Ice Age) period and minimum sedimentation rate is found during LIA period.*

3.3.2.2 Environmental magnetic parameters

Various environmental magnetic parameters showing magnetic mineral concentration are plotted against age in fig. 3.8. The χlf represents bulk magnetic susceptibility and varies from 5×10^{-8} m^3 kg^{-1} to 60×10^{-8} m^3 kg^{-1}. The χlf values throughout the core indicate that the bulk magnetic mineralogy is mostly contributed by weak magnetic minerals, with little contribution from ferrimagnetic, ferromagnetic and canted antiferromagnetic minerals. The χlf values are minimum within a period of 1450 AD to 1800 AD. The percentage frequency-dependent susceptibility (χfd %) tells about the proportion of supra paramagnetic (SP) grains. The supra paramagnetic grains are formed mostly due to pedogenic processes, which directly depends upon rainfall (Shankar, 2006). The χfd % value varies from ~0 to ~13 %. Down core variation of χfd % increases significantly after the LIA period. Within the LIA period, χfd % shows periodic fluctuations. The Sporer minimum, Munder minimum and the Dalton minimum show minimum values comparative to the rest of the LIA period. The 16th century shows the highest peaks of χlf and χfd %. The susceptibility anhysteretic remnant magnetism (χARM) depends upon the amount of single domain (SD)

ferrimagnetic minerals. The χARM values vary from 1.15 × 10^{-5} m^3 kg^{-1} to 0.021 × 10^{-5} m^3 kg^{-1}. The saturation isothermal remnant magnetization depends upon the total concentration of magnetic minerals, and varies from 627.0126× 10^{-5} Am^2 kg^{-1} to 33.094× 10^{-5} Am^2 kg^{-1}. The SIRM and χARM curves show a similar trend as χlf and χfd %.

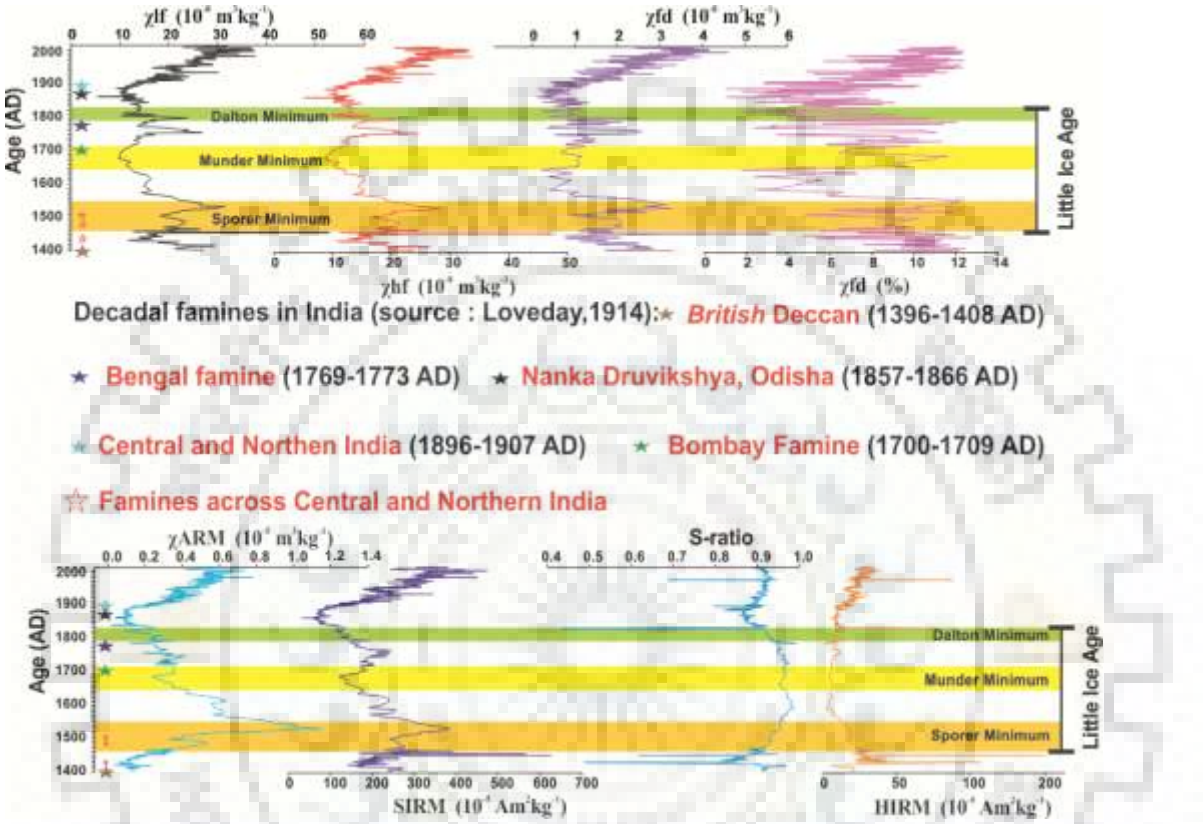

Figure 3.8 *Mineral magnetic measurements of Anshupa Lake core.*

This low range χlf values indicate less concentration of ferrimagnetic minerals, probably since source rocks are mostly sandstones, which contain more amount of diamagnetic minerals. S-ratio (IRM300mT/IRM1000mT) is characteristic of ferrimagnetic and antiferromagnetic minerals in sediments (Walden et al., 1999, Evans and Heller, 2003). S-ratio close to one means magnetically "soft" minerals like magnetite and maghemite, while low values indicate the predominance of magnetically "hard" minerals like hematite and goethite. Estimations of S-ratio in Anshupa core range from high and low values somewhere in the range of 0.4 and 0.9 (Fig. 3.8), indicating the presence of both magnetically soft and hard minerals. The bottom of the core is predominantly dominated by magnetically hard minerals like Hematite, as

indicated by lower S-ratio and high HIRM. HIRM values range from 238.86 $\times 10^{-5}$ Am^2 kg^{-1} to 1.13 $\times 10^{-5}$ Am^2 kg^{-1}.

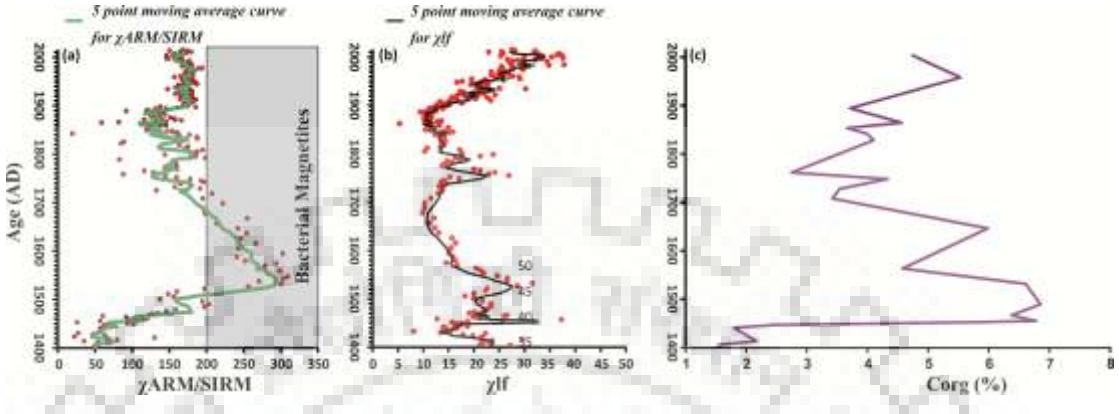

Figure 3.9 *(a) χARM/SIRM vs Age plot showing dominance of bacterial magnetite towards lower end of core (b) χlf values plotted against date and (c) Corg (%) variation with age.*

Magnetic grain size is indicated by interparametric ratios like χARM/SIRM (Fig.3.9) and χARM/ χlf (Fig.3.10). Higher the values finer is the grain size and *vice-versa*. Values of χARM/SIRM > 200 (Oldfield, 2013b) are indicative of bacterial magnetite. In the Anshupa core, the values show the exceptionally higher range at the bottom part of core i.e. >200 at around 16th to 17th centuries, which indicates the dominance of bacterial magnetite towards the lower part of the core. The χARM/SIRM plot shows dominance of bacterial magnetite at about 16th century, where Corg percentage also increases. χARM/SIRM values increase with an increase in χlf and Corg values and vice versa. Similarly, bi-logarithmic χARM/χlf and χARM/χfd is also a representative plot for bacterial magnetite. A bi-logarithmic plot of χARM/χfd (χfd is frequency-dependent magnetic susceptibility) versus χARM/χlf (Fig. 3.10) helps in distinguishing between samples rich in biogenic magnetite and those rich in ferromagnetic minerals derived from eroded soils (Oldfield, 2013b). The 16th to 17th-century χARM/χfd vs χARM/χlf data cluster in the upper right-hand corner of the plot and are characterized by high values of both χARM/χfd and χARM/χlf, which indicates a dominance of SD magnetite (magnetofossils). In contrast, data from the 17th century onwards cluster in the lower left-hand corner of the plot.

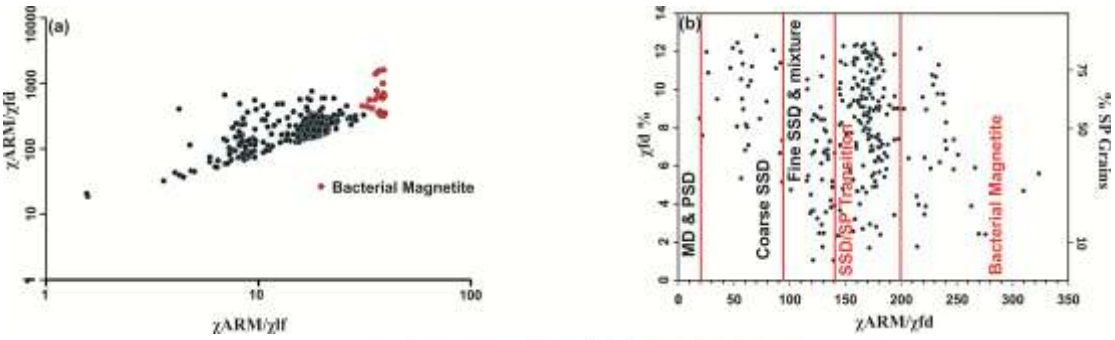

Figure 3.10 *(a) Bi-logarithmic plot of χARM/χlf and χARM/χfd. The samples with bacterial magnetite plots towards the upper right corner, while those with pedogenic origin plots towards the lower left corner of the graph. (b) The plot shows wide distribution of grainsize values, ranging from coarse SSD to SP grains.*

3.3.2.3 C/N Ratio and δ13C analysis

The total organic carbon (TOC), nitrogen, Corg/N ratio, and $\delta^{13}C$ reflect significant down core variation (Fig.3.11). Since the number of samples used for the present analysis are very few, determining small scale fluctuations are not possible. Hence, broad divisions in climate change has been documented with C/N and carbon isotope analysis. TOC ranges from 1.5 to 6 % while nitrogen content varies in range from 0.07 to 0.7 %. There is no positive variation of nitrogen content with age (Fig. 3.11). Additionally, there is a high positive connection ($r^2 = 0.549$) between the organic carbon and nitrogen (Fig. 3.11), suggesting that they are naturally derived and decline in C/N ratio is because of degradation of the organic carbon. The $\delta^{13}C$ of organic carbon fluctuates from − 26.52 to – 21.02 ‰ (Fig. 3.11). The $\delta^{13}C$ values reflect a mixed vegetation source. The bottom part of the core shows the dominance of C_4 plants, which is indicated by a more positive isotopic record. After 1450, C_3 plants and algal organic matter dominated the lake sediment. Further, the more negative trend with high rainfall events indicates that the carbon isotope records in the Anshupa core are correlated with more/less precipitation events. The C/N ratio also corroborates the $\delta^{13}C$ isotopic record. The increasing C/N ratio at the bottom of the core indicates the dominance of detrital organic matter from surrounding catchments. Further, the increasing/decreasing trend in C/N ratio are correlated with high/low precipitation events. The downcore variation reflects two phases of climate during LIA. Phase-I (1450 to 1700 AD) reflects relatively high content of TOC, more negative values $\delta^{13}C$ reflective relatively warmer climatic

condition. During Phase-II (1700-1900 AD), TOC deposition has relatively decreased and $\delta^{13}C$ became comparatively positive reflecting relatively cold climate.

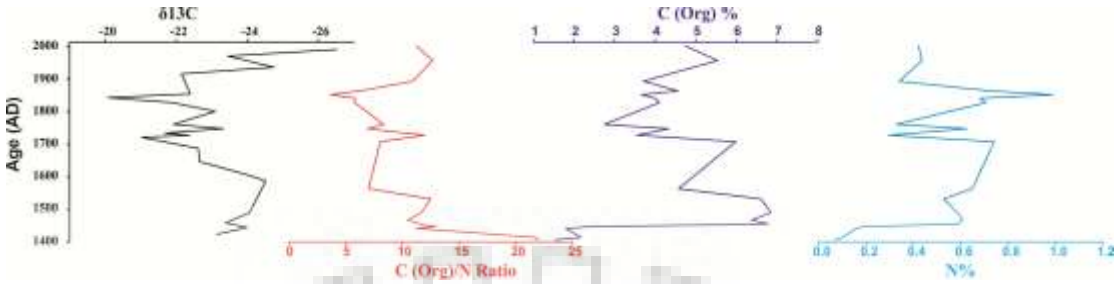

Figure 3.11 *Down core variations of δ13C, C/N ratio, C%, and N %.*

3.3.2.4 Spectral analysis

Previous works (Bhattacharyya et al., 2015; Prabhu and Shankar, 2005; Shankar, 2006; Warrier et al., 2017) suggest that χlf values show a positive correlation with instrumental rainfall data. For the present study reconstructed TSI data (Foukal and Lean, 1990) from sunspot numbers show a positive correlation with χlf values (fig. 3.12)

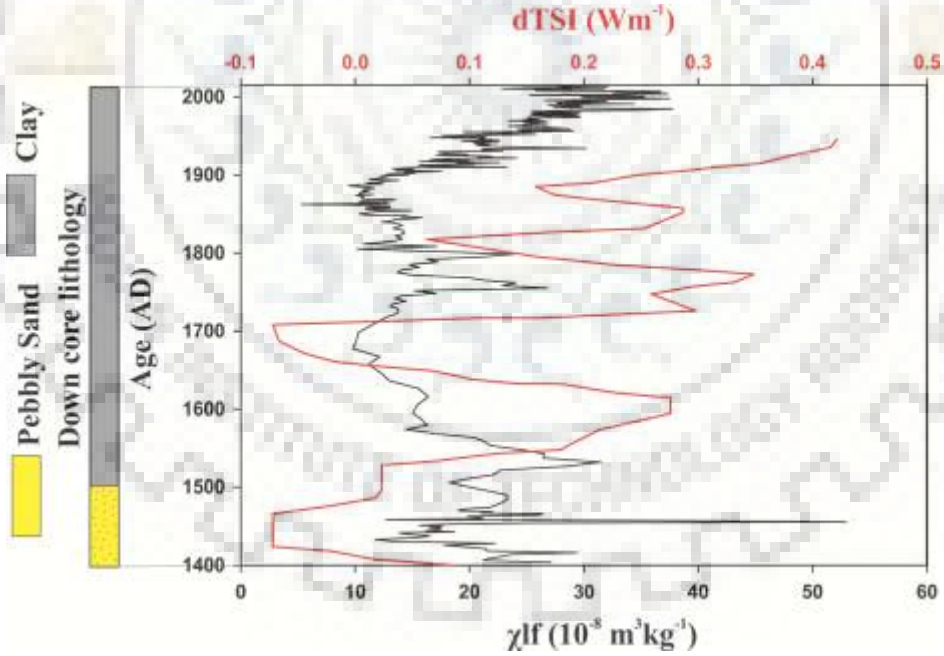

Figure 3.12 *Plot showing relation between χlf and d-TSI with at different periods. The variation trend in both the data sets show a positive correlation.*

Fig. 3.13 shows the various detrending methods and resultant detrended peaks after r-LOWESS smoothening. Major peaks were sorted out leaving a smoothened curve. Significant periodicities using multi-taper method (Fig. 3.14) (at 95% certainty

level) observed are 74, 64, 40, 36 and 11 years (fig.3.15). A significant number of them are linked to solar activity (Agnihotri et al., 2002; Thamban et al., 2007; Von Rad et al., 1999).

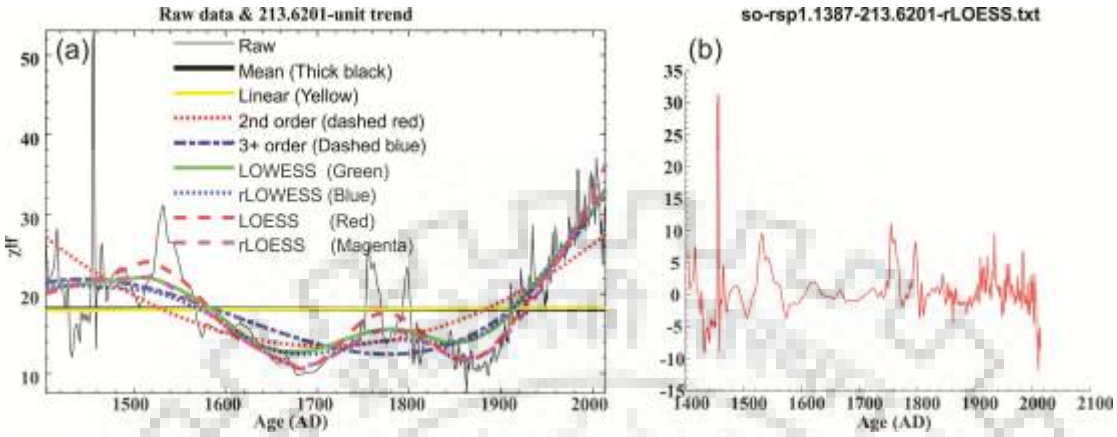

Figure 3.13 *(a) Various detrending curves applied to raw χlf data. (b) χlf values after detrended with r-LOWESS.*

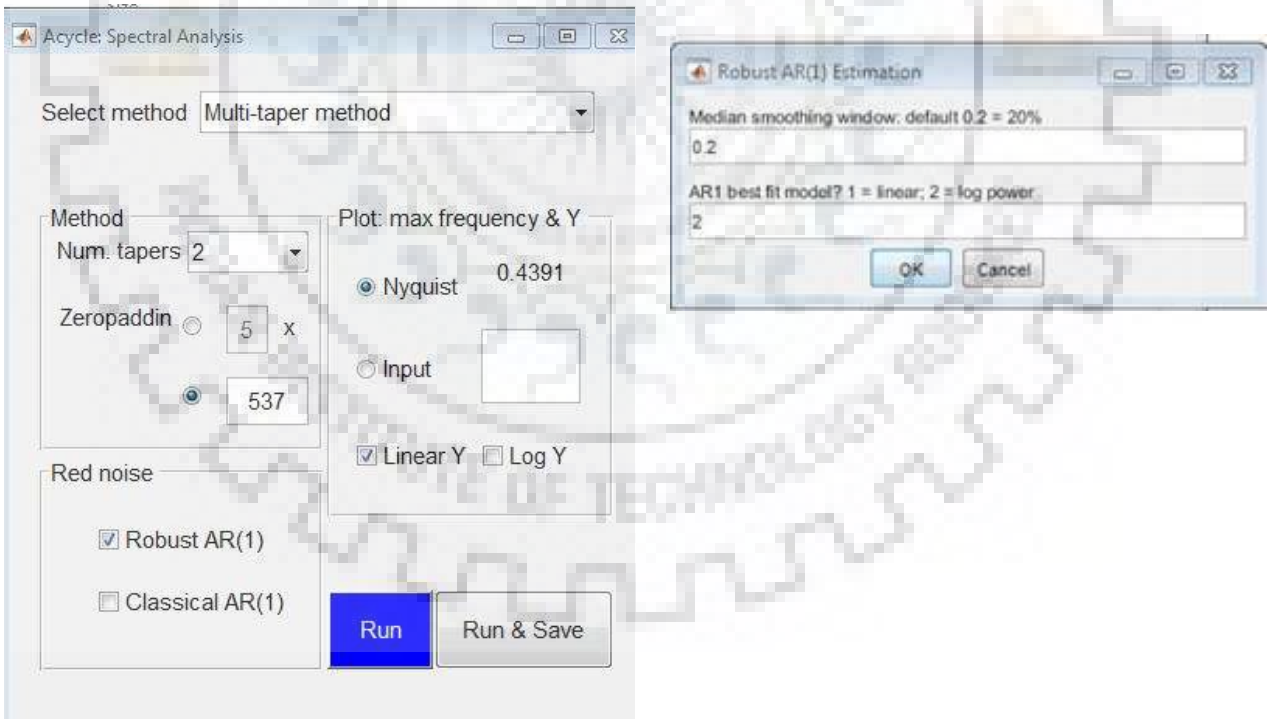

Figure 3.14 *Acycle screenshots showing application of Multi Taper Method.*

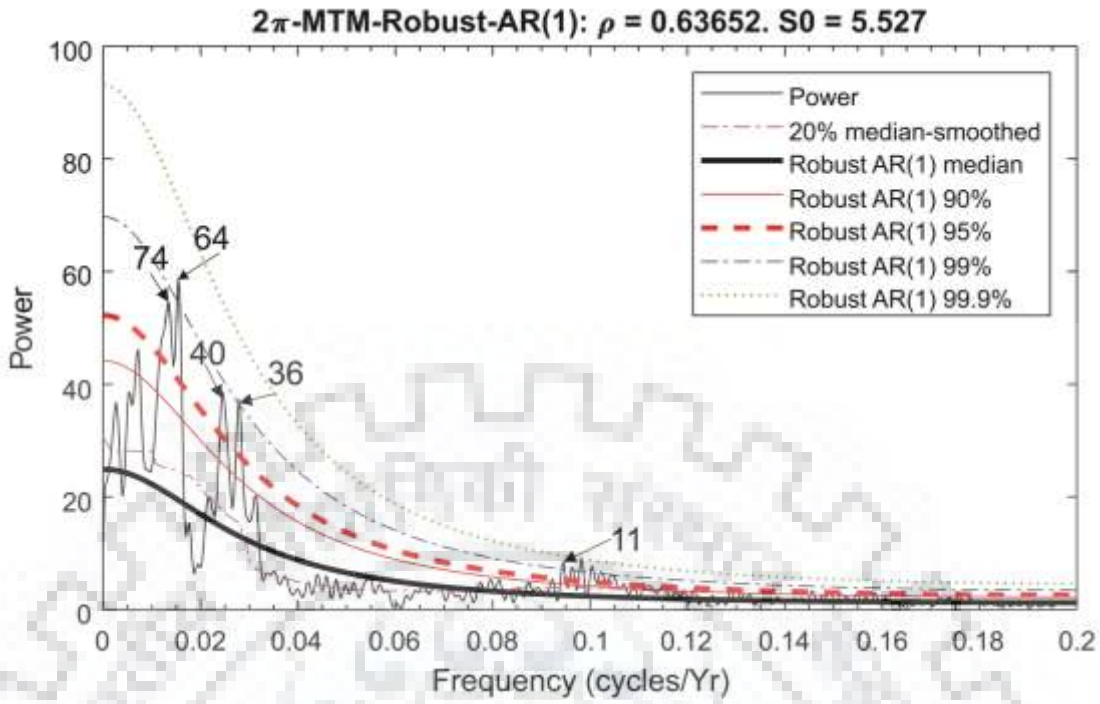

Figure 3.15 *Results of spectral analysis showing periodicities in χlf values.*

Some of the important periodicities observed in the present study are discussed below:

11 Year periodicity:

Study on sunspot numbers, geophysical data, flares and coronal lines of intensity indicates that the 11 yr. cycle consists of two maximums (Gnevyshev, 1977). The 11-year cycle coincides with the maximum of wolf numbers during the first half of the maximal. It is maximum at about the latitude of 25°. The second maxima come 2-3 years after the first maxima at about the latitude of 10°. The second maxima coincide with the biggest solar spots, geomagnetic disturbances and flares, with a 27-day cycle.

64 Year periodicity:

The 64-year periodicity is equivalent to 60-year periodicity, which has been observed in Indian Summer Monsoon by Agnihotri et al., (2002) and Agnihotri & Dutta, (2003). The 60-year cyclicity is one of the most widely spread observed cyclicity in many of the atmospheric phenomenons. The cyclicity is observed in both regional and global temperatures, north Atlantic surface temperature oscillations etc. (Chambers et al., 2012; Eisma, 1998; Knudsen et al., 2011; Schlesinger and Ramankutty, 1994). Xu et al. (2012) has observed 59-year cyclicity from $\delta^{18}O_{\text{tree ring}}$ data, which is equivalent

to 60-year cyclicity of ISM. Indian Summer Monsoon proxy from the Arabian sea also indicates a similar periodicity of 60 years (Agnihotri et al., 2002; Von Rad et al., 1999).

36 Year Periodicity

The 36-year periodicity is equivalent to 35 year Bruckner cycle (Bruckner, 1912; Halberg et al., 2010), defined by analysis of sunspot numbers. Wavelet analysis indicates that this climate cycle varies in the range of 30 to 40 years (Ponyavin, 2004). Tan et al. (2009) recorded 35-year cyclicity in Asian Summer Monsoon precipitation from stalagmite oxygen isotope variations at the south flank of the Qinling Mountains, central China. Varikoden and Babu (2015), observed SSTA over mid –Atlantic and Pacific for a period of about 100 years and correlated with Indian Summer Monsoon Rainfall. The SSTA and Indian Summer Monsoon both showed a periodicity of 32 years over the Mid-Atlantic and Pacific regions.

3.3.3 Discussion

The sediment core from Anshupa Lake covers a wide temporal range from Little Ice Age (LIA) to recent. The sedimentation rate varies from 0.09 cm/.yr during LIA to 0.4 during post-LIA times. The mineral magnetic data showed significant changes from LIA to post-LIA times. During the LIA χlf values were significantly lower than post-LIA times, except few intermediate peaks. The χlf values showed significantly higher peaks in the bottom horizon, reaching the value up to ~ 60×10^{-8} m^3 kg^{-1} .

Similarly, the grain size-dependent parameters also show the dominance of lithogenic magnetic minerals in the bottom horizon. The S- ratio values are lowest and the HIRM values are highest at the bottom of the core, suggesting the dominance of magnetically hard minerals. The χARM values are lowest in this horizon, indicating the less concentration of SD magnetite.

The mineral magnetic values show a good correlation with solar minima. The Sporer minimum (1450-1540) show a decrease in χlf values. While the 16^{th} century showed an increase in magnetic susceptibility values. Based on sunspot activity records during the period 1400–1600 AD, Jiang, and Xu, (1986) observed that the 16^{th} century witnessed more sunspot numbers than the 15^{th} century. The outcomes are as following: (l) the distributions of the 20 unaided eye sunspot records are inhomogeneous. There are 2 sightings in the fifteenth century and 18 sightings in the sixteenth century; (2) the

occurrence of auroral records is similar to sunspot activity. There are 33 records in the fifteenth century and 315 records in the sixteenth century; (3) the climatic changes in China demonstrate that the period AD 1430–1520 was cold while the period AD 1520–1620 was warm. These records indicate that the Spörer Minimum, extended from 1450-1510 AD rather than 1450-1540 AD. The mineral magnetic data from the Anshupa core showed that the 16th century witnessed higher rainfall, indicated by higher χlf values from 1520 - 1560 AD. The values decrease significantly from 1600 AD to 1700 AD. Period from 1645 – 1715 AD is marked as Munder minimum; the χlf values corroborate the previous precipitation record. The Dalton Minimum extends from 1790-1830 AD, this time period is well recorded in the magnetic susceptibility data showing a significant decrease in the values between 1790 AD-1850 AD. After 1850 AD the susceptibility values increase gradually up to the present day. Most of the decadal-scale famines occurred during the LIA period in the Indian subcontinent (Loveday, 1914). The Indian summer Monsoon deterioration during the LIA was solely responsible for such decadal-scale famines which prevailed throughout the Indian subcontinent. Two most devastating famines which occurred nearest to the present study area, the Bengal famine and the Nankadruvikshya are well recorded in the sediment mineral magnetic data.

Percentage frequency-dependent susceptibility (χfd %) values are well correlated with the susceptibility data. Frequency-dependent susceptibility (χfd) is a useful magnetic parameter for detecting the presence of ultra-fine grained superparamagnetic (SP) grains (≤ 0.02 μm diameter), which owe their origin to pedogenesis (Oldfield, 2013a, 2007). Apart from χfd, Anhysteritic Remnant Magnetism (χARM) indicates the proportion of SD grains. Oldfield, (2007) used χARM values to distinguish between various sources of fine-grained magnetic minerals. Bi-logarithmic plots between ratios of χARM with χlf and χfd were used to distinguish between pedogenic and biogenic magnetite.

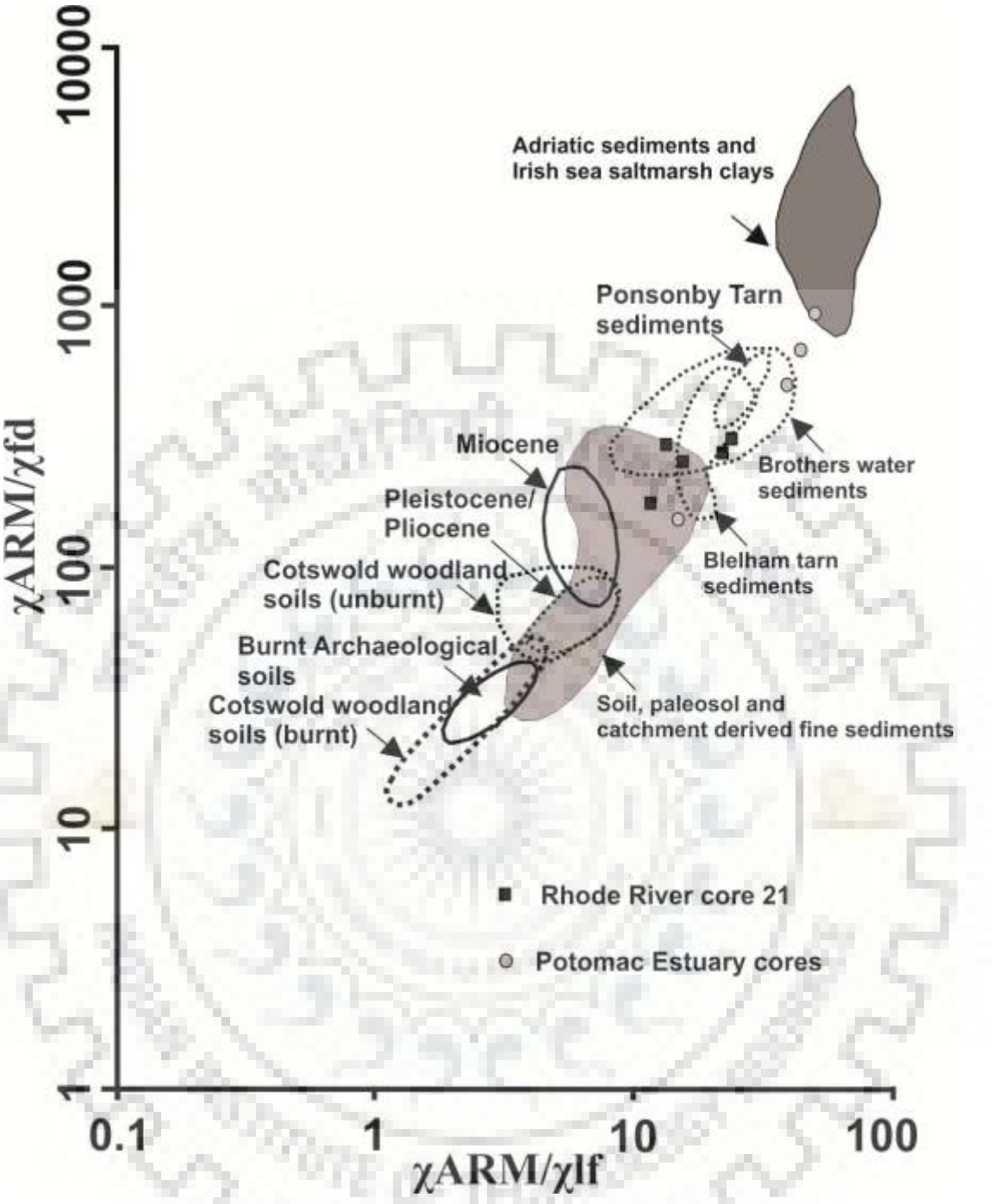

Figure 3.16 *Bi-logarithmic plot of χARM/χlf and χARM/χfd distinguishing between various sources of fine grained magnetite (after Oldfield, 2007).*

Oldfield (2007), stated that the sediment samples towards the upper right corner (fig. 3.16) of the bi-logarithmic plot indicated the presence of biogenic magnetite. With an increase in distance from the estuary, the biogenic magnetic content increased.

Biogenic magnetite is produced by magnetotactic bacteria (MTB), which utilizes a process known as biomineralization to control the arrangement of the mineral grains inside the magnetosomes (Liu et al., 2015). The procedure of biomineralization

enables the MTB to control the shape and size along with the arrangement of every individual magnetite grains. These magnetite grains vary in shape, size and arrangement between various species. They are used to follow the geomagnetic fields and its formation depends upon suitable climatic conditions (Gehring et al., 2012). These magnetite grains are contained inside an organelle envelope. This envelope is called as a magnetosome. Inside the organelle, there can either ferrimagnetic grains of magnetite (Fe_3O_4) or the iron sulfide greigite (Fe_3S_4).

For Anshupa core bi-logarithmic plot of χARM/χlf vs χARM/χfd shows a concentration towards upper right corner. Another interparametric ratio χARM/SIRM > 200 indicates the presence of bacterial magnetite (Liu et al., 2015; Oldfield, 2013b). The χARM/SIRM for the present core shows values > 200 around the 16th century. The values show maxima at around 1520 AD and gradually decrease towards the end of the 16th century. These results are further corroborated by high S-ratio, which indicates the dominance of magnetite over Hematite. S-ratio values show a gradual decrease after the 17th century, which indicates an increase in detrital input. Further increase and decrease in HIRM values also indicate less detrital input around the 16th and 17th centuries. The bacterial magnetites are dependent upon the supply of nutrients and the preservation potential (Liu et al., 2015). Fig. 3.8 shows higher organic carbon content at around the 16th century and predominance of bacterial magnetite. During 16th-century precipitation was comparatively higher and the overall sedimentation rate was lower, which offered good preservation potential for the bacterial magnetites,

The δ13C values show a mixed vegetation type. The bottom part of the core shows the dominance of C4 plants, which is indicated by a more positive isotopic record. After 1450, C3 plants and algal organic matter dominated the lake sediment. Further, the more negative trend with high rainfall events indicates that the carbon isotope records in the Anshupa core are correlated with more/less precipitation events. The C/N ratio also corroborates the δ13C isotopic record. The increasing C/N ratio at the bottom of the core indicates the dominance of detrital organic matter from surrounding catchments. Further, the increasing/decreasing trend in C/N ratio is correlated with high/low precipitation events.

Spectral analysis shows strong periodicities at 64, 40, 74, 36 years. The 64-year periodicity (Agnihotri et al., 2002; Sinha et al., 2005; Warrier et al., 2017; Yadava and

Ramesh, 2007) has been recorded in many sediment proxies and has been correlated with solar cyclicity. The 44-year periodicity also has been correlated with solar cyclicity in previous studies (Berger et al., 2002).

The χlf data for the present core demonstrate a strong 64-year periodicity. This cycle is accepted to be a significant component of the ongoing changeability of the Indian precipitation (Sinha et al., 2005). Current instrumental precipitation records likewise uncover the nearness of this cycle (Parthasarathy et al., 1993; Sontakke et al., 1993). Agnihotri et al. (2002) recorded the 60-year periodicity in a sedimentary core with organic carbon, nitrogen from the Arabian Sea. Sinha et al. (2005) recorded this cycle somewhere in the range of 11.7 and 15.2 ka B.P. in the δ18O record of a speleothem from the western Himalaya. Yadava and Ramesh (2007) recorded a 59-year cycle in the δ13C record of Akalagavi speleothem.

3.3.4 Summary

The Anshupa Lake provides a high-resolution paleoclimatic record of LIA. The magnetic susceptibility data show a good correlation with reconstructed sunspot numbers. The coldest part of the region was the Dalton Minimum. The sedimentation rate also suggests that sedimentation was minimum during LIA and later increased after the 18^{th} century. The bottom part of the core is dominated by bacterial magnetites, which are positively correlated with organic carbon content and low sedimentation rate. The magnetic susceptibility data shows a periodicity of 60 yr, 35 yr and 11 yr which are directly correlated with periodicities in ISM, and many other equivalent periodicities. Mineral magnetic, organic carbon and the $\delta^{13}C$ values indicate that the 16^{th} century was a period of higher rainfall during the entire LIA time and 17^{th} to 18^{th} century (Munder Minimum) was the driest period. All the major famines in the Indian subcontinent are correlated with a decreasing trend in mineral magnetic parameters,

which indicates that the mineral magnetic parameters of Anshupa Lake are correlated with the variability of ISM.

3.4 PALEOCLIMATIC RECONSTRUCTION FROM CHILKA LAKE

3.4.1 Study Area

The Chilka Lagoon is one of the largest lagoons along the coast of Bay of Bengal. It owes its significance due to its environmental and socio-economic importance (Fig.3.17). It covers eastern margins of three major districts along coastal Odisha i.e. Puri, Khurda and Ganjam. The tidal lagoon is around 65 km long (NE- SW), 20 km wide and the water-covered area varies between 950 km^2 during the summers, which reaches 1165 km^2 during the monsoon seasons (Siddiqui and Rama Rao, 1995). Recently, due to land degradation and siltation the water spread area of the lagoon reduced to 706 km^2 (Das and Samal, 1998). The average water depth varies from 1.73 - 3.7 m to 0.93 - 2.6 m during rainy seasons and summer respectively. The salinity differs from 0.1 to 30.6 ppt. The lagoon can be extensively isolated into four characteristic biological areas: Northern (Freshwater zone), Central (brackish water zone), Southern (marine in nature), and the Outer Channel (marine). Several hillock islands which are part of Eastern Ghats Mobile Belt are exposed in the lagoon, some important ones are Nalabana, Kalijai, Somola, Honeymoon, Breakfast and Birds islands. The lagoon receives sediment and water supply from the mostly Mahanadi delta, along with the Bay of Bengal from the west. The Chilika Development Authority (2008) reports that around 4912 million m^3 of fresh water is supplied by distributaries of Mahanadi River and around 1259 million m^3 inflow comes from the western catchment. The natural habitat of the lagoon draws in thousands of tourists, and it is additionally notable for around hundreds of varieties of seasonal birds; half of the species are intercontinental migrants far away from parts of Asia, including the Caspian Sea, Lake Baikal and Siberia. The neighborhood population around the abutting zones of the lagoon isn't just subject to it for their occupations yet additionally for religious, social and cultural activities. Over the past few decades, Chilka Lagoon has undergone an ecological imbalance because of the increase in anthropogenic activities. Overwhelming siltation is one of the main issues prompting shrinkage of the lagoon. On the southwest, the lagoon is outlined by some rocky hills (locally known as

Dipamundia, Kalijugeswar, Mamubhanaja, Solari, Valeri, Jatianasi and Ghantasila). The lagoon is bounded by alluvial plain of Mahanadi River to its north and the Bay of Bengal towards the east. It is isolated from the Bay of Bengal by a tidal gulf channel with sand bars (width differs from 100 m to 1.5 km).

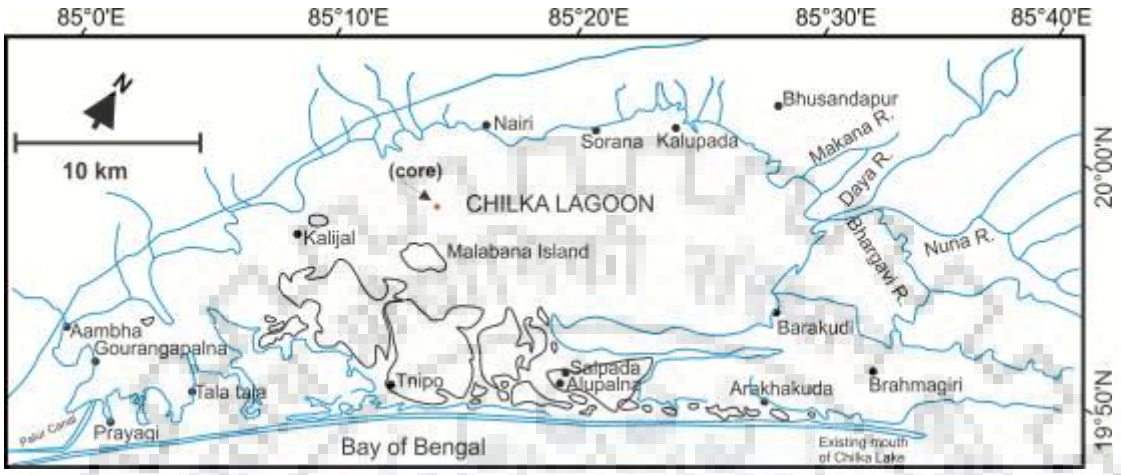

Figure 3.17 *Study area and core location of Chilka Lake (Modified after Pandey et al., 2014).*

3.4.2 Results

3.4.2.1 Chronology

The chronology of the sediment core is obtained by AMS 14C dates from marine shells (Table 3.3). The calibrated age with likelihood and median values were obtained using BACON (Fig.3.18). The age varies from 9039 cal yr. BP to recent. Sedimentation rate fluctuates from ~ 0.2 cm/year to ~ 0.007 cm/year (Fig. 3.19). The minimum sedimentation rate is encountered between 6,000 cal yr BP to 2,000 cal yr BP.

Table 3.3 Radiocarbon dates used for age modeling

LabId	Age	Error	Depth (cm)
18C1812	2225	25	46
18C1806	514	25	45
18C1805	5301	28	79
18C1808	6467	31	110
18C1804	6944	39	128
18C1814	6315	30	154
17C1254	6305	48	161
18C1802	6076	29	164
18C1803	6490	29	196

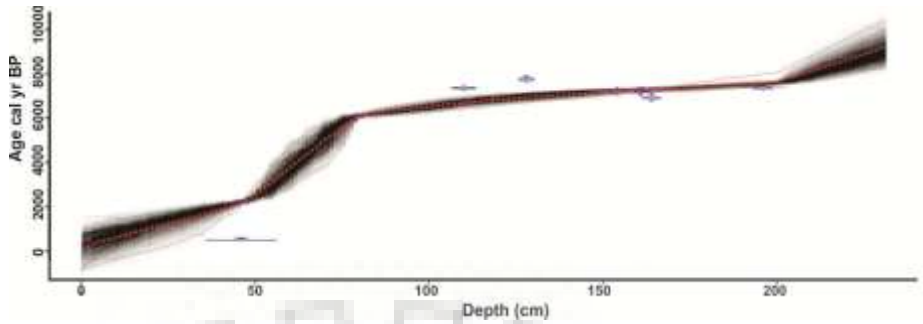

Figure 3.18 *Radiocarbon Age modeling using BACON. Lightly shaded region represents likelihood, the dark shade represents more likely hood and the red line represents median age. Blue balloons indicate calibrated age with error bars.*

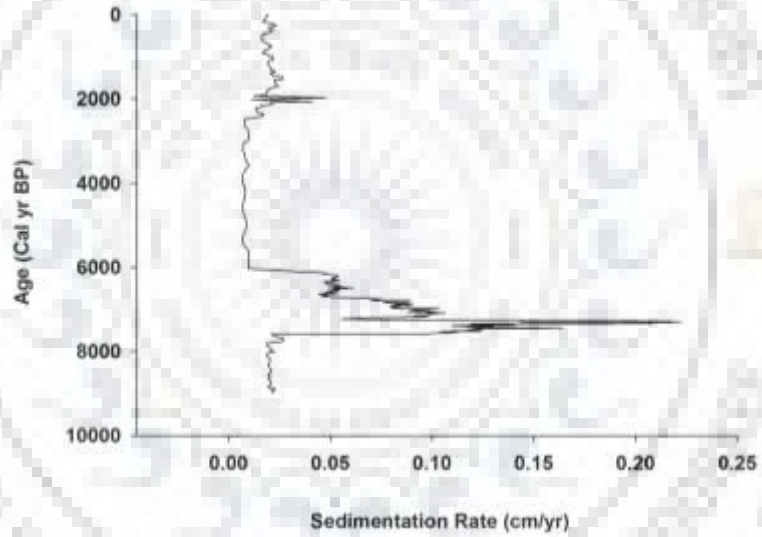

Figure 3.19 *Sedimentation rate of Chilka Lake core.*

3.4.2.2 Mineral magnetic measurements from Chilka Lake Sediments

Environmental magnetic measurements showing concentration-dependent parameters, mineralogy and grain size are plotted against age in Fig 3.20. The bulk magnetic susceptibility is represented by χlf value and varies from 6.4× 10^{-8} m^3 kg^{-1} to 43.16 × 10^{-8} m^3 kg^{-1}. The χlf values throughout the core indicate that the magnetic mineralogy is mostly contributed by ferrimagnetic minerals, with little contribution from paramagnetic, antiferromagnetic and canted antiferromagnetic minerals. The χlf values remain low throughout all depths of core, except few isolated peaks. From around 9,000 cal yr BP to 6,000 cal yr BP the values remain constant and further drop

around 6,000 cal yr BP. After 6,000 cal yr BP χlf show periodic fluctuations, with minimum values till 2,000 cal yr BP. χlf Values show a significant increase after 2,000 cal yr BP, except the LIA period which shows lower values. The susceptibility anhysteretic remnant magnetism (χARM) depends upon the amount of stable single domain (SSD) minerals. The χARM varies from $0.71 \times 10^{-5}\ m^3\ kg^{-1}$ to $0.021 \times 10^{-5}\ m^3\ kg^{-1}$. χARM remains constant throughout the core and there is a sudden increase in the values after 2,000 cal yr BP. The LIA period shows significantly lowered χARM values. The saturation isothermal remnant magnetization (SIRM) depends upon the total concentration of magnetic minerals, and varies from $636.33 \times 10^{-5}\ Am^2\ kg^{-1}$ to $44.905 \times 10^{-5}\ Am^2\ kg^{-1}$. SIRM values increase significantly towards the bottom and top part of the core. At about 6,000 cal yr BP the SIRM values show a sudden drop and remain constant till 2,000 cal yr BP. After 2,000 cal yr, BP the SIRM values show a significant increase, except for the LIA period. HIRM shows the concentration of magnetically hard minerals like hematite and goethite. HIRM values range from $58.32 \times 10^{-5}\ Am^2\ kg^{-1}$ to $1.62 \times 10^{-5}\ Am^2\ kg^{-1}$. HIRM curve show parallelism with SIRM, with an increasing trend towards the top and bottom part of the core similar to the SIRM trend. S-ratio (IRM300mT/IRM1000mT) is characteristic of ferrimagnetic and antiferromagnetic minerals in sediments (Evans and Heller, 2003; Oldfield et al., 1990). S-ratio close to one means magnetically "soft" minerals like magnetite and maghemite, while low values indicate the predominance of magnetically "hard" minerals like hematite and goethite. Estimations of S-ratio in Chilka Lake core is around 0.9, with minimum values towards the bottom part of the core.

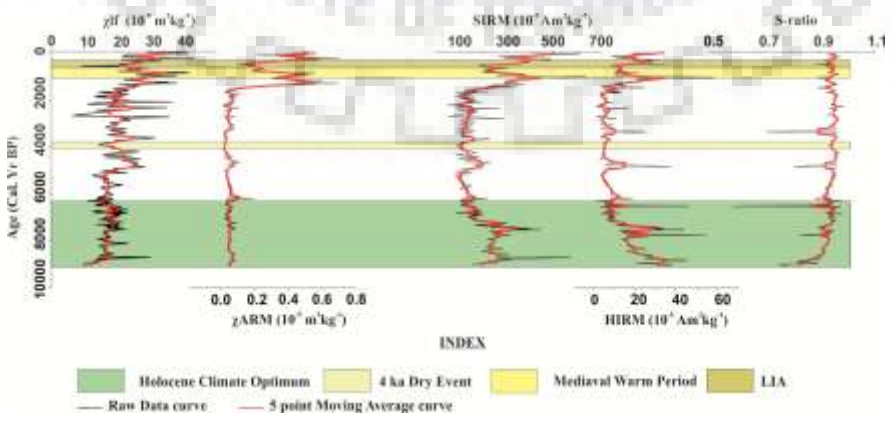

Figure 3.20 *Mineral magnetic parameters of Chilka Lake sediments.*

3.4.2.3 Spectral analysis

Spectral analysis was carried out using similar methods, as discussed in section 3.3.2.4. Detrending was carried out using r-LOESS algorithm. Various detrending methods and the r-LOESS method are shown in Fig. 3.21 and Fig.3.22 respectively.

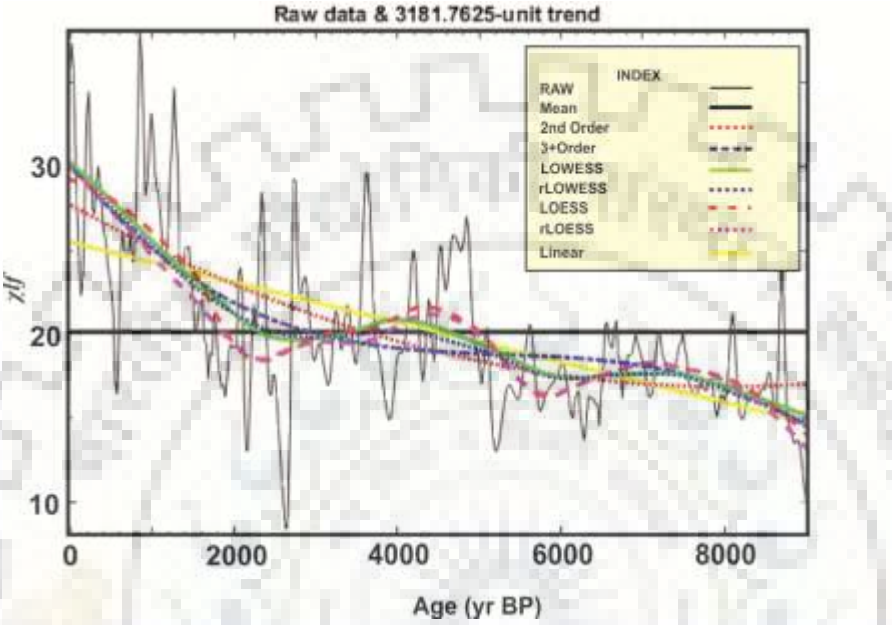

Figure 3.21 *Various detrending methods for spectral analysis.*

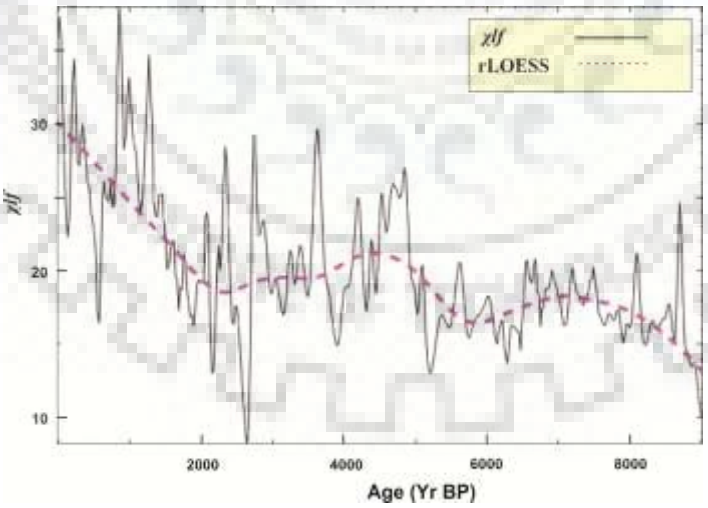

Figure 3.22 *r-LOESS detrending on χlf values.*

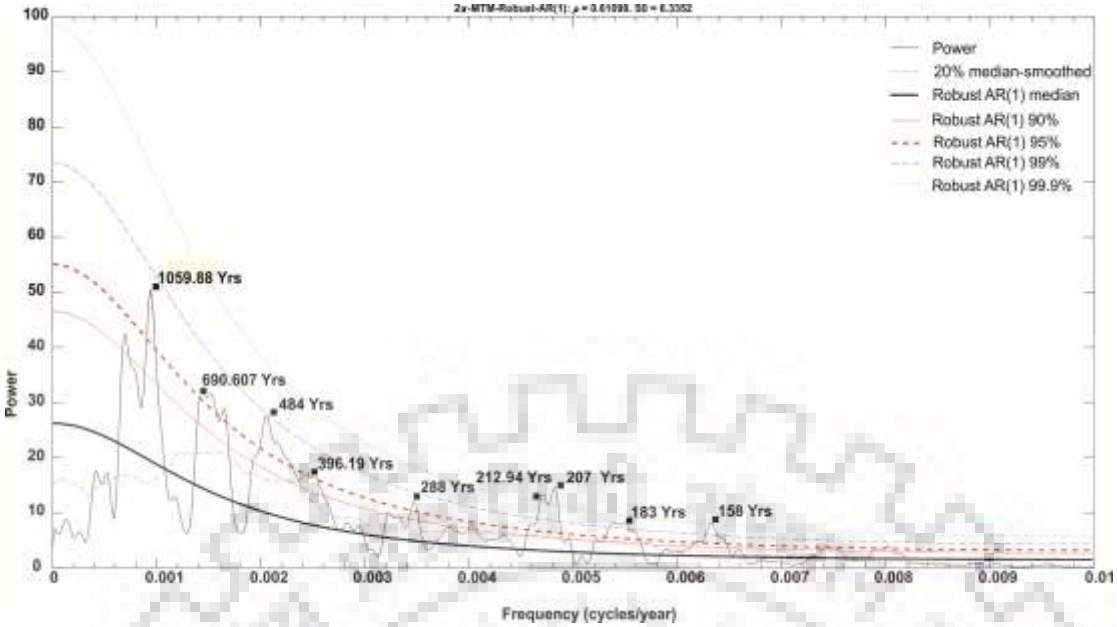

Figure 3.23 *Spectral analysis of χlf showing climate periodicities.*

Spectral analysis shows significant periodicities at 1058, 690, 484, 396, 288, 212, 207, 183 and 158 years (Fig.3.23). Many of these are linked to solar activities. The 1058 yr. periodicity is similar to 950 yr. periodicity found using mineral magnetic data from the Arabian Sea (Thamban et al., 2007), from stalagmite records (Neff et al., 2001) and from reconstructed 14 C data (Lean, 2002). The 1000 year periodicity has been found from sunspot numbers by Zhao and Feng (2015). The 690 and 288-year periodicity are similar to the 700 years and 300-year periodicities respectively found from spectral analysis of ^{10}Be and ^{14}C records (Soon et al., 2014). The 484-year periodicity is equivalent to the 500-year periodicity observed in reconstructed sunspot numbers (Zhao and Feng, 2015) and from ^{14}C or ^{10}Be data (Soon et al., 2014). The 212 and 207-year periodicities are equivalent to the 210 year Suess cycle (the de Varies Cycle, Usoskin and Mursula, 2003). The Suess cycle was one of the most intense cycles recorded in Holocene. The Suess cycle has been reported by Agnihotri et al. (2002) from Arabian sea sediments. Tiwari and Ramesh (2007) documented 215 and 230-year periodicities from foraminiferal records of the Arabian Sea. The 158-year periodicity recorded in the analysis of χlf may coincide with the 130-year cyclicity recorded from spectral analysis of atmospheric ^{14}C variations (Damon and Peristykh, 2000). The 130-year periodicity has also been recorded from aurora observations, lake sediments of Northern Great Plains (North America) (Yu and Ito, 1999), speleothem records of Oman (Fleitmann et al., 2003) and Southern India (Yadava and Ramesh, 2007).

3.4.3 Discussion

The sediment accumulation rate of Chilka Lake suggests that maximum sedimentation occurred from 8,000 cal yr BP to 6,000 cal yr BP BP, which diminished at the beginning of the Mid-Holocene period around 4,000 cal yr BP. The former period between 9,000 cal yr BP to 6,000 cal yr BP is known was Holocene warm period (HWP) or Holocene Climate Optimum (HCO). During the Mid-Holocene times, the sedimentation rate decreased (~ 0.007 cm/yr) due to initiation of arid phase in ISM, as reported in many other studies in the Indian sub-continent (Jain and Tandon, 2003; Ponton et al., 2012; Prabhu et al., 2004; Sridhar, 2007). Further, after 2,000 cal yr BP the sedimentation rate increased to ~ 0.02 cm/yr. The χlf, χARM, HIRM and SIRM curves show an increasing trend from 9,000 cal yr BP to 6,000 cal yr BP. This period corresponds to the Holocene Climate Optimum (HCO) (Fig.3.24). During Mid-Holocene (6,000 cal yr BP to 2,000 cal yr BP) period these values show a significant decreasing trend. The Mid-Holocene period witnessed a comparatively dry period with significant weakening in ISM (as cited in Fig. 3.24). High SIRM and HIRM values during HCO indicate a significant contribution of antiferromagnetic minerals like Hematite and Goethite. A high concentration of antiferromagnetic minerals indicates strong lithogenic weathering, which implies high precipitation and chemical weathering. SIRM and HIRM show a decreasing trend during the Mid-Late Holocene period (6,000 cal yr BP-2,000 cal yr BP), indicating a relatively dry period. These curves show an increasing trend after 2,000 cal yr BP indicating enhanced Indian Summer Monsoon. The bulk magnetic susceptibility, SIRM and HIRM show a decreasing trend at about 500 cal yr BP, which corresponds to the time of LIA. χARM indicate the concentration of stable single-domain ferromagnetic minerals. χARM curve shows a similar trend till 2,000 cal yr BP, after which the values increase significantly. Though HCO was a period of strengthened ISM, lower χARM indicates that the contribution of SD ferrimagnetic minerals was suppressed by the contribution of canted antiferromagnetic minerals. This indicates that the lithogenic contribution was much higher than the pedogenic contribution. Enhanced contribution from pedogenic magnetites increases the χARM values. The increasing trend of χARM after 2,000 cal yr BP indicates increased input from catchment weathered pedogenic particles. S-ratio (ratio of IRM 300to IRM 1000) varies around 0.9, with lowest values

at the bottom of the core around 9,000 cal yr BP, which indicates the dominance of canted antiferromagnetic minerals around HCO.

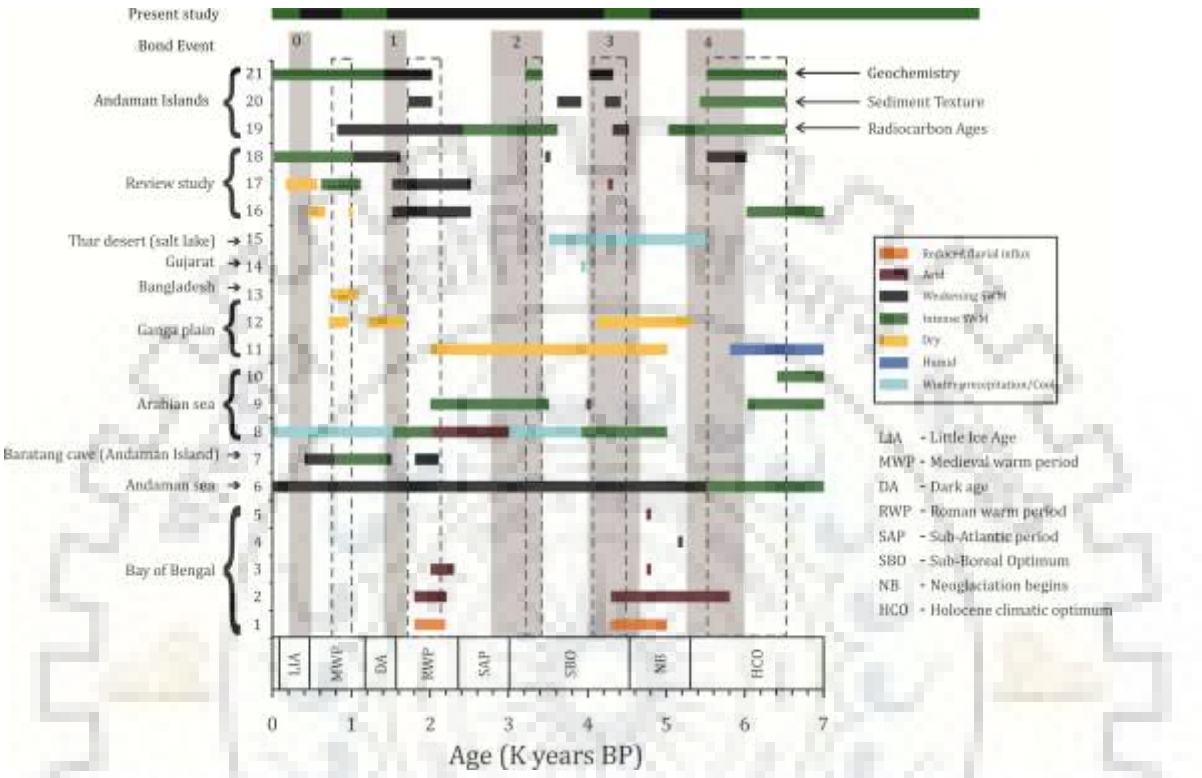

Figure 3.24 *Paleomonsoonal changes inferred from present study compared with regional paleoclimatic records during Holocene. After 1) Chauhan et al. (2004); 2)Chauhan and Vogelsang (2006); 3) Chauhan and Suneethi (2001); 4) Mathien and Bassinot (2008); 5) Chauhan et al. (2000a); Chauhan et al.,(2000); 6) Rashid et al. (2007); 7) Laskar et al. (2013); 8) Lückge et al. (2001); 9) Sarkar et al, (2000); 10)Thamban et al. (2002); 11) Sharma et al. (2006); 12) Saxena et al. (2013); 13) Alam et al. (2009); 14) Singh et al. (2007); 15) Enzel et al. (1999) 16) Patnaik et al. (2012) 17) Kuppusamy and Ghosh (2012); 18) Thamban et al. (2007); 19, 20, 21) Achyuthan et al. (.2014).*

Giosan et al. (2017) estimated Late Holocene erosion rates from Godavari delta towards south of Mahanadi delta and found that massive erosion of the delta occurred since the past 2,000 ka BP. Massive erosion towards Late Holocene was linked to land degradation due to the dominance of anthropogenic activities during the past 2,000 yrs. Fig. 3.25 shows that most of the civilizations flourished during Mid- Holocene and at around 3.5 ka BP the river valley civilizations became rare. Comparison of river valley civilizations with variation of magnetic susceptibility data indicates that the period around 3500 cal yr BP was coldest during the Mid-Holocene times and the number of

river valley settlements in the Indian subcontinent reduced. The initiation of tank irrigation around 500 cal yr BP indicates both scarcity of rainfall and the dominance of industrial activities.

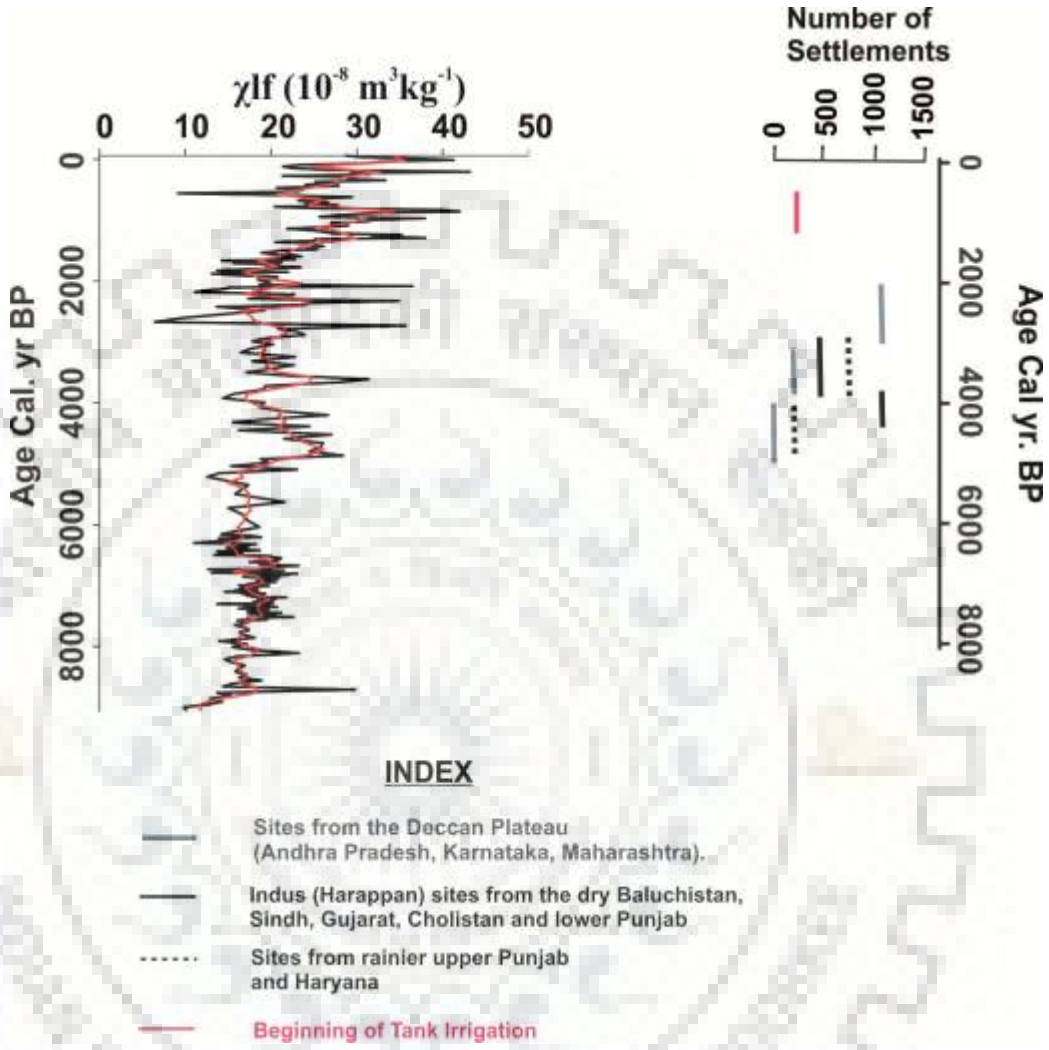

Figure 3.25 *Comparison of Magnetic susceptibility data with Historical settlements. (Historical settlement data obtained from* (Giosan et al., 2017).

The increasing trend in χARM values and sedimentation rates after 2,000 cal yr BP indicates a higher rate of catchment erosion around Chilka Lake. Though strengthening of ISM around the Medieval Warm Period may have contributed to the χARM values when compared to the rest of the core, the extremely high values may indicate additional contributing factors. Increased anthropogenic activities in the catchment area such as high deforestation, an increase in a number of settlements and industrial activity may have provided favorable conditions for land degradation and exposure to deeper erosion of the soil profile, which may have supplied more finer magnetic particles into the lake sediments. The climatic control on χARM values is

indicated by a lower trend during the LIA period. Spectral analysis shows a wide range of periodicities, all connected to solar influence. Hence it may be concluded that fluctuation in ISM has been controlled by solar cycles throughout the Holocene.

3.4.4 Summary

Though the mineral magnetic values indicate ferrimagnetic minerals, they respond to regional scale paleoclimatic fluctuations. The χlf, SIRM, and HIRM values represent a strong relationship with the variation in Indian Summer Monsoon precipitation. During strengthened ISM, downcore variation of concentration-dependent mineral magnetic parameters showed an increasing trend and *vice versa*. The Early to Mid-Holocene period corresponding to 9,000 cal BP to 6,000 cal BP was the warmest phase, represented by high sedimentation rates and increased concentration of magnetic minerals. The Mid-Late Holocene period was the coldest phase of Holocene found in the present study, represented by the lowest sedimentation rate and lowest concentration of magnetic mineral. The Late Holocene witnessed an increased sedimentation rate and a higher trend in mineral magnetic properties. Major climatic changes of Holocene like Holocene Warm Period, 4 ka dry event, the medieval warm period and LIA can be studied from the Chilka Lake core. Majority of Mid-Holocene river valley civilizations which flourished during 5 ka BP and became rare towards 3.5 ka BP. The probable dry event at about 3,5 ka BP reduced the number of settlements of river valley civilizations.

Chapter 4 CONCLUSIONS

The present study deals with two major aspects of Mahanadi Delta geology i.e. paleogeography and paleoclimatic reconstructions. Paleogeography of the delta is mostly controlled by various stages of progradation and retrogression owing to sea-level fluctuations. East coast of India witnessed major fluctuations in sea level starting from Mio-Pliocene to recent times, this led to a different sequence of fluvial and marine sedimentation along the coastal tracts. Different rivers draining into the Bay of Bengal build deltas along the eastern coast of India forming sequence of fluvial deposits. These fluvial sediment sequences were punctuated by sequences of marine depositions. Borehole data from Mahanadi delta shows the sequence of marine and fluvial deposition from Mio-Pliocene to the present day. The fluvial distributaries forming Mahanadi delta evolved through changing environmental conditions due to marine transgression and regression events. Paleochannels along different strandlines of Mahanadi delta show evidence of marine transgression and regression events. The transgressive strandlines show anastomosing channels and the regressive strandlines show meandering or straight channels. Marine transgression/regression events throughout Quaternary has been correlated with interglacial/glacial cycles. The interglacial periods are relatively warm compared to intermittent glacial periods. The warmer interglacials supplied abundant sediments for river anastomosis; hence the transgressive coastlines are marked by anastomosing channels. During glacial periods the fluvial sediment load was lesser and the rivers could adjust to the changing base level by marine transgression; hence the regressive strandlines have meandering or straight channels. Avulsion related river mouth shifts also are evidence of higher sediment load during interglacials/transgressive marine phases. Higher sedimentation rates during interglacials and decreasing accommodation space due to marine transgression led to avulsion of the fluvial channels along the coast. The river mouth shifts observed along paleo-strandlines are indicative of transgression related avulsion processes. Dendritic channels along the coastlines are formed due to flow accumulation at lower gradients. The dendritic channels are more common to low laying swampy or marshy areas along the coast. When coast line advances due to marine regression, these dendritic channels are left abandoned as paleochannels. Low base level erosion capacity of these channels leads to their abandonment during sea-level regression. Mio-Pliocene and Pleistocene strandlines along the Mahanadi delta do not show evidence of paleo-

dendritic channels as these may have been buried or altered by long-duration exposure to deltaic fluvio-geomorphic processes. Evidence of paleo-dendritic channels are found along the Holocene strandlines due to the recent exhumation history of these channels. OSL chronology of paleochannels along the Holocene strandlines correlates with the timing of sea-level fluctuations. Paleochannel of Kushabhadra River is parallel to the Early Holocene strandline and dates back to ~7ka BP. The dendritic channels along the Konark swamp dates back to ~6.5 ka BP. The Kushabhadra paleochannel indicates that the mouth of Kushabhadra River shifted parallel to the Early Holocene strandline. The dendritic channels at Konark swamp indicate the presence of paleo-coastline at the paleo-mouth position of Kushabhadra River. The paleo-dendritic channels around Chilka swamp and Kujang swamp are of Mid-Late Holocene age and ends abruptly along the Early-Mid and Mid-Late Holocene strandline, which indicates that these dendritic channels were exhumed along the Holocene strandlines. The paleo-meander scars to the NE of the study area are formed by shifting of flow paths of Brahmani and Baitarani Rivers. OSL ages of these meander scars are Early to Mid-Holocene. This indicates that these meander scars were formed by shifting of river mouths parallel to Early-Mid Holocene strandline. A comparison of fluvial morphologic changes of Mahanadi delta with other deltas around the world suggests that these types of dendritic channels are common along paleo-strandline positions. Detailed study of these strandline positions will give evidence of paleo-strandline positions and sea-level changes throughout the geological time scale.

The second objective of the study focused on paleoclimatic studies from lake sediments of Mahanadi Delta. The Anshupa Lake core dated back to 1400 AD covering the entire Little Ice Age. High-resolution paleoclimatic analysis using mineral magnetic, organic carbon percentage and the carbon isotopic analysis of organic matter revealed periodical climatic changes from the 14th century to the present day. Mineral magnetic variations show that the little ice age received low precipitation than the post LIA period. Sedimentation rates were also lower during LIA than the post LIA period. During LIA various short term climatic changes related to the solar activity such as Sporer Minimum, Munder Minimum and Dalton Minimum were distinguishable from the mineral magnetic data. The Munder minimum showed the lowest values of magnetic susceptibility, indicating the coolest period of LIA with the lowest rainfall. The 16th century showed an increasing trend in mineral magnetic parameters indicating

increasing precipitation. As opposed to previous studies that the Sporer Minimum extended up to 1560 AD, this study finds that the 16th century was a period of highest rainfall during LIA and the Sporer Minimum extended up to 1520 AD. The historical database of famines is well correlated with the mineral magnetic data. This study confirms that the most devastating famines in eastern India occurred around the 17th century. Interparametric ratios indicate that bacterial magnetite dominated the sediment core during the 16th century and detrital magnetic minerals dominate during pre and post 16th century. Organic carbon percentage shows an increasing trend during the 16th century, indicating a period of higher precipitation. The dominance of bacterial magnetite during the 16th century is correlated with high precipitation and high organic carbon input to the lake. The carbon isotopic values show a positive trend during periods of low precipitation and a negative trend during periods of high rainfall. The 16th century shows a relatively negative trend and the 18th century showed a relatively positive trend indicating periods of high and low rainfall during LIA. The Chilka Lake sediment core dates back to 9,000 cal year BP and shows major climatic fluctuations during Holocene. Major climatic changes like Holocene Climate Optimum, 4 ka climate event and LIA are evident from the sediment core. The Holocene Climate Optimum is evident from increase in sedimentation rate and mineral magnetic parameters from bottom of the core to 6,000 cal yr BP. After 6,000 cal yr BP to 2,000 cal yr BP the core shows evidence of weakening monsoon, with intermittent peaks in mineral magnetic data. The lowest value of mineral magnetic parameters are encountered at about 3,500 cal yr BP. This period was the driest period during the Mid-Holocene. The weakening of monsoon continued till the medieval warm period. Most of the river valley civilizations which flourished during Mid-Holocene became rare during 3.5 ka BP. The Medieval warm period shows the strengthening of ISM until the advent of LIA. The LIA period is marked by decreasing mineral magnetic values. The post LIA period shows strengthening of ISM. Periodicities shown by χlf values in both the cores matches with previously studied periodicities on ISM. The present study finds that χlf shows good correlation with paleoprecipitation data, hence it may be concluded that high resolution mineral magnetic analysis is useful to study decadal to millennial-scale climatic periodicities.

References

Achyuthan, H., Nagasundaram, M., Gourlan, A. T., Eastoe, C., Ahmad, S. M., & Padmakumari, V. M. (2014). Mid-Holocene Indian summer monsoon variability off the Andaman Islands, Bay of Bengal. *Quaternary international*, *349*, 232-244.

Agnihotri, R., & Dutta, K. (2003). Centennial scale variations in monsoonal rainfall (Indian, east equatorial and Chinese monsoons): Manifestations of solar variability. *Current Science*, 459-463.

Agnihotri, R., Dutta, K., Bhushan, R., & Somayajulu, B. L. K. (2002). Evidence for solar forcing on the Indian monsoon during the last millennium. *Earth and Planetary Science Letters*, *198*(3-4), 521-527.

Alam, A. M., Xie, S., & Wallis, L. A. (2009). Reconstructing late Holocene palaeoenvironments in Bangladesh: phytolith analysis of archaeological soils from Somapura Mahavihara site in the Paharpur area, Badalgacchi Upazila, Naogaon District, Bangladesh. *Journal of Archaeological Science*, *36*(2), 504-512.

Alley, R. B., Mayewski, P. A., Sowers, T., Stuiver, M., Taylor, K. C., & Clark, P. U. (1997). Holocene climatic instability: A prominent, widespread event 8200 yr ago. *Geology*, *25*(6), 483-486.

Altabet, M. A., Higginson, M. J., & Murray, D. W. (2002). The effect of millennial-scale changes in Arabian Sea denitrification on atmospheric CO 2. *Nature*, *415*(6868), 159.

Anoop, A., Prasad, S., Plessen, B., Basavaiah, N., Gaye, B., Naumann, R., ... & Brauer, A. (2013). P alaeoenvironmental implications of evaporative gaylussite crystals from Lonar Lake, central India. *Journal of Quaternary Science*, *28*(4), 349-359.

Arthur, M. A., Dean, W. E., & Schlanger, S. O. (1985). Variations in the global carbon cycle during the Cretaceous related to climate, volcanism, and changes in atmospheric CO2. *The carbon cycle and atmospheric CO2: Natural variations Archean to present*, *32*, 504-529.

Aslan, A., & Blum, M. D. (1999). Contrasting styles of Holocene avulsion, Texas Gulf coastal plain, USA. *Fluvial sedimentology VI*, *28*, 193-209.

Babu, P. V. L. P. (1973). Morphostructure of the Krishna and the Godavari delta region. *Journal of the Indian Society of Photo-Interpretation*, *1*(1-2), 65-67.

Babu, P. V. (1975). Morphological evolution of the Krishna delta. *Journal of the Indian Society of Remote Sensing*, *3*(1), 21-27.

Bakker, J. G. M., Kleinendorst, T. W., & Geirnaert, W. (1989). Tectonic and sedimentary history of a late Cenozoic intramontane basin (The Pitalito Basin, Colombia). *Basin Research*, *2*(3), 161-187.

Banerjee, P. K. (2000). Holocene and Late Pleistocene relative sea level fluctuations along the east coast of India. *Marine Geology*, *167*(3-4), 243-260.

Banerjee, P. K. (1993). Imprints of late quaternary climatic and sea level changes on East and South Indian coast. *Geo-marine letters*, *13*(1), 56-60.

Barboza, E. G., Dillenburg, S. R., Rosa, M. L. C. C., Tomazelli, L. J., & Hesp, P. A. (2009). Ground-penetrating radar profiles of two Holocene regressive barriers in southern Brazil. *Journal of Coastal Research*, 579-583.

B Barboza, E. G., Rosa, M. L. C. C., & Caron, F. (2014). Metodologia de aquisição e processamento em dados de Georradar (GPR) nos depósitos quaternários da porção emersa da Bacia de Pelotas. *VI Simpósio Brasileiro de Geofísica. Resumos Expandidos*, *1*, 1-6.

Barboza, E. G., Rosa, M. L. C. C., Dillenburg, S. R., Tomazelli, L. J., & Ayup-Zouain, R. N. (2011). Comportamento Regressivo/Transgressivo da linha de costa na Bacia de Pelotas durante o Holoceno Médio e Tardio. *Problemática de Los Ambientes Costeros. 1ed. Buenos Aires-Argentina: Editorial Croquis*, *1*, 15-30.

Barboza, E. G., Rosa, M. L. C. C., Hesp, P. A., Dillenburg, S. R., Tomazelli, L. J., & Ayup-Zouain, R. N. (2011). Evolution of the Holocene Coastal Barrier of Pelotas Basin (Southern Brazil)-a new approach with GPR data. *Journal of Coastal Research*, 646-650.

Barboza, E. G., Rosa, M. L. C., Dillenburg, S. R., & Tomazelli, L. J. (2013). Preservation potential of foredunes in the stratigraphic record. *Journal of Coastal Research*, *65*(sp2), 1265-1270.

Barboza, E. G., Rosa, M. L. C., Dillenburg, S. R., Watanabe, D. S., Esteves, T., Martins, E. M., & Gruber, N. L. (2018). Diachronic Condition Between Maximum Transgressive and Maximum Eustatic Sea-Level in Holocene: Subsidies for Coastal Management. *Journal of Coastal Research*, *85*(sp1), 446-450.

Barnhardt, W. A., Belknap, D. F., & Kelley, J. T. (1997). Stratigraphic evolution of the inner continental shelf in response to late Quaternary relative sea-level change, northwestern Gulf of Maine. *Geological Society of America Bulletin*, *109*(5), 612-630.

Bateman, M.D., Homes, P.J., Carr, A.S., Horton, B.P., Jaiswal, M.K., (2004). Aeolanite and barier dune barrier construction spanning the last two glacial--interglacial cycles from the southern cape coast, South Africa. *Quat. Sci. Rev*. 23, 1681–1698.

Beer, J., Tobias, S., & Weiss, N. (1998). An active Sun throughout the Maunder minimum. *Solar Physics*, *181*(1), 237-249.

Begin, Z. E. B. (1988). Application of a diffusion-erosion model to alluvial channels which degrade due to base-level lowering. *Earth Surface Processes and Landforms*, *13*(6), 487-500.

Begin, Z. E. B., Meyer, D. F., & Schumm, S. A. (1981). Development of longitudinal profiles of alluvial channels in response to base-level lowering. *Earth Surface Processes and Landforms*, *6*(1), 49-68.

Bennett, M. R., Cassidy, N. J., & Pile, J. (2009). Internal structure of a barrier beach as

revealed by ground penetrating radar (GPR): Chesil beach, UK. *Geomorphology*, *104*(3-4), 218-229.

Bera, S. K., & Farooqui, A. (2000). Mid-Holocene vegetation and climate of south Indian Montane. *J Palaeontol Soc India*, *45*, 551-562.

Berger, A. L. (1978). Long-Term Variations of Caloric Insolation Resulting from the Earth's Orbital Elements 1. *Quaternary research*, *9*(2), 139-167.

Berger, W. V., & Von Rad, U. (2002). Decadal to millennial cyclicity in varves and turbidites from the Arabian Sea: hypothesis of tidal origin. *Global and Planetary Change*, *34*(3-4), 313-325.

Berger, W. H., Pätzold, J., & Wefer, G. (2002). A case for climate cycles: Orbit, Sun and Moon. In *Climate development and history of the North Atlantic realm* (pp. 101-123). Springer, Berlin, Heidelberg.

Bharali, B. (1991). A brief review of Mahanadi delta and the deltaic sediments in Mahanadi basin. *Mem. Geol. Soc. Ind.*, *22*, 31-49.

Bhatt, N., & Bhonde, U. A. (2003). Quaternary fluvial sequences of south Saurashtra, western India. *Current Science*, 1065-1071.

Bhattacharyya, A., Sandeep, K., Misra, S., Shankar, R., Warrier, A. K., Weijian, Z., & Xuefeng, L. (2015). Vegetational and climatic variations during the past 3100 years in southern India: evidence from pollen, magnetic susceptibility and particle size data. *Environmental earth sciences*, *74*(4), 3559-3572.

Bianchi, G. G., & McCave, I. N. (1999). Holocene periodicity in North Atlantic climate and deep-ocean flow south of Iceland. *Nature*, *397*(6719), 515.

Bloemendal, J., & Demenocal, P. (1989). Evidence for a change in the periodicity of tropical climate cycles at 2.4 Myr from whole-core magnetic susceptibility measurements. *Nature*, *342*(6252), 897.

Bolton, E. W., Maasch, K. A., & Lilly, J. M. (1995). A wavelet analysis of Plio-Pleistocene climate indicators: A new view of periodicity evolution. *Geophysical Research Letters*, *22*(20), 2753-2756.

Bond, G., Showers, W., Cheseby, M., Lotti, R., Almasi, P., DeMenocal, P., ... & Bonani, G. (1997). A pervasive millennial-scale cycle in North Atlantic Holocene and glacial climates. *science*, *278*(5341), 1257-1266.

Bowler, J. M. (1978). Quaternary stratigraphy of the Darling river near Tilpa, New South wales. *Proc. Roy. Soc. Vic.*, *90*, 79-88.

Bristow, C. S., Chroston, P. N., & Bailey, S. D. (2000). The structure and development of foredunes on a locally prograding coast: insights from ground-penetrating radar surveys, Norfolk, UK. *Sedimentology*, *47*(5), 923-944.

Bristow, C. S., & Jol, H. M. (2003). An introduction to ground penetrating radar (GPR) in sediments. *Geological Society, London, Special Publications*, *211*(1), 1-7.

Bristow, C. S., & Pucillo, K. (2006). Quantifying rates of coastal progradation from sediment volume using GPR and OSL: the Holocene fill of Guichen Bay, south-east South Australia. *Sedimentology*, *53*(4), 769-788.

Brock, F., Higham, T., Ditchfield, P., & Ramsey, C. B. (2010). Current pretreatment methods for AMS radiocarbon dating at the Oxford Radiocarbon Accelerator Unit (ORAU). *Radiocarbon*, *52*(1), 103-112.

Brown, L. J., Wilson, D. D., Moar, N. T., & Mildenhall, D. C. (1988). Stratigraphy of the late Quaternary deposits of the northern Canterbury Plains, New Zealand. *New Zealand journal of geology and geophysics*, *31*(3), 305-335.

Bruckner, E., (1912). The settlement of the United States as controlled by climate and climatic oscillations. Meml. Vol. Transcontinental Excursion 125–139.

Burke, K., & Dewey, J. F. (1973). Plume-generated triple junctions: key indicators in applying plate tectonics to old rocks. *The Journal of Geology*, *81*(4), 406-433.

Butzer, K. W. (1980). Holocene alluvial sequences: problems of dating and correlation. *Timescales in geomorphology*, 131-142.

C Camenisch, C., Keller, K. M., Salvisberg, M., Amann, B., Bauch, M., Blumer, S., ... & Fernández-Donado, L. (2016). The 1430s: a cold period of extraordinary internal climate variability during the early Spörer Minimum with social and economic impacts in north-western and central Europe. *Climate of the Past*, *12*(11), 2107-2126.

Chamberlain, E. L., Törnqvist, T. E., Shen, Z., Mauz, B., & Wallinga, J. (2018). Anatomy of Mississippi Delta growth and its implications for coastal restoration. *Science advances*, *4*(4), eaar4740.

Chambers, D. P., Merrifield, M. A., & Nerem, R. S. (2012). Is there a 60-year oscillation in global mean sea level?. *Geophysical Research Letters*, *39*(18).

Chauhan, M. S., Mazari, R. K., & Rajagopalan, G. (2000). Vegetation and climate in upper Spiti region, Himachal Pradesh during late Holocene. *Current Science*, *79*(3), 373-377.

Chauhan, O. S., Patil, S. K., & Suneethi, J. (2004). Fluvial influx and weathering history of the Himalayas since Last Glacial Maxima–isotopic, sedimentological and magnetic records from the Bay of Bengal. *Current Science*, 509-515.

Chauhan, O. S., Sukhija, B. S., Gujar, A. R., Nagabhushanam, P., & Paropkari, A. L. (2000). Late-Quaternary variations in clay minerals along the SW continental margin of India: evidence of climatic variations. *Geo-Marine Letters*, *20*(2), 118-122.

Chauhan, O. S., & Suneethi, J. (2001). 18 Ka BP records of climatic changes, Bay of Bengal: Isotopic and sedimentological evidences. *Current Science*, 1231-1234.

Chauhan, O. S., & Vogelsang, E. (2006). Climate induced changes in the circulation and dispersal patterns of the fluvial sources during late Quaternary in the middle

Bengal Fan. *Journal of earth system science*, *115*(3), 379-386.

Chen, R., Shen, J., Li, C., Zhang, E., Sun, W., & Ji, M. (2015). Mid-to late-Holocene East Asian summer monsoon variability recorded in lacustrine sediments from Jingpo Lake, Northeastern China. *The Holocene*, *25*(3), 454-468.

Chodankar, A. R., Banakar, V. K., & Oba, T. (2005). Past 100 ky surface salinity-gradient response in the Eastern Arabian Sea to the summer monsoon variation recorded by δ18O of G. sacculifer. *Global and Planetary Change*, *47*(2-4), 135-142.

Choi, K., Hong, C. M., Kim, M. H., Oh, C. R., & Jung, J. H. (2013). Morphologic evolution of macrotidal estuarine channels in Gomso Bay, west coast of Korea: Implications for the architectural development of inclined heterolithic stratification. *Marine Geology*, *346*, 343-354.

Chu, Z. X., Sun, X. G., Zhai, S. K., & Xu, K. H. (2006). Changing pattern of accretion/erosion of the modern Yellow River (Huanghe) subaerial delta, China: Based on remote sensing images. *Marine Geology*, *227*(1-2), 13-30.

Clemens, S. C., Murray, D. W., & Prell, W. L. (1996). Nonstationary phase of the Plio-Pleistocene Asian monsoon. *Science*, *274*(5289), 943-948.

Clemens, S. C., & Prell, W. L. (1990). Late Pleistocene variability of Arabian Sea summer monsoon winds and continental aridity: Eolian records from the lithogenic component of deep-sea sediments. *Paleoceanography*, *5*(2), 109-145.

Coleman, J. M. (1988). Dynamic changes and processes in the Mississippi River delta. *Geological Society of America Bulletin*, *100*(7), 999-1015.

Colin, C., Kissel, C., Blamart, D., & Turpin, L. (1998). Magnetic properties of sediments in the Bay of Bengal and the Andaman Sea: impact of rapid North Atlantic Ocean climatic events on the strength of the Indian monsoon. *Earth and Planetary Science Letters*, *160*(3-4), 623-635.

Colman, S. M., & Mixon, R. B. (1988). The record of major Quaternary sea-level changes in a large coastal plain estuary, Chesapeake Bay, eastern United States. *Palaeogeography, Palaeoclimatology, Palaeoecology*, *68*(2-4), 99-116.

Costas, S., Alejo, I., Rial, F., Lorenzo, H., & Nombela, M. A. (2006). Cyclical evolution of a modern transgressive sand barrier in Northwestern Spain elucidated by GPR and aerial photos. *Journal of sedimentary Research*, *76*(9), 1077-1092.

Curray, J. R., & Moore, D. G. (1971). Growth of the Bengal deep-sea fan and denudation in the Himalayas. *Geological Society of America Bulletin*, *82*(3), 563-572.

d'Arrigo, R., Villalba, R., & Wiles, G. (2001). Tree-ring estimates of Pacific decadal climate variability. *Climate Dynamics*, *18*(3-4), 219-224.

D'Arrigo, R. D., Jacoby, G. C., & Free, R. M. (1992). Tree-ring width and maximum latewood density at the North American tree line: parameters of climatic

change. *Canadian Journal of Forest Research*, *22*(9), 1290-1296.

da Silva, A. B., Barboza, E. G., Rosa, M. L. C., & Dillenburg, S. R. (2014). Meandering fluvial system influencing the evolution of a Holocene regressive barrier in southern Brazil. *Journal of Coastal Research*, *70*(sp1), 205-211.

Damon, P. E., & Peristykh, A. N. (2000). Radiocarbon calibration and application to geophysics, solar physics, and astrophysics. *Radiocarbon*, *42*(1), 137-150.

Das, C. R., & Mohanty, S. (2008). Integrated sustainable environmental conservation of Ansupa lake: A famous water resource of Orissa, India. *Water and Energy International*, *65*(4), 62-66.

Das, N.K., Samal, R.C. (1998). Environmental Survey of Chilka, in: Chilka: The Pride of Our Wetland Heritage. Orissa Environmental Society, pp. 96–103.

Das, S. N., Das, R., & Thakur, R. S. (2005). Estimation of methane emitted by natural wetlands of Orissa: Based on case studies on three representative wetlands. *Toxicological & Environmental Chemistry*, *87*(3), 351-363.

Dash, D. (2000). Hydrocarbon potential of Mahanadi coastal basin. *Mahanadi Delta—Geology, Resources and Biodiversity, India, AITAA, India*, 132.

David Knighton, A., & Nanson, G. C. (1993). Anastomosis and the continuum of channel pattern. *Earth Surface Processes and Landforms*, *18*(7), 613-625. 5

Davis, J. L., & ANNAN, A. P. (1989). Ground-penetrating radar for high-resolution mapping of soil and rock stratigraphy 1. *Geophysical prospecting*, *37*(5), 531-551.

De Lange, W. P., & Moon, V. G. (2007). Tsunami washover deposits, Tawharanui, New Zealand. *Sedimentary Geology*, *200*(3-4), 232-247.

Dean, W. E., Forester, R. M., & Bradbury, J. P. (2002). Early Holocene change in atmospheric circulation in the Northern Great Plains: an upstream view of the 8.2 ka cold event. *Quaternary Science Reviews*, *21*(16-17), 1763-1775.

Dillenburg, S. R., & Barboza, E. G. (2014). The strike-fed sandy coast of Southern Brazil. *Geological Society, London, Special Publications*, *388*(1), 333-352.

Dillenburg, S. R., & Barboza, E. G. (2009). Long-and short-term progradation of a regressive barrier in southern Brazil. *Journal of Coastal Research*, 599-601.

Dillenburg, S. R., Barboza, E. G., Hesp, P. A., & Rosa, M. L. C. C. (2011). Ground Penetrating Radar (GPR) and Standard Penetration Test (SPT) records of a regressive barrier in southern Brazil. *Journal of Coastal Research*, 651-655.

Dillenburg, S. R., Barboza, E. G., Hesp, P. A., Rosa, M. L. C., Angulo, R. J., Souza, M. C., ... & Sawakuchi, A. O. (2014). Discussion:"Evidence for a transgressive barrier within a regressive strandplain system: implications for complex response to environmental change" by Hein, et al.(2013), Sedimentology 60, 469–502: A transgressive barrier at Pinheira, Southern Brazil around 3 ka?. *Sedimentology*, *61*(7), 2205-2212.

Dillenburg, S. R., Barboza, E. G., Rosa, M. L. C., Caron, F., & Sawakuchi, A. O. (2017). The complex prograded Cassino barrier in southern Brazil: Geological and morphological evolution and records of climatic, oceanographic and sea-level changes in the last 7–6 ka. *Marine Geology*, *390*, 106-119.

Dillenburg, S. R., Barboza, E. G., Tomazelli, L. J., Ayup-Zouain, R. N., Hesp, P. A., & Clerot, L. C. (2009). The Holocene Coastal Barriers of Rio Grande do Sul. In *Geology and Geomorphology of Holocene Coastal Barriers of Brazil* (pp. 53-91). Springer, Berlin, Heidelberg.

Dillenburg, S. R., Tomazelli, L. J., Hesp, P. A., Barboza, E. G., Clerot, L. C. P., & Silva, D. D. (2006). Stratigraphy and evolution of a prograded transgressive dunefield barrier in southern Brazil. *Journal of Coastal Research*, 132-135.

Divakar Naidu, P. (1995). High-resolution studies of Asian quaternary monsoon climate and carbonate records from the equatorial Indian Ocean.

Dolphin, L. T., Beatty, W. B., & Tanzi, J. D. (1978). Radar probing of Victorio Peak, New Mexico. *Geophysics*, *43*(7), 1441-1448.

Dominguez, J. M., Martin, L., & Bittencourt, A. C. (1987). Sea-Level History and Quaternary Evolution of River Mouth–Associated Beachridge Plains Along the East–Southeast Brazilian Coast: A Summary.

Dougherty, A. J., FitzGerald, D. M., & Buynevich, I. V. (2004). Evidence for storm-dominated early progradation of Castle Neck barrier, Massachusetts, USA. *Marine Geology*, *210*(1-4), 123-134.

Eddy, J. A. (1983). The Maunder minimum: a reappraisal. *Solar Physics*, *89*(1), 19

Eisma, D. (1998). *Intertidal deposits: river mouths, tidal flats, and coastal lagoons* (Vol. 16). CRC Press.

Ékes, C., & Friele, P. (2003). Sedimentary architecture and post-glacial evolution of Cheekye fan, southwestern British Columbia, Canada. *Geological Society, London, Special Publications*, *211*(1), 87-98.

Enzel, Y., Ely, L. L., Mishra, S., Ramesh, R., Amit, R., Lazar, B., ... & Sandler, A. (1999). High-resolution Holocene environmental changes in the Thar Desert, northwestern India. *Science*, *284*(5411), 125-128.

Evans, M., & Heller, F. (2003). *Environmental magnetism: principles and applications of enviromagnetics* (Vol. 86). Elsevier.

Fairbanks, R. G. (1989). A 17,000-year glacio-eustatic sea level record: influence of glacial melting rates on the Younger Dryas event and deep-ocean circulation. *Nature*, *342*(6250), 637.

Fan, L., Jiezao, Z., Jianjun, Y., Quansheng, D., Tailu, D., & Xiuhang, J. (1990). Buried paleo-channel system and records of sea level changes on the continental shelf in Yingge Sea Basin. *Chinese Journal of Oceanology and Limnology*, *8*(3), 240-248.

Farooqui, A., Ranjana, & Nautiyal, C. M. (2016). Deltaic land subsidence and sea level fluctuations along the east coast of India since 8 ka: A palynological study. *The Holocene*, *26*(9), 1426-1437.

Fisk, H.N. (1945). Geological investigation of the alluvial valley of the lower Mississippi River.

Buynevich, I. V., & FitzGerald, D. M. (2002). Organic-rich facies in paraglacial barrier lithosomes of northern New England: preservation and paleoenvironmental significance. *Journal of Coastal Research*, 109-117.

Fitzgerald, D. M., & Van Heteren, S. (1999). Classification of paraglacial barrier systems: coastal New England, USA. *Sedimentology*, *46*(6), 1083-1108.

Fleitmann, D., Burns, S. J., Mudelsee, M., Neff, U., Kramers, J., Mangini, A., & Matter, A. (2003). Holocene forcing of the Indian monsoon recorded in a stalagmite from southern Oman. *science*, *300*(5626), 1737-1739.

Foukal, P. V., & Lean, J. (1990). An empirical model of total solar irradiance variation between 1874 and 1988. *Science*, *247*(4942), 556-558.

Frihy, O. E., Nasr, S. M., El Hattab, M. M., & El Raey, M. (1994). Remote sensing of beach erosion along the Rosetta promontary, northwestern Nile delta, Egypt. *International Journal of Remote Sensing*, *15*(8), 1649-1660.

Galbraith, H., Jones, R., Park, R., Clough, J., Herrod-Julius, S., Harrington, B., & Page, G. (2002). Global climate change and sea level rise: potential losses of intertidal habitat for shorebirds. *Waterbirds*, 173-183.

Gallais, J. (1967). *Le delta intérieur du Niger et ses bordures: étude morphologique* (Vol. 1). Éditions du Centre national de la recherche scientifique.

Ganju, J. L., Mitra, D. S., & Shaktawat, K. S. (1982). Geomorphology of a part of east coast between Balasore and Indo-Bangladesh border. In *Proceedings of the Symposium on Resources Survey for Landuse Planning and Environmental Conservation: 20-22 October, 1982/organised by: Indian Society of Photo-Interpretation and Remote Sensing*. Dehra Dun, India.

Garner, H. F. (1959). Interpretation of globally distributed anastomosing channel drainages. *Geological Society of America Bulletin*, *70*(12), 1607.

Gasse, F., & Van Campo, E. (1994). Abrupt post-glacial climate events in West Asia and North Africa monsoon domains. *Earth and Planetary Science Letters*, *126*(4), 435-456.

Gawthorpe, R. L., Collier, R. L., Alexander, J., Bridge, J. S., & Leeder, M. R. (1993). Ground penetrating radar: application to sandbody geometry and heterogeneity studies. *Geological Society, London, Special Publications*, *73*(1), 421-432.

Gehring, A. U., Kind, J., Charilaou, M., & García-Rubio, I. (2013). S-band ferromagnetic resonance spectroscopy and the detection of magnetofossils. *Journal of The Royal Society Interface*, *10*(80), 20120790.

Giosan, L., Ponton, C., Usman, M., Glusztajn, J., Fuller, D. Q., Galy, V., ... & Eglinton, T. I. (2017). Massive erosion in monsoonal central India linked to late Holocene land cover degradation. *Earth surface dynamics*.

Gnevyshev, M. N. (1977). Essential features of the 11-year solar cycle. *Solar Physics*, *51*(1), 175-183.

Grant, J. A., Brooks, M. J., & Taylor, B. E. (1998). New constraints on the evolution of Carolina Bays from ground-penetrating radar. *Geomorphology*, *22*(3-4), 325-345.

Grosse, G., Ulrich, M., & Schirrmeister, L. (2006). Characterization of periglacial surfaces in the Arctic Lena Delta using satellite data and field spectrometry.

Grudd, H., Briffa, K. R., Karlén, W., Bartholin, T. S., Jones, P. D., & Kromer, B. (2002). A 7400-year tree-ring chronology in northern Swedish Lapland: natural climatic variability expressed on annual to millennial timescales. *The Holocene*, *12*(6), 657-665.

Halberg, F., Cornelissen, G., Sothern, R. B., Czaplicki, J., & Schwartzkopff, O. (2010). Thirty-five-year climatic cycle in heliogeophysics, psychophysiology, military politics, and economics. *Izvestiya, Atmospheric and Oceanic Physics*, *46*(7), 844-864.

Hall, S. A. (1990). Channel trenching and climatic change in the southern US Great Plains. *Geology*, *18*(4), 342-345.

Hedges, J. I., & Stern, J. H. (1984). Carbon and nitrogen determinations of carbonate-containing solids 1. *Limnology and oceanography*, *29*(3), 657-663.

Heteren, S. V., Fitzgerald, D. M., Mckinlay, P. A., & Buynevich, I. V. (1998). Radar facies of paraglacial barrier systems: coastal New England, USA. *Sedimentology*, *45*(1), 181-200.

Hodgkinson, J., Cox, M. E., McLoughlin, S., & Huftile, G. J. (2008). Lithological heterogeneity in a back-barrier sand island: Implications for modelling hydrogeological frameworks. *Sedimentary Geology*, *203*(1-2), 64-86.

Hoegh-Guldberg, O., & Bruno, J. F. (2010). The impact of climate change on the world's marine ecosystems. *Science*, *328*(5985), 1523-1528.

Hoorn, C., Wesselingh, F. P., Ter Steege, H., Bermudez, M. A., Mora, A., Sevink, J., ... & Jaramillo, C. (2010). Amazonia through time: Andean uplift, climate change, landscape evolution, and biodiversity. *science*, *330*(6006), 927-931.

Horwitz, M., & Wang, P. (2005). Sedimentological characteristics and internal architecture of two overwash fans from Hurricanes Ivan and Jeanne.

Horwitz, M. H. (2008). Sedimentological characteristics and 3-D internal architecture of washover deposits from Hurricanes Frances, Ivan, and Jeanne.

Howarth, R. J., & McArthur, J. M. (1997). Statistics for strontium isotope stratigraphy:

a robust LOWESS fit to the marine Sr-isotope curve for 0 to 206 Ma, with look-up table for derivation of numeric age. *The Journal of Geology*, *105*(4), 441-456.

Hughes, Z. J. (2012). Tidal channels on tidal flats and marshes. In *Principles of Tidal Sedimentology* (pp. 269-300). Springer, Dordrecht.

Hunt, C. B., Averitt, P., & Miller, R. L. (1953). *Geology and geography of the Henry Mountains region, Utah* (No. 228). US Government Printing Office.

Lambiase, J. J. (2013). Sediment dynamics and depositional systems of the Mahakam Delta, Indonesia: ongoing delta abandonment on a tide-dominated coast. *Journal of Sedimentary Research*, *83*(7), 503-521.

Narula, P. L., Acharyya, S. K., & Banerjee, J. (2000). Seismotectonic atlas of India and its environs. Geological Survey of India.

Jagannathan, C. R., Ratnam, C., Baishya, N. C., & Dasgupta, U. (1983). Geology of the offshore Mahanadi basin. *Petroleum Asia Journal*, *6*(4), 101-104.

Jain, M., & Tandon, S. K. (2003). Fluvial response to Late Quaternary climate changes, western India. *Quaternary Science Reviews*, *22*(20), 2223-2235.

Jaiswal, M. K., Bhat, M. I., Bali, B. S., Ahmad, S., & Chen, Y. G. (2009). Luminescence characteristics of quartz and feldspar from tectonically uplifted terraces in Kashmir Basin, Jammu and Kashmir, India. *Radiation Measurements*, *44*(5-6), 523-528.

Jiang, Y., Xu, Z. (1986). On the Spörer Minimum, in: Third Asian-Pacific Regional Meeting of the International Astronomical Union. Springer Netherlands, Dordrecht, pp. 159–162.

Jol, H. M., & Bristow, C. S. (2003). GPR in sediments: advice on data collection, basic processing and interpretation, a good practice guide. *Geological Society, London, Special Publications*, *211*(1), 9-27.

Jol, H. M., Lawton, D. C., & Smith, D. G. (2003). Ground penetrating radar: 2-D and 3-D subsurface imaging of a coastal barrier spit, Long Beach, WA, USA. *Geomorphology*, *53*(1-2), 165-181.

Jol, H. M., & Smith, D. G. (1991). Ground penetrating radar of northern lacustrine deltas. *Canadian Journal of Earth Sciences*, *28*(12), 1939-1947.

Jol, H. M., Smith, D. G., & Meyers, R. A. (1997). Digital ground penetrating radar (GPR): a new geophysical tool for coastal barrier research (examples from the Atlantic, Gulf and Pacific coasts, USA). *Oceanographic Literature Review*, *7*(44), 688.

Jol, H. M., Smith, D. G., & Meyers, R. A. (1996). Digital ground penetrating radar (GPR): a new geophysical tool for coastal barrier research (examples from the Atlantic, Gulf and Pacific Coasts, USA). *Journal of Coastal Research*, 960-968.

Kaila, K. L. (1987). Crustal structure and delineation of Gondwana basin in Mahanadi

delta area, India, from Deep Seismic Soundings. *J. Geol. Soc. India*, *29*, 293-308.

Kasse, C., Vandenberghe, J., & Bohncke, S. J. P. (1995). Climatic change and fluvial dynamics of the Maas during the Late Weichselian and Early Holocene. In *European river activity and climatic change during the Lateglacial and early Holocene: Paläoklimaforschung/Palaeoclimate Research, Vol. 14, Special Issue: ESF Project" European Palaeoclimate and Man" 9* (pp. 123-150).

Knight, R., & Endres, A. (1990). A new concept in modeling the dielectric response of sandstones: Defining a wetted rock and bulk water system. *Geophysics*, *55*(5), 586-594.

Knudsen, M. F., Seidenkrantz, M. S., Jacobsen, B. H., & Kuijpers, A. (2011). Tracking the Atlantic Multidecadal Oscillation through the last 8,000 years. *Nature communications*, *2*, 178.

Koss, J. E., Ethridge, F. G., & Schumm, S. A. (1994). An experimental study of the effects of base-level change on fluvial, coastal plain and shelf systems. *Journal of Sedimentary Research*, *64*(2b), 90-98.

Kozarski, S. (1991). Warta: A case study of a lowland river. In *Temperate palaeohydrology. Fluvial processes in the temperate zone during the last 15 000 years* (pp. 189-215).

Krishna Rao, B. (1990). Sedimentary characteristics of Holocene beach ridges in western delta of Krishna River. *Sea leval variation and its impact on coastal environment*, *131*, 133-143.

Kuppusamy, M., & Ghosh, P. (2012). Cenozoic climatic record for monsoonal rainfall over the Indian region. *Modern Climatology*.

Lachniet, M. S. (2009). Climatic and environmental controls on speleothem oxygen-isotope values. *Quaternary Science Reviews*, *28*(5-6), 412-432.

Lambeck, K., & Chappell, J. (2001). Sea level change through the last glacial cycle. *Science*, *292*(5517), 679-686.

Lane, E. W. (1955). The im por tance of flu vial mor phol ogy in hy drau lic en gi neer ing. *Am. Soc. Civil En gi neers, Proc*, *81*, 745.

Larson, R. L. (1977). Early Cretaceous breakup of Gondwanaland off western Australia. *Geology*, *5*(1), 57-60.

Larson, R. L. (1975). Late Jurassic sea-floor spreading in the eastern Indian Ocean. *Geology*, *3*(2), 69-71.

Laskar, A. H., Yadava, M. G., Sharma, N., & Ramesh, R. (2013). Late-Holocene climate in the Lower Narmada valley, Gujarat, western India, inferred using sedimentary carbon and oxygen isotope ratios. *The Holocene*, *23*(8), 1115-1122.

Leal, R. A., Barboza, E. G., Bitencourt, V., da Silva, A. B., & Manzolli, R. P. (2016). Geological and stratigraphic characteristics of a holocene regressive barrier in

Southern Brazil: GIS and GPR applied for evolution analysis. *Journal of Coastal Research*, *75*(sp1), 750-755.

Lean, J. (2002). Solar forcing of climate change in recent millennia. In *Climate development and history of the North Atlantic realm* (pp. 75-88). Springer, Berlin, Heidelberg.

Lean, J., Beer, J., & Bradley, R. (1995). Reconstruction of solar irradiance since 1610: Implications for climate change. *Geophysical Research Letters*, *22*(23), 3195-3198.

Leckie, D. A. (1994). Canterbury Plains, New Zealand--implications for sequence stratigraphic models. *AAPG bulletin*, *78*(8), 1240-1256.

Leigh, D. S., & Feeney, T. P. (1995). Paleochannels indicating wet climate and lack of response to lower sea level, southeast Georgia. *Geology*, *23*(8), 687-690.

Leigh, D. S., Srivastava, P., & Brook, G. A. (2004). Late Pleistocene braided rivers of the Atlantic coastal plain, USA. *Quaternary Science Reviews*, *23*(1-2), 65-84.

Leopold, L. B., & Bull, W. B. (1979). Base level, aggradation, and grade. *Proceedings of the American Philosophical Society*, *123*(3), 168-202.

Leopold, L. B., & Maddock, T. (1953). *The hydraulic geometry of stream channels and some physiographic implications* (Vol. 252). US Government Printing Office.

Li, M., Hinnov, L., & Kump, L. (2019). Acycle: Time-series analysis software for paleoclimate research and education. *Computers & geosciences*, *127*, 12-22.

Liu, S., Deng, C., Xiao, J., Li, J., Paterson, G. A., Chang, L., ... & Zhu, R. (2015). Insolation driven biomagnetic response to the Holocene Warm Period in semi-arid East Asia. *Scientific reports*, *5*, 8001.

Liu, X., Dong, H., Yang, X., Herzschuh, U., Zhang, E., Stuut, J. B. W., & Wang, Y. (2009). Late Holocene forcing of the Asian winter and summer monsoon as evidenced by proxy records from the northern Qinghai–Tibetan Plateau. *Earth and Planetary Science Letters*, *280*(1-4), 276-284.

Loveday, A. (1914). history & economics of Indian famines.

Lückge, A., Doose-Rolinski, H., Khan, A. A., Schulz, H., & Von Rad, U. (2001). Monsoonal variability in the northeastern Arabian Sea during the past 5000 years: geochemical evidence from laminated sediments. *Palaeogeography, Palaeoclimatology, Palaeoecology*, *167*(3-4), 273-286.

Mackin, J. H. (1948). Concept of the graded river: Geologi cal Society of America Bulletin, v. 59. *doi*, *10*(0016), 7606.

Madhupratap, M., Gauns, M., Ramaiah, N., Kumar, S. P., Muraleedharan, P. M., De Sousa, S. N., ... & Muraleedharan, U. (2003). Biogeochemistry of the Bay of Bengal: physical, chemical and primary productivity characteristics of the central and western Bay of Bengal during summer monsoon 2001. *Deep Sea Research*

Part II: Topical Studies in Oceanography, *50*(5), 881-896.

Maejima, W., & Mahalik, N. K. (2001). The Role of Prevalent Wind on the Geomorphic Development of the Marine-Marginal Zone of the Mahanadi Delta, India. *JOURNAL OF GEOSCIENCES-OSAKA CITY UNIVERSITY*, *44*, 173-180.

Mahadevan, C. (1958). Causes of the growth of sand spit north of Godavari confluence. *Andhra University, Memories of Oceanography*, *2*, 69-74.

Mahalik, N. K. (2006). A study of the morphological features and borehole cuttings in understanding the evolution and geological processes in Mahanadi delta, east coast of India. *JOURNAL-GEOLOGICAL SOCIETY OF INDIA*, *67*(5), 595.

Mahalik, N. K. (2000). *Mahanadi Delta: geology, resources & biodiversity*. AIT Alumni Association, India Chapter.

Mahalik, N. K. (1995). Subsurface geology and ground-water occurrence in the south-western sector of Mahanadi delta along the Eastern Coast of India. In *Proc. XV Annual Conf., National Assoc. Geograph. India (Spatial Dimensions in Geography)* (pp. 1-14).

Mahalik, N. K. (1984). Satellite imageries in geological mapping of Orissa and geomorphological study of Mahanadi-Baitarani compound data. *Res Bull Eastern Geographic Soc, Bhubaneswan*, *22*, 1-12.

Mahalik, N. K., & Maejima, W. (1996). Geomorphology and evolution of the Mahanadi delta, India. *JOURNAL OF GEOSCIENCES-OSAKA CITY UNIVERSITY*, *39*, 111-122.

Makaske, B. (2001). Anastomosing rivers: a review of their classification, origin and sedimentary products. *Earth-Science Reviews*, *53*(3-4), 149-196.

Makaske, B. (1998). *Anastomosing rivers: forms, processes and sediments*. Koninklijk Nederlands Aardrijkskundig Genootschap.

Mantelli, L. R., de Fátima Rossetti, D., Albuquerque, P. G., & de Morisson Valeriano, M. (2009). Applying SRTM digital elevation model to unravel Quaternary drainage in forested areas of Northeastern Amazonia. *Computers & Geosciences*, *35*(12), 2331-2337.

Markl, R. G. (1978). Further evidence for the Early Cretaceous breakup of Gondwanaland off southwestern Australia. In *Elsevier Oceanography Series* (Vol. 21, pp. 41-48). Elsevier.

Martinez, A., & Brynes, A. P. (2001). *Modeling dielectric-constant values of geologic materials: An aid to ground-penetrating radar data collection and interpretation* (Vol. 247). Lawrence, Kansas: Kansas Geological Survey.

Mathien, E., & Bassinot, F. (2008). Abrupt hydrographic changes in the Bay of Bengal

during the Holocene. *Geophy. Res. Abst*, *10*.

Maurya, D. M., Chouksey, V., Joshi, P. N., & Chamyal, L. S. (2013). Application of GPR for delineating the neotectonic setting and shallow subsurface nature of the seismically active Gedi fault, Kachchh, western India. *Journal of Geophysics and Engineering*, *10*(3), 034006.

McCave, I. (1969). Correlation using a sedimentological model of part of the Hamilton group (middle Devonian), New York State. *American Journal of Science*, *267*(5), 567-591.

McGuire, W. J., Howarth, R. J., Firth, C. R., Solow, A. R., Pullen, A. D., Saunders, S. J., ... & Vita-Finzi, C. (1997). Correlation between rate of sea-level change and frequency of explosive volcanism in the Mediterranean. *Nature*, *389*(6650), 473.

McIntosh, R. J. (1983). Floodplain geomorphology and human occupation of the upper inland delta of the Niger. *Geographical Journal*, 182-201.

Meijerink, A. M. J. (1982). Dynamic geomorphology of Mahanadi delta. *International Training Center Journal*, 243-250.

Meyers, P. A. (1994). Preservation of elemental and isotopic source identification of sedimentary organic matter. *Chemical geology*, *114*(3-4), 289-302.

Meyers, P. A., & Lallier-Vergès, E. (1999). Lacustrine sedimentary organic matter records of Late Quaternary paleoclimates. *Journal of Paleolimnology*, *21*(3), 345-372.

Milankovitch, M. (1930). Mathematische klimalehre und astronomische theorie der klimaschwankungen. *Handbuch der Klimatologie 1*.

Mischke, S., & Zhang, C. (2010). Holocene cold events on the Tibetan Plateau. *Global and Planetary Change*, *72*(3), 155-163.

Mishra, V., Tiwari, A. D., Aadhar, S., Shah, R., Xiao, M., Pai, D. S., & Lettenmaier, D. (2019). Drought and Famine in India, 1870–2016. *Geophysical Research Letters*, *46*(4), 2075-2083.

Mixon, R. B. (1985). *Stratigraphic and geomorphic framework of uppermost Cenozoic deposits in the southern Delmarva Peninsula, Virginia and Maryland* (No. 1067-G). USGPO,.

Miyahara, H., Sokoloff, D., & Usoskin, I. G. (2006). The solar cycle at the Maunder minimum epoch. In *Advances in Geosciences: Volume 2: Solar Terrestrial (ST)* (pp. 1-20).

Mohanti, M., & Swain, M. R. (2003). Mahanadi river delta, east coast of India: an overview on evolution and dynamic processes.

Morgan, J. P., & McINTIRE, W. G. (1959). Quaternary geology of the Bengal basin, East Pakistan and India. *Geological Society of America Bulletin*, *70*(3), 319-342.

Muñoz, A., Bartolomé, M., Muñoz, A., Sancho, C., Moreno, A., Hellstrom, J. C., ... & Cacho, I. (2015). Solar influence and hydrological variability during the Holocene from a speleothem annual record (Molinos Cave, NE Spain). *Terra Nova*, *27*(4), 300-311.

Murray, A. S., & Wintle, A. G. (2000). Luminescence dating of quartz using an improved single-aliquot regenerative-dose protocol. *Radiation measurements*, *32*(1), 57-73.

Murray, A. S., & Wintle, A. G. (2003). The single aliquot regenerative dose protocol: potential for improvements in reliability. *Radiation measurements*, *37*(4-5), 377-381.

Nageswara Rao, J. (1987). Geomorphology quaternary geology and neotectonic structure of Krishna delta: East coast Andhra Pradesh. *Visesa Prakasana-Bharatiya Bhuvaijñanika Sarveksana*, (11), 317-322.

Naidu, A. S., & Shankar, R. (1999). Palaeomonsoon history during the late quaternary: results of a pilot study on sediments from the laccadive trough, southeastern Arabian sea. *Journal of the Geological Society of India*, *53*(4), 401-406.

Naidu, P. D., & Malmgren, B. A. (1996). A high-resolution record of late Quaternary upwelling along the Oman Margin, Arabian Sea based on planktonic foraminifera. *Paleoceanography*, *11*(1), 129-140.

Nayak, G. K., Rao, C. R., & HV, R. (2006). Aeromagnetic evidence for the arcuate shape of Mahanadi Delta, India. *Earth, planets and space*, *58*(8), 1093-1098.

Neal, A. (2004). Ground-penetrating radar and its use in sedimentology: principles, problems and progress. *Earth-science reviews*, *66*(3-4), 261-330.

Neal, A., Pontee, N. I., Pye, K., & Richards, J. (2002a). Internal structure of mixed-sand-and-gravel beach deposits revealed using ground-penetrating radar. *Sedimentology*, *49*(4), 789-804.

Neal, A., Richards, J., & Pye, K. (2003). Sedimentology of coarse-clastic beach-ridge deposits, Essex, southeast England. *Sedimentary Geology*, *162*(3-4), 167-198.

Neal, A., Richards, J., & Pye, K. (2002b). Structure and development of shell cheniers in Essex, southeast England, investigated using high-frequency ground-penetrating radar. *Marine Geology*, *185*(3-4), 435-469.

Neff, U., Burns, S. J., Mangini, A., Mudelsee, M., Fleitmann, D., & Matter, A. (2001). Strong coherence between solar variability and the monsoon in Oman between 9 and 6 kyr ago. *Nature*, *411*(6835), 290.

Nelson, C. H., & Maldonado, A. (1988). Factors controlling depositional patterns of Ebro turbidite systems, Mediterranean Sea. *AAPG bulletin*, *72*(6), 698-716.

Němec, M., Wacker, L., & Gäggeler, H. (2010). Optimization of the graphitization process at AGE-1. *Radiocarbon*, *52*(3), 1380-1393.

Nigam, R. (1993). Foraminifera and changing pattern of monsoon rainfall. *Current Science*, 935-937.

Nigam, R., & Khare, N. (1992). Oceanographic evidences of the great floods in 2,000 and 1,500 BC documented in Archaeological records.

Niyogi, D. (1971). Morphology and evolution of the Balashore shoreline, Orlssa, in: Studles In Earth Sclences West Volume, Today and Tomorrow's Pnnters and Publ~shers New Delh. pp. 289–304.

Niyogi, D. (1970). *Geological background of beach erosion at Digha, West Bengal* (No. 43). Geology Dept., Calcutta University.

Northfelt, D. W., DeNiro, M. J., & Epstein, S. (1981). Hydrogen and carbon isotopic ratios of the cellulose nitrate and saponifiable lipid fractions prepared from annual growth rings of a California redwood. *Geochimica et Cosmochimica Acta*, *45*(10), 1895-1898.

Ojala, A. E. K., Launonen, I., Holmström, L., & Tiljander, M. (2015). Effects of solar forcing and North Atlantic oscillation on the climate of continental Scandinavia during the Holocene. *Quaternary Science Reviews*, *112*, 153-171.

Oldfield, F. (2013a). Mud and magnetism: records of late Pleistocene and Holocene environmental change recorded by magnetic measurements. *Journal of paleolimnology*, *49*(3), 465-480.

Oldfield, F. (2013b). Mud and magnetism: records of late Pleistocene and Holocene environmental change recorded by magnetic measurements. *Journal of paleolimnology*, *49*(3), 465-480.

Oldfield, F. (2007). Sources of fine-grained magnetic minerals in sediments: a problem revisited. *The Holocene*, *17*(8), 1265-1271.

Walden, J. (Ed.). (1999). *Environmental magnetism: a practical guide*. Quaternary Research Association.

Oliveira Jr, J. G. D., & Medeiros, W. E. D. (2008). Influência do conteúdo de água, granulometria e minerais pesados sobre as reflexões de GPR em corpos arenosos inconsolldados. *Revista Brasileira de Geofísica*, *26*(4), 437-449.

Paillou, P., Schuster, M., Tooth, S., Farr, T., Rosenqvist, A., Lopez, S., & Malezieux, J. M. (2009). Mapping of a major paleodrainage system in eastern Libya using orbital imaging radar: the Kufrah River. *Earth and Planetary Science Letters*, *277*(3-4), 327-333.

Pandey, S., Scharf, B. W., & Mohanti, M. (2014). Palynological studies on mangrove ecosystem of the Chilka Lagoon, east coast of India during the last 4165 yrs BP. *Quaternary international*, *325*, 126-135.

Panin, N. (2003). The Danube Delta. Geomorphology and Holocene Evolution: a synthesis/Le delta du Danube. Géomorphologie et évolution holocène: une synthèse. *Géomorphologie: relief, processus, environnement*, *9*(4), 247-262.

Parthasarathy, B., Kumar, K. R., & Munot, A. A. (1993). Homogeneous Indian monsoon rainfall: variability and prediction. *Proceedings of the Indian Academy of Sciences-Earth and Planetary Sciences*, *102*(1), 121-155.

Patel, M. P., & Bhatt, N. (1995). Evidence of Paleoclimatic fluctuations in Miliolite rocks of Saurashtra, Western India. *Journal of the Geological Society of India*, *45*(2), 191-200.

Patnaik, R., Gupta, A. K., Naidu, P. D., Yadav, R. R., Bhattacharyya, A., & Kumar, M. (2012). Indian monsoon variability at different time scales: marine and terrestrial proxy records.

Pavelsky, T. M., & Smith, L. C. (2009). Remote sensing of suspended sediment concentration, flow velocity, and lake recharge in the Peace-Athabasca Delta, Canada. *Water Resources Research*, *45*(11).

Penck, A., & Brückner, E. (1909). *Die alpen im Eiszeitalter* (Vol. 3). CH Tauchnitz.

Ponton, C., Giosan, L., Eglinton, T. I., Fuller, D. Q., Johnson, J. E., Kumar, P., & Collett, T. S. (2012). Holocene aridification of India. *Geophysical Research Letters*, *39*(3).

Ponyavin, D. I. (2004). Solar cycle signal in geomagnetic activity and climate. *Solar Physics*, *224*(1-2), 465-471.

Powell, J. W. (1875). *Exploration of the Colorado River of the West and its Tributaries*.

Prabhu, C. N., & Shankar, R. (2005). Palaeoproductivity of the eastern Arabian Sea during the past 200 ka: A multi-proxy investigation. *Deep Sea Research Part II: Topical Studies in Oceanography*, *52*(14-15), 1994-2002.

Prabhu, C. N., Shankar, R., Anupama, K., Taieb, M., Bonnefille, R., Vidal, L., & Prasad, S. (2004). A 200-ka pollen and oxygen-isotopic record from two sediment cores from the eastern Arabian Sea. *Palaeogeography, Palaeoclimatology, Palaeoecology*, *214*(4), 309-321.

Prasad, S., Kusumgar, S., & Gupta, S. K. (1997). A mid to late Holocene record of palaeoclimatic changes from Nal Sarovar: a palaeodesert margin lake in western India. *Journal of Quaternary Science: Published for the Quaternary Research Association*, *12*(2), 153-159.

Prasad, V., Farooqui, A., Sharma, A., Phartiyal, B., Chakraborty, S., Bhandari, S., ... & Singh, A. (2014). Mid–late Holocene monsoonal variations from mainland Gujarat, India: A multi-proxy study for evaluating climate culture relationship. *Palaeogeography, Palaeoclimatology, Palaeoecology*, *397*, 38-51.

Prizomwala, S. P., Das, A., Chauhan, G., Solanki, T., Basavaiah, N., Bhatt, N., ... & Rastogi, B. K. (2016). Late Pleistocene–Holocene uplift driven terrace formation and climate-tectonic interplay from a seismically active intraplate setting: An example from Kachchh, western India. *Journal of Asian Earth Sciences*, *124*, 55-67.

Radhakrishna, I. (2001). Saline fresh water interface structure in Mahanadi delta region, Orissa, India. *Environmental Geology*, *40*(3), 369-380.

Raiverman, V., Singh, G., & Murti, K. V. S. (1966). Fracture pattern in Cauvery basin. *Bull. ONGC*, *3*(1), 13-20.

Rajagopalan, G., Sukumar, R., Ramesh, R., Pant, R. K., & Rajagopalan, G. (1997). Late Quaternary vegetational and climatic changes from tropical peats in southern India–an extended record up to 40,000 years BP. *Current Science*, 60-63.

Ramasamy, S. M., Saravanavel, J., Yadava, M. G., & Ramesh, R. (2006). Radiocarbon dating of some palaeochannels in Tamil Nadu and their significance. *Current Science*, *91*(12), 1609-1613.

Ramasamy, S. M. (1992). A remote sensing study of river deltas of Tamil Nadu.

Ramasamy, S. M., Panchanathan, S., & Palanivelu, R. (1987). Pleistocene earth movements in peninsular India-evidences from Landsat MSS and thematic mapper data. In *IGARSS'87-International Geoscience and Remote Sensing Symposium* (pp. 1157-1161).

Ramasamy, S. M., Venkatasubramanian, V., Abdullah, S. R., & Balaji, S. (2005). The phenomenon of river migration in northern Tamil Nadu-evidence from satellite data, archaeology and Tamil literature. *Remote Sensing in Geomorphology*, 133.

Rao, K. N. (1985). Evolution of land forms in the area between the Krishna and Godawari delta. *Indian Geographical Journal*, *60*, 30-34.

Rao, M. S. (1979). Morphology and evolution of Godavari delta, India.

Raper, S. C., & Braithwaite, R. J. (2006). Low sea level rise projections from mountain glaciers and icecaps under global warming. *Nature*, *439*(7074), 311.

Rashid, H., Flower, B. P., Poore, R. Z., & Quinn, T. M. (2007). A∼ 25 ka Indian Ocean monsoon variability record from the Andaman Sea. *Quaternary Science Reviews*, *26*(19-21), 2586-2597.

Rashid, T. (2014). Sea Level Changes Scenarios During Holocene in Bangladesh. In *Holocene Sea-level Scenarios in Bangladesh* (pp. 61-69). Springer, Singapore.

Raymo, M. E., & Ruddiman, W. F. (1992). Tectonic forcing of late Cenozoic climate. *Nature*, *359*(6391), 117.

Reineck, H. E., & Singh, I. B. (2012). *Depositional sedimentary environments: with reference to terrigenous clastics*. Springer Science & Business Media.

Ren, Z., & Shunan, X. (1990). Prognosis of aggradation in the lower Yellow River by historic analysis of the morphology of its abandoned ancient channel. *Int.J.Sediment Res. 5(2),15–29* .

Rich, J. L. (1935). Origin and evolution of rock fans and pediments. *Bulletin of the Geological Society of America*, *46*(6), 999-1024.

Ridd, M. F. (1971). South-East Asia as a part of Gondwanaland. *Nature*, *234*(5331), 531.

Ritter, D. F. (1972). The significance of stream capture in the evolution of a piedmont region, southern Montana. *Zietschrift fur Geomorphologie*, *16*, 83-92.

Roberts, M. S., Smart, P. L., & Baker, A. (1998). Annual trace element variations in a Holocene speleothem. *Earth and Planetary Science Letters*, *154*(1-4), 237-246.

Rockett, G. C., Barboza, E. G., & Rosa, M. L. C. (2016). Ground penetrating radar applied to the characterization of the Itapeva Dunefield, Torres, Brazil. *Journal of Coastal Research*, *75*(sp1), 323-328.

Rosa, M. L. C. C., Barboza, E. G., Dillenburg, S. R., Tomazelli, L. J., & Ayup-Zouain, R. N. (2011). The Rio Grande do Sul (southern Brazil) shoreline behavior during the Quaternary: a cyclostratigraphic analysis. *Journal of Coastal Research*, 686-690.

Rosa, M. L. C. C., Hoyal, D. C., Barboza, E. G., Fedele, J. U. A. N., & Abreu, V. S. (2016). River-dominated deltas: upscaling autogenic and allogenic processes observed in laboratory experiments to field examples of small deltas in southern Brazil. *Autogenic dynamics and self-organization in sedimentary systems. SEPM Special Publication*, *106*, 176-197.

Rossetti, D. D. F. (2010). Multiple remote sensing techniques as a tool for reconstructing late Quaternary drainage in the Amazon lowland. *Earth Surface Processes and Landforms*, *35*(10), 1234-1239.

Rotnicki, K. (1991). Retrodiction of palaeodischarges of meandering and sinuous alluvial rivers and its palaeohydroclimatic implications. In *Temperate palaeohydrology. Fluvial processes in the temperate zone during the last 15 000 years* (pp. 431-471).

Russell, R.J. (1957). Instability of sea level. Am. Sci. 45, 414–430.

Russell, R.J. (1954). Alluvial Morphology of Anatolian Rivers. Ann. Assoc. Am. Geogr. 44, 363–391.

Sadangi, A., Mishra, B. (2015). Petrography and geochemical characteristics of the athgarh sandstones, upper Gondwana, Eastern India: Implications on provenance and source area weathering, International Journal of Earth Sciences and Engineering.

Samadder, R. K., Kumar, S., & Gupta, R. P. (2011). Paleochannels and their potential for artificial groundwater recharge in the western Ganga plains. *Journal of Hydrology*, *400*(1-2), 154-164.

Sambasiva Rao, M. (1987). Influence of coastal processes along the modern delta front of Godavari in Andhra Pradesh. *Journal of the Geological Society of India*, *29*(4), 399-404.

Sambasiva Rao, M. (1979). New Coastal landforms at the confluence of Godavari

River. *Indian journal of earth science*, *6*, 222-227.

Sandeep, K., Shankar, R., Warrier, A. K., Yadava, M. G., Ramesh, R., Jani, R. A., ... & Xuefeng, L. (2017). A multi-proxy lake sediment record of Indian summer monsoon variability during the Holocene in southern India. *Palaeogeography, palaeoclimatology, palaeoecology*, *476*, 1-14.

Sandeep, K., Shankar, R., Warrier, A. K., Weijian, Z., & Xuefeng, L. (2015). The environmental magnetic record of palaeoenvironmental variations during the past 3100 years: a possible solar influence?. *Journal of Applied Geophysics*, *118*, 24-36.

Sangode, S. J., & Bloemendal, J. (2004). Pedogenic transformation of magnetic minerals in Pliocene–Pleistocene palaeosols of the Siwalik Group, NW Himalaya, India. *Palaeogeography, Palaeoclimatology, Palaeoecology*, *212*(1-2), 95-118..

Sarkar, A., Ramesh, R., Somayajulu, B. L. K., Agnihotri, R., Jull, A. T., & Burr, G. S. (2000). High resolution Holocene monsoon record from the eastern Arabian Sea. *Earth and Planetary Science Letters*, *177*(3-4), 209-218.

Sarkar, A., Sarangi, S., Bhattacharya, S. K., & Ray, A. K. (2003). Carbon isotopes across the Eocene-Oligocene boundary sequence of Kutch, western India: Implications to oceanic productivity and pCO2 change. *Geophysical Research Letters*, *30*(11).

Sarkar, A., Sarangi, S., Ebihara, M., Bhattacharya, S. K., & Ray, A. K. (2003). Carbonate geochemistry across the Eocene/Oligocene boundary of Kutch, western India: implications to oceanic O2-poor condition and foraminiferal extinction. *Chemical Geology*, *201*(3-4), 281-293.

Saxena, A., Prasad, V., & Singh, I. B. (2013). Holocene palaeoclimate reconstruction from the phytoliths of the lake-fill sequence of Ganga Plain. *Current science*, 1054-1062.

Saxena, A., & Singh, D. S. (2017). Multiproxy records of vegetation and monsoon variability from the lacustrine sediments of eastern Ganga Plain since 1350 AD. *Quaternary international*, *444*, 24-34.

Saxena, A., Trivedi, A., Chauhan, M. S., & Sharma, A. (2015). Holocene vegetation and climate change in Central Ganga Plain: a study based on multiproxy records from Chaudhary-Ka-Tal, Raebareli District, Uttar Pradesh, India. *Quaternary international*, *371*, 164-174.

Schlesinger, M. E., & Ramankutty, N. (1994). An oscillation in the global climate system of period 65–70 years. *Nature*, *367*(6465), 723.

Schröder, W. (1994). Aurorae during the so-called Spoerer minimum. *Solar physics*, *151*(1), 199-201.

Schumm, S. A. (1993). River response to baselevel change: implications for sequence stratigraphy. *The Journal of Geology*, *101*(2), 279-294.

Schumm, S. A. (1968). Speculations concerning paleohydrologic controls of terrestrial sedimentation. *Geological Society of America Bulletin*, *79*(11), 1573-1588.

Schumm, S. A. (1985). Explanation and extrapolation in geomorphology: seven reasons for geologic uncertainty. *Transactions of the Japanese Geomorphological Union*, *6*, 1-18.

Schumm, S. A., & Schumm, S. A. (1998). *To Interpret the Earth: Ten ways to be wrong*. Cambridge University Press.

Selby, M. J. (1985). *Earth's changing surface: an introduction to geomorphology*. Oxford University Press.

Shankar, R., Prabhu, C. N., Warrier, A. K., Kumar, G. V., & Sekar, B. (2006). A multi-decadal rock magnetic record of monsoonal variations during the past 3,700 years from a tropical Indian tank. *Journal-Geological Society of India*, *68*(3), 447.

Shankar, R., & Pandarinath, K. (2008). Mineral magnetic signature of the early Holocene intense monsoon conditions recorded in sediments from the Southwestern Indian continental margin. *JOURNAL-GEOLOGICAL SOCIETY OF INDIA*, *71*(5), 670.

Sharma, K., Bhatt, N., Shukla, A. D., Cheong, D. K., & Singhvi, A. K. (2017). Optical dating of late Quaternary carbonate sequences of Saurashtra, western India. *Quaternary Research*, *87*(1), 133-150.

Sharma, S., Joachimski, M. M., Tobschall, H. J., Singh, I. B., Sharma, C., & Chauhan, M. S. (2006). Correlative evidences of monsoon variability, vegetation change and human inhabitation in Sanai lake deposit: Ganga Plain, India. *Current Science*, 973-978.

Shenoi, S. S. C., Shankar, D., & Shetye, S. R. (2002). Differences in heat budgets of the near-surface Arabian Sea and Bay of Bengal: Implications for the summer monsoon. *Journal of Geophysical Research: Oceans*, *107*(C6), 5-1.

Shimmield, G. B., Mowbray, S. R., & Weedon, G. P. (1990). A 350 ka history of the Indian Southwest Monsoon—evidence from deep-sea cores, northwest Arabian Sea. *Earth and Environmental Science Transactions of The Royal Society of Edinburgh*, *81*(4), 289-299.

Shukla, S. B., Chowksey, V. M., Prizomwala, S. P., Ukey, V. M., Bhatt, N. P., & Maurya, D. M. (2013). Internal sedimentary architecture and coastal dynamics as revealed by ground penetrating radar, Kachchh coast, western India. *Acta Geophysica*, *61*(5), 1196-1210.

Siddiqui, N.Z., Rama Rao, K.V. (1995). Limnology of Chilka Lake, in: Fauna of Chilka Lake. Zoological Survey of India, pp. 11–136.

Singh, D. S., Dubey, C. A., Kumar, D., & Ravindra, R. (2018). Climate events between 47.5 and 1 ka BP in glaciated terrain of the Ny-Alesund region, Arctic, using geomorphology and sedimentology of diversified morphological zones. *Polar Science*, *18*, 123-134.

Singh, D. S., Dubey, C. A., Kumar, D., Vishawakarma, B., Singh, A. K., Tripathi, A., ... & Sharma, R. (2019). Monsoon variability and major climatic events between 25 and 0.05 ka BP using sedimentary parameters in the Gangotri Glacier region, Garhwal Himalaya, India. *Quaternary International*, *507*, 148-155.

Singh, S., Parkash, B., Awasthi, A. K., & Kumar, S. (2014). Do stable isotopes in carbonate cement of Mio-Pleistocene Himalayan sediments record paleoecological and paleoclimatic changes?. *Palaeogeography, Palaeoclimatology, Palaeoecology*, *399*, 363-372.

Singh, S., Parkash, B., Awasthi, A. K., & Singh, T. (2012). Palaeoprecipitation record using O-isotope studies of the Himalayan Foreland Basin sediments, NW India. *Palaeogeography, Palaeoclimatology, Palaeoecology, 331*, 39-49.

Singh, V., Prasad, V., & Chakraborty, S. (2007). Phytoliths as indicators of monsoonal variability during mid–late Holocene in mainland Gujarat, western India. *Current Science*, 1754-1759.

Sinha, A., Cannariato, K. G., Stott, L. D., Li, H. C., You, C. F., Cheng, H., ... & Singh, I. B. (2005). Variability of Southwest Indian summer monsoon precipitation during the Bølling-Allerød. *Geology*, *33*(10), 813-816.

Sirocko, F., Sarnthein, M., Lange, H., & Erlenkeuser, H. (1991). Glacial to interglacial changes in Arabian Sea sediment accumulation rates: history of atmospheric summer circulation and coastal upwelling over the last 30,000 years. *Quaternary Research*, *36*, 72-93.

Smith, D.G. (1973). Aggradation of the Aleandra-North Sasktchewan River, Banff Park, Alberta, in: Fluvial Geomorphology. pp. 201–219.

Snowball, I. F. (1991). Magnetic hysteresis properties of greigite (Fe3S4) and a new occurrence in Holocene sediments from Swedish Lappland. *Physics of the Earth and Planetary Interiors*, *68*(1-2), 32-40.

Sontakke, N. A., Pant, G. B., & Singh, N. (1993). Construction of all-India summer monsoon rainfall series for the period 1844–1991. *Journal of Climate*, *6*(9), 1807-1811.

Soon, W., Herrera, V. M. V., Selvaraj, K., Traversi, R., Usoskin, I., Chen, C. T. A., ... & Severi, M. (2014). A review of Holocene solar-linked climatic variation on centennial to millennial timescales: Physical processes, interpretative frameworks and a new multiple cross-wavelet transform algorithm. *Earth-Science Reviews*, *134*, 1-15.

Sridhar, A. (2007). Mid–late Holocene hydrological changes in the Mahi River, arid western India. *Geomorphology*, *88*(3-4), 285-297.

Stefani, M., & Vincenzi, S. (2005). The interplay of eustasy, climate and human activity in the late Quaternary depositional evolution and sedimentary architecture of the Po Delta system. *Marine Geology*, *222*, 19-48.

Straffin, E., Blum, M., Colls, A., & Stokes, S. (1999). Alluvial stratigraphy of the Loire

and Arroux rivers (Burgundy, France)[Stratigraphie des alluvions de la Loire et de l'Arroux, Bourgogne, France]. *Quaternaire*, *10*(4), 271-282.

Street, F. A., & Grove, A. T. (1979). Global maps of lake-level fluctuations since 30,000 yr BP. *Quaternary Research*, *12*(1), 83-118.

Stuiver, M., & Reimer, P. J. (1993). Extended 14 C data base and revised CALIB 3.0 14 C age calibration program. *Radiocarbon*, *35*(1), 215-230.

Switzer, A. D., Bristow, C. S., & Jones, B. G. (2006). Investigation of large-scale washover of a small barrier system on the southeast Australian coast using ground penetrating radar. *Sedimentary Geology*, *183*(1-2), 145-156.

Tamura, T., Murakami, F., Nanayama, F., Watanabe, K., & Saito, Y. (2008). Ground-penetrating radar profiles of Holocene raised-beach deposits in the Kujukuri strand plain, Pacific coast of eastern Japan. *Marine Geology*, *248*(1-2), 11-27.

Tan, L., Cai, Y., Cheng, H., An, Z., & Edwards, R. L. (2009). Summer monsoon precipitation variations in central China over the past 750 years derived from a high-resolution absolute-dated stalagmite. *Palaeogeography, Palaeoclimatology, Palaeoecology*, *280*(3-4), 432-439.

Thamban, M., Kawahata, H., & Rao, V. P. (2007). Indian summer monsoon variability during the Holocene as recorded in sediments of the Arabian Sea: timing and implications. *Journal of oceanography*, *63*(6), 1009-1020.

Thamban, M., Rao, V. P., & Schneider, R. R. (2002). Reconstruction of late Quaternary monsoon oscillations based on clay mineral proxies using sediment cores from the western margin of India. *Marine Geology*, *186*(3-4), 527-539.

Ta, T. K. O., Nguyen, V. L., Tateishi, M., Kobayashi, I., Tanabe, S., & Saito, Y. (2002). Holocene delta evolution and sediment discharge of the Mekong River, southern Vietnam. *Quaternary Science Reviews*, *21*(16-17), 1807-1819.

Thompson, C., McMechan, G., Szerbiak, R., & Gaynor, N. (1995). Three-dimensional GPR imaging of complex stratigraphy within the Ferron sandstone, Castle Valley, Utah. In *Symposium on the Application og Geophysics to Engineering and Environmental Problems* (pp. 435-443).

Tiwari, M., Managave, S., Yadava, M. G., & Ramesh, R. (2009). Spatial and temporal coherence of paleomonsoon records from marine and land proxies in the Indian region during the past 30 ka. *Platinum Jubilee publication of the Indian Academy of sciences, Bangalore, India*, 1-19.

Tiwari, M., & Ramesh, R. (2007). Solar variability in the past and palaeoclimate data pertaining to the southwest monsoon. *Current Science*, *93*(4), 477-487.

Tornqvist, T. E. (1993a). Holocene alternation of meandering and anastomosing fluvial systems in the Rhine-Meuse delta (central Netherlands) controlled by sea-level rise and subsoil erodibility. *Journal of Sedimentary Research*, *63*(4), 683-693.

Törnqvist, T. E. (1993b). *Fluvial sedimentary geology and chronology of the Holocene*

Rhine-Meuse delta, The Netherlands (Vol. 166). Koninklijk Nederlands Aardrijkskundig Genootschap.

Usoskin, I. G., & Mursula, K. (2003). Long-term solar cycle evolution: review of recent developments. *Solar Physics*, *218*(1-2), 319-343.

Babu Rao,V., Atchuta Rao,D., & Ratnam,C. (1982). Aeromagnetic survey over parts of Mahanadi basin and the adjoining offshore region. Indian Geophys. Res. Bull. 20, 219–226.

Vaidyanadhan, R. (1991). *Quaternary deltas of India* (No. 22). Geological Society of India.

Vaidyanadhan, R., & Ghosh, R. N. (1993). Quaternary of the east coast of India. *Current science*, 804-816.

Van Heteren, S., FitzGerald, D. M., & Barber, D. C. (1997). Volumetric analysis of a New England barrier system using ground-penetrating-radar and coring techniques. *Oceanographic Literature Review*, *3*(44), 284.

van Heteren, S., FitzGerald, D. M., Barber, D. C., Kelley, J. T., & Belknap, D. F. (1996). Volumetric analysis of a New England barrier system using ground-penetrating-radar and coring techniques. *The Journal of Geology*, *104*(4), 471-483.

Van Overmeeren, R. A. (1998). Radar facies of unconsolidated sediments in The Netherlands: A radar stratigraphy interpretation method for hydrogeology. *Journal of Applied Geophysics*, *40*(1-3), 1-18.

Varikoden, H., & Babu, C. A. (2015). Indian summer monsoon rainfall and its relation with SST in the equatorial Atlantic and Pacific Oceans. *International Journal of Climatology*, *35*(6), 1192-1200.

Vaz, G. G., & Banerjee, P. K. (1997). Middle and late Holocene sea level changes in and around Pulicat Lagoon, Bay of Bengal, India. *Marine Geology*, *138*(3-4), 261-271.

Von Rad, U., Schaaf, M., Michels, K. H., Schulz, H., Berger, W. H., & Sirocko, F. (1999). A 5000-yr record of climate change in varved sediments from the oxygen minimum zone off Pakistan, Northeastern Arabian Sea. *Quaternary Research*, *51*(1), 39-53.

Wacker, L., Bonani, G., Friedrich, M., Hajdas, I., Kromer, B., Němec, M., ... & Vockenhuber, C. (2010). MICADAS: routine and high-precision radiocarbon dating. *Radiocarbon*, *52*(2), 252-262.

Wacker, L., Němec, M., & Bourquin, J. (2010). A revolutionary graphitisation system: fully automated, compact and simple. *Nuclear Instruments and Methods in Physics Research Section B: Beam Interactions with Materials and Atoms*, *268*(7-8), 931-934.

Walker, H. J., & Coleman, J. M. (1987). Atlantic and Gulf coastal

province. *Geomorphic systems of North America. Centennial Special*, *2*, 51-110.

Walker, M., Johnsen, S., Rasmussen, S. O., Popp, T., Steffensen, J. P., Gibbard, P., ... & Cwynar, L. C. (2009). Formal definition and dating of the GSSP (Global Stratotype Section and Point) for the base of the Holocene using the Greenland NGRIP ice core, and selected auxiliary records. *Journal of Quaternary Science: Published for the Quaternary Research Association*, *24*(1), 3-17.

Wang, N., Yao, T., Thompson, L. G., Henderson, K. A., & Davis, M. E. (2002). Evidence for cold events in the early Holocene from the Guliya ice core, Tibetan Plateau, China. *Chinese Science Bulletin*, *47*(17), 1422-1427.

Wang, P., & Horwitz, M. H. (2007). Erosional and depositional characteristics of regional overwash deposits caused by multiple hurricanes. *Sedimentology*, *54*(3), 545-564.

Warrick, R. A., Barrow, E. M., & Wigley, T. M. (Eds.). (1993). *Climate and sea level change: observations, projections and implications*. Cambridge University Press.

Warrier, A. K., Sandeep, K., & Shankar, R. (2017). Climatic periodicities recorded in lake sediment magnetic susceptibility data: Further evidence for solar forcing on Indian summer monsoon. *Geoscience Frontiers*, *8*(6), 1349-1355.

Warrier, A. K., Sandeep, K., & Shankar, R. (2017). Climatic periodicities recorded in lake sediment magnetic susceptibility data: Further evidence for solar forcing on Indian summer monsoon. *Geoscience Frontiers*, *8*(6), 1349-1355.

Wasson, R. J., Sundriyal, Y. P., Chaudhary, S., Jaiswal, M. K., Morthekai, P., Sati, S. P., & Juyal, N. (2013). A 1000-year history of large floods in the Upper Ganga catchment, central Himalaya, India. *Quaternary Science Reviews*, *77*, 156-166.

Weng, Q. (2002). Land use change analysis in the Zhujiang Delta of China using satellite remote sensing, GIS and stochastic modelling. *Journal of environmental management*, *64*(3), 273-284.

White, J. C. (2011). Emergence of cultural diversity in mainland Southeast Asia: a view from prehistory. *Dynamics of human diversity. Canberra: Pacific Linguistics*, 9-46.

White, K., & El Asmar, H. M. (1999). Monitoring changing position of coastlines using Thematic Mapper imagery, an example from the Nile Delta. *Geomorphology*, *29*(1-2), 93-105.

Wintle, A. G., & Murray, A. S. (2006). A review of quartz optically stimulated luminescence characteristics and their relevance in single-aliquot regeneration dating protocols. *Radiation measurements*, *41*(4), 369-391.

Wintle, A. G., & Murray, A. S. (1998). Towards the development of a preheat procedure for OSL dating of quartz. *Radiation Measurements*, *29*(1), 81-94.

Wood, L. J., Ethridge, F. G., & Schumm, S. A. (2009). The effects of rate of base-level fluctuation on coastal-plain, shelf and slope depositional systems: an experimental

approach. *Sequence stratigraphy and facies associations*, *100*, 43.

Woodroffe, S. A., & Horton, B. P. (2005). Holocene sea-level changes in the Indo-Pacific. *Journal of Asian Earth Sciences*, *25*(1), 29-43.

Wyrtki, K. (1973). Physical oceanography of the Indian Ocean. In *The biology of the Indian Ocean* (pp. 18-36). Springer, Berlin, Heidelberg.

Xu, H., Hong, Y., & Hong, B. (2012). Decreasing Asian summer monsoon intensity after 1860 AD in the global warming epoch. *Climate dynamics*, *39*(7-8), 2079-2088.

Xue, C. (1993). Historical changes in the Yellow River delta, China. *Marine geology*, *113*(3-4), 321-330.

Yadava, M. G., & Ramesh, R. (2007). Significant longer-term periodicities in the proxy record of the Indian monsoon rainfall. *New Astronomy*, *12*(7), 544-555.

Yadava, M. G., & Ramesh, R. (1999). Speleothems—useful proxies for past monsoon rainfall.

Yang, S., & Ding, Z. (2008). Advance–retreat history of the East-Asian summer monsoon rainfall belt over northern China during the last two glacial–interglacial cycles. *Earth and Planetary Science Letters*, *274*(3-4), 499-510.

Yoxall, W. H. (1969). The relationship between falling base level and lateral erosion in experimental streams. *Geological Society of America Bulletin*, *80*(7), 1379-1384.

Yu, Z., & Ito, E. (1999). Possible solar forcing of century-scale drought frequency in the northern Great Plains. *Geology*, *27*(3), 263-266.

Zani, H., Assine, M. L., & McGlue, M. M. (2012). Remote sensing analysis of depositional landforms in alluvial settings: method development and application to the Taquari megafan, Pantanal (Brazil). *Geomorphology*, *161*, 82-92.

Zhao, X. H., & Feng, X. S. (2015). Correlation between solar activity and the local temperature of Antarctica during the past 11,000 years. Journal of Atmospheric and Solar-Terrestrial Physics, 122, 26-33.

India Water Portal (http://www.indiawaterportal.org/met_data/), accessed on 02 June 2018.

Appendix I

Brief Principle of OSL dating:

The minerals like Quartz and feldspar are insulators in pure state but behave like semiconductors due to defects in crystal structure or due to presence of some impurities in the lattice. The defects behave as attractive potential for electrons and holes and are known as 'traps'. These traps are present in the forbidden energy gap and act as storage site for electrons and holes, where they can stay for millions of years. In Optically Stimulated Luminescence (OSL) dating we target these traps. Small amount of radioactive elements such as U, Th, K40 are present in the sediment. The alpha, beta and gamma radiations from elements act as ionizing radiation and generate electron hole pairs in the minerals such as quartz. These electrons may get trapped in the traps and stay there for millions of years until and unless are ejected from them due to external stimuli. In case of OSL dating the stimulation is done by light. So, when these minerals are exposed to light during sediment transport the traps get emptied and the clock is reset to zero. When these sediments are deposited somewhere else and are cut off from light, due to exposure to ionizing radiation the electrons start accumulating in the traps and the clock starts ticking again. Larger the time period of burial, higher is the number of electrons being trapped and thus higher is the luminescence counts.

The age is given by the formula

Age=Paleodose/Dose rate

Paleodose is the amount of energy accumulated in the grains over the time period of burial. The paleodose is the amount of given ionizing radiation by experimental setup which induces luminescence equivalent to originally found in grain. The rate at which ionizing radiation is given to the mineral is called the paleodose.

Paleodose Estimation

The paleodose is estimated in the laboratory by comparing the signal obtained by artificial radiation with the burial signal. The paleodose is estimated by two methods: (i) additive method (ii) regenerative method (Aitken, 1998).

Additive Method

For this method, aliquots are divided into a minimum of six groups. All the groups are primarily preheated before giving any laboratory radiation. Among these groups, one group is used for calculating natural signal and all other groups are exposed to a known amount of ionizing radiation of different magnitudes. Luminescence signals/counts are plotted against the dose to obtain paleodose. The main limitation of this method is that the dose-response curve is non-linear at high doses as the rate of increment falls off with increasing doses (Fig.1).

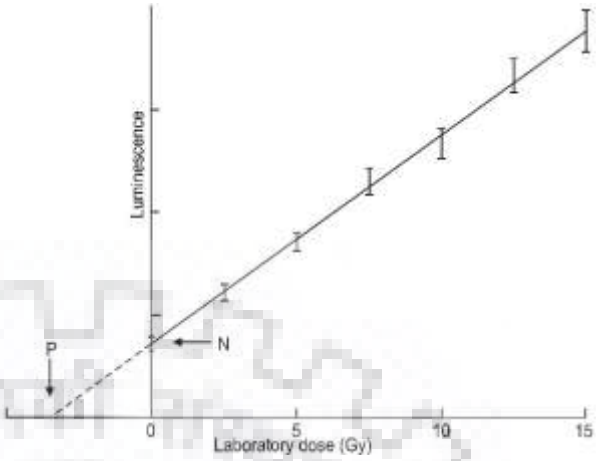

Figure 1 *Additive method of paleodose evaluation. Each data point is average OSL from a group of aliquots. Laboratory dose is zero for N. P is read off as paleodose (Aitken, 1998).*

Regeneration Method

In this process, the laboratory signal is compared with a natural signal to obtain the paleodose. Prior to giving artificial radiation the mineral grains need to be bleached properly. The growth curves are not extrapolated manually as in additive method; hence the limitations of nonlinear curves are overcome in this method (Fig.2).

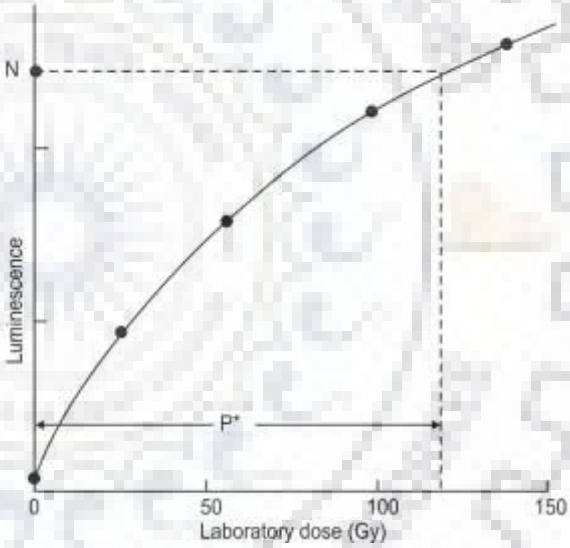

Figure 2 *The regeneration plot. The aliquots have been bleached and dosed. N is the natural OSL. P is read off as paleodose by regeneration.*

Dose-Rate

The dose rate is determined by estimating the concentration of radioactive minerals present in the sediment. It is generally by doing elemental analysis using XRF, ICP-MS or combination of both. It can be also estimated by using devices such as High Purity Germanium (HPGe) Radiation Detectors. In the present study, a combination of XRF and ICP-MS was used to measure the dose rate.